A Substantia Innominata-midbrain Circuit Controls a General Aggressive State

Zhenggang Zhu[1,3], Qingqing Ma[1,3], Hongbin Yang[1,3], Lu Miao[1], Lina Pan[1], Kaiyuan Li[1], Xiaoxing Zhang[2], Jintao Wu[1], Sijia Hao[1], Shen Lin[1], Xiulin Ma[1], Weihao Mai[1], Yizhe Hao[1], Yan-qin Yu[1]* and Shumin Duan[1,4]*

[1]Department of Neurobiology and Department of Neurology of Second Affiliated Hospital, Zhejiang University School of Medicine, Hangzhou 310058, China

[2]Institute of Neuroscience and Key Laboratory of Primate Neurobiology, Shanghai Institutes for Biological Sciences, Chinese Academy of Sciences, Shanghai 200031, China.

[3]These authors contributed equally

[4]Lead Contact

*Correspondence: yanqinyu@zju.edu.cn (Y.Y.Q.) and duanshumin@zju.edu.cn (D.S.)

SUMMARY

Animals display various aggressive behaviors essential for survival, while 'uncontrollable' attacks and abnormal aggressive states have massive social costs. Neural circuits regulating specific forms of aggression under defined conditions have been described, but whether there are circuits governing a general aggressive state to promote diverse aggressive behaviors remains unknown. Here, we found that posterior substantia innominata (pSI) neurons responded to multiple aggression-provoking cues with graded activity of differential dynamics, predicting the aggressive state and the topography of aggression in mice. Activation of pSI neurons projecting to the periaqueductal gray (PAG) increased aggressive arousal and robustly initiated/promoted all the types of aggressive behavior examined in an activity level-dependent manner. Inactivation of the pSI circuit largely blocked diverse aggressive behaviors, but not mating. By encoding a general aggressive state, the pSI-PAG circuit universally drives multiple aggressive behaviors and thus may provide a potential target for alleviating human pathological aggression.

KEYWORDS

Posterior substantia innominata, periaqueductal gray, aggression, aggressive state, arousal, synergistic circuit, female, defensive behavior

INTRODUCTION

Animals exhibit a range of aggressive behaviors (Blanchard et al., 2003; Moyer, 1968) essential for survival, reproduction, and social hierarchy establishment (Nelson and Trainor, 2007), while pathological aggression and the inability to control aggressive states cause serious social problems (Coccaro, 2012; Davidson, 2000; Siegel and Victoroff, 2009). Distinct regions in the mouse brain have been shown to be essential for male (Chamero et al., 2007; Hong et al., 2014; Lee et al., 2014; Leroy et al., 2018; Lin et al., 2011; Stagkourakis et al., 2018; Stowers et al., 2002; Todd et al., 2018; Unger et al., 2015; Yang et al., 2013; Yang et al., 2017; Zelikowsky et al., 2018), female (Hashikawa et al., 2017; Unger et al., 2015), predatory (Han et al., 2017; Li et al., 2018; Park et al., 2018; Shang et al., 2019; Zhao et al., 2019), and infant-directed (Autry et al., 2019; Chen et al., 2019; Isogai et al., 2018; Trouillet et al., 2019) aggressive behaviors. Furthermore, studies from some brain regions that have been examined for more than one type of aggressive behaviors suggest that different behaviors are regulated by distinct, dedicated neural circuits under specific internal and external conditions (Chen and Hong, 2018; Chen et al., 2019; Han et al., 2017; Hashikawa et al., 2017; Isogai et al., 2018; Yang et al., 2017; Zelikowsky et al., 2018). For example, aggression initiated in the ventromedial hypothalamus requires a specific genetic background (Swiss Webster or C57), sexual-reproductive state (male or female; virgin, sexually-experienced, or lactating), and social-contextual conditions (Hashikawa et al., 2017; Lee et al., 2014; Yang et al., 2017). Activation of the GABAergic neurons in the medial amygdala (MeA) promotes pup-directed aggression in male but hardly in female mice (Chen et al., 2019). In addition, activation of neurons in the central amygdala (Han et al., 2017), zona incerta (Shang et al., 2019; Zhao et al., 2019), or medial preoptic area (Park et al., 2018) triggers predatory aggression but not intra-conspecific aggression.

On the other hand, social behavior-related conditions have been reported to activate similar brain structures and overlapping circuits (Dulac et al., 2014; Hashikawa et al., 2017; Kim et al., 2015; Lin et al., 2011; Renier et al., 2016). Furthermore, stereotyped attack displays or patterns (e.g., biting, chasing, threatening, and aggression-related autonomic arousal) are expressed in most aggressive behaviors in rodents (Chen and Hong, 2018; Hashikawa et al., 2018; Siegel and Victoroff, 2009), suggesting the involvement of convergent pathways for diverse aggressive behaviors. Besides, human pathological aggression, such as “Intermittent Explosive Disorder”, are characterized by a variety of inappropriate and uncontrollable impulsive attacks (Coccaro, 2012) that may break out in the absence of an external threat, implying that some circuits in the brain may encode a general aggressive state and govern diverse aggressive behaviors, bypassing the various internal and external conditions required for natural aggression (Anderson, 2016; Asahina et al., 2014; Davidson, 2000). It is plausible that diverse aggressive behaviors are not only the results of parallel information processing by multiple dedicated circuits, but are also implemented

in some synergistic and interacting circuits. However, whether such synergistic circuits exist in the brain and how they regulate the internal state and behavioral activity patterns that together comprise diverse aggressive behaviors remain unclear.

The amygdala is known to be a key node for regulating aggression-related emotional state, and abnormalities of the amygdala are associated with human pathological aggression (Coccaro, 2012; Davidson, 2000; McCloskey et al., 2016; Nelson and Trainor, 2007; Siegel and Victoroff, 2009). However, the role of subdivisions of the amygdala in diverse aggressive behaviors and aggressive states remains elusive. The substantia innominata (SI), a sub-region of the basal forebrain that extends >2 mm rostrocaudally in the mouse brain, can be divided into the anterior SI (aSI) and the posterior SI (pSI), which has also been classified as the extended amygdala (Grove, 1988a; Heimer et al., 1997). Notably, the SI sends widespread descending projections to regions related to social behavior (Grove, 1988a), including the periaqueductal gray (PAG, see http://www.brain-map.org experiment id: 120281646), a region involved in the motor control of social behaviors (Behbehani, 1995; Chen and Hong, 2018). Remarkably, the SI is also involved in the regulation of motivation and fear behavior (Cui et al., 2017; Yu et al., 2017), an aggression-related emotional state.

Using electrophysiological recording and Ca^{2+} imaging, we found here that mouse pSI neurons exhibited increased activity with differential intensity and dynamics when exposed to various social-contextual cues and during many subsequent aggressive behaviors. This graded neuronal activity was correlated with the biological significance (threatening/attack-provoking or neutral) of the different social-contextual cues and predicted the topography of diverse aggressive behaviors. Acute optogenetic or chronic pharmacogenetic manipulation of the three largely overlapped pSI neuron populations, thymus cell antigen 1-positive (pSI^{Thy1} neurons), calcium/calmodulin-dependent protein kinase IIα-positive ($pSI^{CaMKIIα}$ neurons), and pSI neurons projecting to the PAG (pSI^{-PAG} neurons) demonstrated that the pSI-PAG circuit universally governs diverse aggressive behaviors.

RESULTS

Posterior SI Neurons Are Highly Active During Inter-male Aggression

To explore the role of the SI in aggressive behaviors, we first examined the c-Fos expression in the SI and nearby regions induced by inter-male aggression (Figure 1A). The number of c-Fos+ neurons in the pSI under aggressive conditions was ~3.4-fold greater than that under the control investigating condition, while less of an increase occurred in the aSI, nearby central amygdala (CeA), and globus pallidus (GP) (Figure 1B, C).

The pSI is a heterogeneous region and contains several intermingled cell populations, such as the cholinergic and non-cholinergic excitatory and inhibitory neurons (http://mouse.brain-map.org/; https://bbp.epfl.ch/nexus/cell-atlas/) (Cui et al., 2017; Heimer et al., 1997). We found

that approximately 81% of the aggression-induced c-Fos+ neurons in the pSI were thymus cell antigen 1-positive (Thy1+) and 77% were calcium/calmodulin-dependent protein kinase IIα-positive (CaMKIIα+), suggesting the preferential involvement of pSI^{Thy1} and $pSI^{CaMKII\alpha}$ neurons in aggression (Figure 1D, E). We then made *in vivo* electrophysiological recordings of the pSI neuronal activity during non-aggressive and aggressive social behaviors (Figure 1F, G). Consistently, we found that the average firing rate of all the recorded pSI neurons (n = 113) was increased during aggression (Figure 1H-J), with 39% showing increased activity during an attack (Figure 1H), which was much higher than that during a sniff (29% for contact with a male and 26% for contact with an object; Figure 1H). Notably, activity in these aggression-excited pSI neurons started to increase during the sniff preceding an attack ('aggressive' sniff, Figure 1K, L). The pSI neurons excited with aggression were less activated when sniffing an object (22%, Figure 1M) than when sniffing a male mouse (38%, Figure 1 N). Moreover, we found that pSI neurons excited by sniffing a male, a provoking cue for aggression, were activated more in attacks than the excitation when sniffing an object (Figure 1O-R; 47% *vs* 35%). Interestingly, none of the recorded neurons showed an increased firing rate under all three conditions (Figure 1S, T).

In summary, we found that pSI neurons are highly active in inter-male aggression and these neurons may encode the aggression and aggression-provoking cues.

Differential Ca^{2+} Dynamics in pSI^{Thy1} Neurons Associated with Different Aggressive States in Inter-male Aggression

To further explore the correlation between the activity in identified subtypes of pSI neurons and the behavioral aspects of aggression processing, we next injected viruses encoding GCaMP6m into the pSI of male Thy1-Cre mice (FVB/N) and used fiber photometry to record Ca^{2+} signaling in pSI^{Thy1} neurons during various aggressive and non-aggressive social behaviors (Figure 2A, B). Male Thy1-Cre mice exhibited robust aggressive behaviors (mean duration, 1.01 ± 0.06 s; Figure 2C, D) and were thus efficient for assessing aggression-associated activity. The tested mice could exhibit single attacks (without a subsequent attack episode in 4 s) or continuous attacks (with subsequent attack episodes in 4 s) toward the intruder mouse (Figure 2I). The average interval between episodes of continuous attacks was 1.53 ± 0.08 s (n = 293), while the average interval between two single attacks or between a single attack and a continuous attack was 48.73 ± 5.35 s (n = 165).

The activity of pSI^{Thy1} neurons started to increase before an attack (~–1.2 s, pre-attack), peaked midway through the attack (duration of attacks, ~1.0 s; peak $\Delta F/F$: 23.43 ± 1.14%), and was sustained for some time after termination of the attack (~4.8 s; post-attack, Figure 2E-H). However, distinct Ca^{2+} dynamics of pSI^{Thy1} neurons were found in attacks of different patterns or in different episodes of continuous attacks (Figure 2J). The Ca^{2+} signal in the post-attack period of each

127 episode of continuous attacks (except for the last episode) was maintained at a much higher level
128 (peak $\Delta F/F$: 29.26 ± 1.93% *vs* 16.21 ± 1.97%) and for a longer time (7.8 s *vs* 5.4 s) than that in
129 single attacks (Figure 2K-N). The subsequent episodes after the first one in continuous attacks
130 were initiated from a much higher basal Ca^{2+} (pre-attack) level than the first episode or single
131 attacks (Figure 2K-N). To study the potential correlation of pSI^{Thy1} neuronal Ca^{2+} signals with
132 different attack episodes, we analyzed the predictive value of these Ca^{2+} signals for the topography
133 of the aggressive behavior by developing a supporting vector machine (SVM) classifier according
134 to the LIBSVM library (https://www.csie.ntu.edu.tw/~cjlin/libsvm). We found that the first
135 episode of a continuous attack was best distinguished from a single attack by increased activity of
136 pSI neurons in the post-attack period (Figure S1I-J), while the last episode of a continuous attack
137 was much better separated from a single attack by an increased pre-attack pSI activity (Figure
138 S1K-L). These results indicate the patterns in different episodes of attack can be largely separated
139 by differential pSI Ca^{2+} signals. To determine whether the differential pSI Ca^{2+} activity between
140 single and continuous attacks results from the attack activity itself, we did the regression analysis
141 and found that no positive correlation between the attack probabilities prior to attacks and the Ca^{2+}
142 activity in the attack episodes (Figure S1A-D). Therefore, the differential Ca^{2+} activity prior to
143 attacks with different aggression topography may reflect different aggressive states, rather than
144 simply contamination from continuous behavior episodes. On the other hand, the peak Ca^{2+} levels
145 during all of these attacks were similar (Figure 2O, P, and Figure S1E). The sustained elevated
146 post-attack Ca^{2+} level of continuous attacks may reflect a higher basal level of the aggressive state
147 so that a subsequent attack episode can be initiated quickly (Figure 2K-M).

148 It is interesting to note that differential Ca^{2+} dynamics in the pSI^{Thy1} neurons were also recorded
149 during other types of social behaviors such as sniffs and rattles, depending on whether these
150 behaviors were followed by attack behavior (Figure 3A, B). Thus, Ca^{2+} activity in the pSI^{Thy1}
151 neurons increased more during the sniff/rattle preceding an attack (peak $\Delta F/F$: 21.23 ± 1.81% for
152 'aggressive' sniff (Hashikawa et al., 2017) and 17.37 ± 3.29% for 'aggressive' rattle (Yang et al.,
153 2017)) than the simple sniff/rattle without an attack (peak $\Delta F/F$: 9.90 ± 0.82% for 'non-aggressive'
154 sniff and 7.03 ± 3.54% for 'non-aggressive' rattle; Figure 3C-F, and 3I-J). The SVM classifier
155 analysis demonstrated that the pre-, during-, and post-behavior Ca^{2+} signals in sniffs or rattles
156 largely differed from those in sniffs or rattles preceding an attack, and the Ca^{2+} levels associated
157 with these sniffs or rattles predicted whether or not an actual attack would follow (Figure 3G-H
158 and 3M-N). In addition, when mice threatened male intruders (with boxing postures but no bites),
159 the pSI^{Thy1} neuronal activity also increased to a high level (peak $\Delta F/F$: 17.06 ± 2.61%) similar to
160 that in 'aggressive' rattles (Figure 3K, L).

161 Collectively, pSI^{Thy1} neurons showed a graded increase in Ca^{2+} activity in various inter-male
162 social behaviors, with the least increase during 'non-aggressive' social behaviors such as a simple

sniff or rattle (peak Δ*F/F*: 7.03–9.90%), relatively high activity during 'aggressive' inter-male social behaviors such as sniff-attack or rattle-attack (peak Δ*F/F*: 17.06–21.23%), and the highest activity in inter-male attacks (peak Δ*F/F*: 23.43%) (Figure 3O). Classifier analysis of the graded Ca^{2+} levels among these distinct social behaviors further suggested that these behaviors in different aggressive states were largely predicted by the associated pSI^{Thy1} neuronal activity (Figure 3P, Q).

Graded Ca^{2+} Activity in pSI^{Thy1} Neurons Associated with Various Aggression-provoking Cues and Different Aggressive Behaviors

Animals exhibit several aggressive behaviors in response to different social-contextual cues. Much of our knowledge regarding aggressive behaviors has been obtained from studies of rodent inter-male aggression in the resident intruder assay (Blanchard et al., 2003; Chen and Hong, 2018), while the mechanisms underlying other types of aggression remain relatively under-studied. We therefore investigated whether aggressive behaviors in male Thy1-Cre mice could be evoked by different social-contextual cues (Figure S2A) and how pSI^{Thy1} neurons responded to various cues that may or may not trigger aggressive or non-aggressive social behaviors (Figure S2E). We found that aggression was not triggered (Figure S2B) and pSI^{Thy1} neurons were not excited by neutral or appetitive stimuli, such as the consumption of food or water, and the detection of a novel object or olfactory urine cue (Figure S2F, G). In contrast, various imminent non-social threat cues (e.g., air-puff, tail suspension, or an intruding flying glove) significantly activated the pSI^{Thy1} neurons (Figure S2H, I) and moderately evoked aggressive behaviors (Figure S2C). Moreover, introducing a conspecific into the home cage of a tested male mouse, a social threat cue, or social provocation that frequently evokes aggressive behaviors (Figure S2C) (Bayless et al., 2019; Blanchard and Blanchard, 1988; Coccaro et al., 2007), immediately induced even higher activity in pSI^{Thy1} neurons than non-social threat cues (Figure S2J-N). Interestingly, the introduction of different types of conspecific evoked differential intensity of pSI^{Thy1} neuronal activity in the order (from weak to strong) female C57 < male C57 < male CD1 < male C57 with a subsequent attack (Figure S2O). Since different social-contextual cues differ in their biological significance, representing different levels of 'social threat' to the tested mouse for evoking aggression (Figure S2D), the graded pSI^{Thy1} neuronal activity thus provides a scalar measure of different aggressive states in a tested mouse.

We next investigated whether and how Ca^{2+} activity in pSI^{Thy1} neurons correlates with different types of aggressive behavior (Figure 4A). First, we recorded the neural activity during male-female attacks when Thy1-Cre male mice occasionally attacked female mice (aggression was observed in 22.7 % of male Thy1-Cre mice, Figure 4B). We found that pSI^{Thy1} neuronal activity was increased

during a male-female attack with a time window from –1.7 s to 7.5 s (Figure 4C) and a peak magnitude ($\Delta F/F$) of 25.62 ± 2.33% (Figure 4D), similar to that in inter-male attacks (from –1.2 s to 5.8 s; peak $\Delta F/F$: 23.43 ± 1.14%; Figures 4M-O and S1M-O). When introduced to the home-cage of male CD-1 mice and attacked by the latter, the Thy1-Cre mice in turn exhibited defensive attacks. Interestingly, the increased neural activity during inter-male defensive attacks (peak $\Delta F/F$: 30.23 ± 0.79%) was even higher than that during inter-male offensive attacks (peak $\Delta F/F$: 23.43 ± 1.14%) (Figure 4E-G). In contrast, although the pSI^{Thy1} neuronal activity was also increased in predatory attacks on crickets, the increase was much less (peak $\Delta F/F$ during investigation or attack: 6.35 ± 1.26% or 8.41 ± 0.47%) and shorter in sustained time (from –0.2 s to 3.3 s) than that in inter-male attacks (Figure 4H-L). The increased pSI^{Thy1} neuronal activity in pup-directed attacks had a similar magnitude (peak $\Delta F/F$ during investigation or attack: 4.50 ± 1.58% or 9.50 ± 0.90%) but a longer time window (from –2.1 s to 4.8 s) than that in a predatory attack (Figure 4M-Q). The female aggression in virgin female mice toward a male mouse, although seldom observed and lasting for a shorter time (duration of attacks in females *vs* males: 0.42 ± 0.03 s *vs* 1.01 ± 0.06 s) (Figures 2E and 4T), was associated with increased pSI^{Thy1} neuronal activity at a similar amplitude (peak $\Delta F/F$ during sniff without or with attack: 7.03 ± 0.76% or 8.76 ± 0.51%) but an even longer time window (from –4.0 s to 7.5 s) than with predatory or pup-directed aggression (Figure 4R-V). Based on the pSI^{Thy1} neuronal Ca^{2+} properties in cricket-directed, pup-directed, and female social behaviors, the SVM algorithm analysis nicely classified the sniffs, sniffs (attack), and attacks (Figure 4K, P, U), and predicted whether or not an actual attack would follow (Figure S1P-AA). Interestingly, the decoding accuracies in 4 types of attack and 4 types of approach (attack) were much higher than those in 4 types of approach (Figure S1AB, AC), suggesting that the aggressive states rather than the non-aggressive states are specially encoded in the dynamics of pSI neuronal activity. Moreover, pSI^{Thy1} neurons in the tested mice showed graded increases in activity in different types of aggressive behavior in the order (from weak to strong) predatory aggression < pup-directed aggression < female aggression < male offensive aggression < male defensive aggression (Figure 4W). Predictive analysis nicely classified six types of aggression by the recorded activity of pSI^{Thy1} neurons (Figure S1AD, AE), pointing out that different levels of pSI neuronal activity were linked with distinct aggressive behaviors of the tested male or female with different attack targets.

In summary, the perception of various aggression-provoking cues and the topography of aggressive behaviors is a critical determinant of the magnitude and dynamics of pSI^{Thy1} neuronal activity.

Activation of pSI Neurons Drives Inter-male Aggression and Enhances Autonomic Arousal

The above results suggest that, based on the perception of various social and non-social-contextual

233 cues, pSI neurons may encode an aggressive state with graded levels to drive aggressive behaviors.
234 We then asked whether the activation of pSI^{Thy1} neurons is sufficient to elicit aggression. We first
235 optimized a behavioral paradigm in which a socially-housed male encountered a singly-housed
236 male in a novel cage, a condition under which the virus-injected male mice showed minimal basic
237 inter-male aggression. The tested male mice were intraperitoneally injected (i.p.) with clozapine-
238 N-oxide (CNO) so that pSI^{Thy1} neurons were selectively activated by pharmacogenetics (Figure
239 5A, B). CNO treatment robustly induced aggressive behaviors in mice with hM3Dq-encoding
240 virus injected into the pSI (Figures 5C and S3K). Interestingly, chemogenetic activation of the
241 pSI^{Thy1} neurons in male mice did not promote their mating behavior (no mating behavior was
242 observed; Figure 5C), suggesting a specific role of pSI^{Thy1} neurons in aggressive behavior.
243 Notably, the SI sends widespread descending projections to social behavior-related regions
244 (Grove, 1988a). Using anterograde trans-synaptic tracing approach, we found that ventral
245 lateral/lateral periaqueductal gray (VL/LPAG), a region involved in the motor control of social
246 behaviors (Behbehani, 1995; Chen and Hong, 2018), was densely innervated by pSI neurons
247 (Figure S3A-D) (also see http://www.brain-map.org experiment id: 120281646). We further
248 labeled the input neurons to the PAG by injecting a retrograde AAV-Retro-EGFP virus into the
249 VL/LPAG (Figure 5D). A dense infection of upstream neurons was found in the pSI, but not or
250 few in the aSI, GP, or MeA (Figure 5D, E), consistent with data shown in the Allen Brain Atlas
251 (http://www.brain-map.org experiment id: 304694870 and 146985623). Since most of the pSI
252 neurons projecting to the PAG (pSI^{-PAG} neurons) were Thy1-positive or CaMKIIα-positive
253 (~87%/75%, Figure S3E-H), we investigated the essential role of the PAG projecting-specific pSI
254 neurons in aggression. The pSI^{-PAG} neurons were then selectively activated by pharmacogenetics
255 in mice unilaterally injected with AAV-Retro-Cre-EGFP virus into the VL/LPAG and Cre-
256 dependent AAV-DIO-hM3Dq-mCherry virus into the pSI (Figure S3I-K). CNO-dependent
257 activation of the pSI^{-PAG} neurons was confirmed by whole-cell electrophysiological recordings
258 (Figure S3L) and double-labeling for mCherry and c-Fos (Figure S3M-O). Activating the pSI^{-PAG}
259 neurons robustly induced inter-male aggression, but no mating behavior observed (Figure S3P-R).
260 In summary, pharmacogenetic activation of either pSI^{Thy1} or pSI^{-PAG} neurons was capable of
261 promoting inter-male aggression, but not mating.
262 We next used an optogenetic approach to establish a causal relationship between pSI^{-PAG}
263 neuronal activity and aggressive behaviors with more precise temporal resolution (Figures 5F and
264 S4A-C). Photostimulation-induced activation of the pSI^{-PAG} neurons was confirmed by whole-cell
265 electrophysiological recordings (Figure S4D). A socially-housed male that exhibited minimal
266 natural inter-male aggression (Figure 5G) immediately attacked a singly-housed male (Movie S1;
267 Figure S4G) when pSI^{-PAG} neurons were optogenetically activated. The success ratio of light-
268 evoked attacks was positively correlated with the frequency of photostimulation (Figure S4F). An

attack was characterized by biting the dorsal surface of an opponent at a mean latency of ~3 s (Figure 5I), closely resembling the most violent elements of aggressive behavior under natural conditions (Figure S4G; Movie S1). Optogenetic activation of $pSI^{CaMKII\alpha}$ neurons similarly increased male aggression (Figure S4P-T).

Diverse types of aggression may be largely classified into proactive and affective forms, characterized by hypoarousal and hyperarousal, respectively (Coccaro, 2012; Nelson and Trainor, 2007; Siegel and Victoroff, 2009). We next determined whether the photoactivation of pSI^{-PAG} neurons modulates the state of arousal, monitored by changes in the size of the pupil and widening of the eye in head-fixed mice (Figure 5J, K) (Wang et al., 2015). Photoactivation of the pSI^{-PAG} neurons resulted in a significant (30%) increase in pupil size (Figure 5L, M; Movie S2), a response that was sustained for >15 s after the stimulation ceased. The eyes were also wider during pSI stimulation (Figure 5N; Movie S2). Moreover, pSI^{-PAG} activation caused an increase in the breathing rate (Figure 5O) and heart rate (Figure 5P), as well as body trembling (Figure 5Q; Movie S2). However, photostimulation of pSI^{-PAG} neurons did not affect the overall level of anxiety (Figure S4I, J), nor trigger the freezing or flight response (Figure S4K-O). In summary, optogenetic activation of pSI^{-PAG} neurons immediately induced robust attacks accompanied by an increased arousal state (Figure 5R), a response consistent with affective aggression (Coccaro, 2012; Siegel and Victoroff, 2009).

Diverse Aggressive Behaviors Controlled by Differential Activity of pSI^{-PAG} Neurons

High levels of arousal have been proposed to diminish the requirements for promoting innate behaviors (Asahina et al., 2014; Tinbergen, 1951). Importantly, indiscriminate and uncontrollable aggressive behaviors, such as "Intermittent Explosive Disorder", have been reported in humans with elevated arousal (Coccaro, 2012; Siegel and Victoroff, 2009). Therefore, we reasoned that the increased arousal induced by pSI activation may establish a 'heightened aggressive state' that overcomes the internal and external requirements (Blanchard et al., 2003; Moyer, 1968) for evoking multiple types of aggression. In the subsequent experiments, we determined whether photo-activation of pSI^{-PAG} neurons induces a variety of aggressive behaviors under various conditions (Figure 6A).

Offensive inter-male aggression is expressed distinctly when animals are under different social-contextual conditions (Chen and Hong, 2018; Yang et al., 2017). Furthermore, activating the identified aggression-associated circuits has been reported to induce inter-male aggression in the home cage of singly-housed but not in socially-housed mice (Yang et al., 2017; Zelikowsky et al., 2018). Surprisingly, photoactivation of pSI^{-PAG} neurons not only facilitated typical territorial inter-male aggression in both singly-housed (Figure 6J) and socially-housed (Figure 5) resident mice in their home cages, but also robustly induced inter-male aggression when a singly-housed

or a socially-housed male encountered a male mouse in a novel cage (Figure 6J) or even when a socially-housed male encountered its male cage mate (Figure 6J). Notably, photoactivation of pSI^{-PAG} neurons even induced inter-male aggression when the tested (optogenetically stimulated) male mice intruded into the home cage of another mouse (Figure 6J). Under normal conditions, male mice do not attack females (Lin et al., 2011). Interestingly, photoactivation of pSI^{-PAG} neurons immediately and reliably induced male aggression against females to an extent similar to attacks against males (Figure 6J). Aggression induced by activating identified aggression-associated circuits rarely seen in virgin female mice, and the induced female aggression differs widely depending on their reproductive state and genetic background (Hashikawa et al., 2017). To find out whether pSI^{-PAG} neurons are involved in female aggression, we used a behavioral paradigm in which a virgin female mouse encountered a male or female, a condition under which the tested female showed little or no natural aggression (Figure 6B). Strikingly, pSI-activation in these females immediately initiated attacks against males (Figure 6C; Movie S3) or females (Figure 6J).

We found that photoactivation of pSI^{-PAG} neurons in sexually-experienced males evoked aggression toward pups (Figure 6D, E), an infanticidal behavior usually committed by adult virgin males but not sexually-experienced males (Chen and Hong, 2018; Isogai et al., 2018). Crickets have been used as prey to test predatory aggression in mice (Han et al., 2017; Li et al., 2018; Park et al., 2018). Photoactivation of pSI^{-PAG} neurons increased predatory attacks in male mice toward crickets (Figure 6J). Interestingly, photoactivation of pSI^{-PAG} neurons also induced object-directed aggression (Figure 6F, G): a moving glove evoked a rage-like response in male mice that never occurred in control mice (Lin et al., 2011). A socially-housed male that had been previously social defeated by a more aggressive CD-1 male for 5 min would flee or freeze without apparent defensive aggression (Blanchard et al., 2003) when encountering the same CD-1 mouse later in the home cage of that CD-1 mouse (Figure 6H). Surprisingly, photoactivation of pSI^{-PAG} neurons in the defeated mouse immediately shifted the flight or freeze into defensive attack towards the aggressive CD-1 male (Figure 6I; Movie S4), a response consistent with the increased activity of pSI neurons recorded during natural defensive aggression (Figure 4). No increased mating behavior was observed under the above conditions. Furthermore, optogenetic or pharmacogenetic activation of pSI$^{CaMKII\alpha/Thy1}$ neurons similarly increased male or female aggression (Figure S5), two types of aggression rarely observed under control conditions. Similar to the activation of pSI^{-PAG} neurons, photoactivation of the pSI^{-PAG} projection terminals in the PAG, but not in the bed nucleus of the stria terminalis (BNST), or ventromedial hypothalamus (VMH) (Lin et al., 2011), universally triggered diverse aggressive behaviors (Figure S6). Besides, optogenetically stimulating the terminals of pSI$^{CaMKII\alpha}$ neurons in the PAG, but not in the BNST, induced robust male and female aggression (Figure S6).

Notably, the extent of an attack was similar among the above thirteen types or conditions of

aggressive behaviors (Figure 6J) induced by the photoactivation of pSI^{-PAG} neurons at the same intensity of laser stimulation (2.7 mW). Considering that graded neuronal responses of pSI neurons were recorded during natural aggressive behaviors (Figure 4), we investigated whether multiple aggressive behaviors could be elicited by different activities of pSI^{-PAG} neurons (Figure 7A). We first optogenetically stimulated pSI^{-PAG} neurons across a wide range of illumination intensities in inter-male aggression, and found that gradually increasing the activation of the pSI^{-PAG} neurons by increasing the light intensity progressively increased the inter-male attack probability (Figure 7B-D), in agreement with our hypothesis that the pSI^{-PAG} neuronal activity determines the attack strength of aggression. Similarly, we found that the strength of photoactivation was strongly correlated with the attack probability or latency to attack onset among all five types of aggressive behaviors tested (Figure 7E-G). However, distinct dose-response curves, obtained by non-linear regression fit of photostimulation intensity with the probability and latency of attack, were created from these five types of evoked aggression (Figure 7F-G). Low-intensity photostimulation (<0.2 mW) mostly initiated predatory and pup-directed aggression, with less evoked female aggression and the least triggered male aggression (Figure 7F-H). As the stimulation intensity increased to intermediate light intensities (0.2 - 1 mW), female-male, male-female, and inter-male aggression were more frequently evoked (Figure 7F, G). Interestingly, under conditions of high-intensity photostimulation (>1 mW), all five types of aggressive behaviors were triggered (Figure7 F and G, see also Figure 6J).

These results suggest that diverse aggressive behaviors are differentially initiated by scalable activation of pSI^{-PAG} neurons, with different threshold in the order: predatory aggression < pup-directed aggression < female aggression < inter-male aggression (Figure 7H). This causal relationship between aggressive behavioral response and photostimulation intensity largely consistent with the graded pSI^{-PAG} neuronal activity observed in diverse aggressive behaviors (Figure 4), consistent with that pSI activity represents a general aggressive state threshold variable for computing diverse aggressive behaviors.

pSI Is Required for Diverse Aggressive Behaviors but not for Mating

The above results showed that diverse aggressive behaviors can be induced by differential activation levels of the pSI circuit. We then asked whether the pSI is also necessary for these natural aggressive behaviors. We first optimized a behavioral paradigm in which a singly-housed Thy1-Cre male in its home cage robustly attacked a socially-housed male intruder (Figure 8A). Pharmacogenetically inhibiting the pSI^{Thy1} neurons in male Thy1-Cre mice by CNO injection (Figures 8B and S7H-K) largely blocked the aggression in tested males (Figures 8C and S7L). Besides, pharmacogenetic inactivation of the pSI^{-PAG} neurons also reduced aggression (Figure S7A-G). Several brain regions known to regulate aggression have also been found to affect mating

behaviors (Hong et al., 2014; Lee et al., 2014; Lin et al., 2011). However, activation of pSI^{-PAG}, $pSI^{CaMKII\alpha}$, or pSI^{Thy1} neurons was not sufficient to induce mating behavior in the present study (Figures 5, 6, and 7). Moreover, mating behavior was not changed during the pharmacogenetic silencing of pSI^{Thy1} neurons (Figure 8D-E), suggesting a specific role of pSI^{Thy1} neurons in aggression rather than mating.

Strikingly, photo-inhibition of pSI^{Thy1} neurons (Figure 8F) by targeting the Cre-dependent expression of *Guillardia theta* anion channel rhodopsin 1 protein (GtACR1) immediately terminated inter-male offensive aggression when a singly-housed male in its home cage encountered a socially-housed male (Figure 8G, J, M; Movie S5). Virgin adult males exhibited robust pup-directed aggression when encountering pups (Chen and Hong, 2018). Optogenetically inhibiting pSI^{Thy1} neurons also decreased the pup-directed aggression in singly-housed virgin adult males (Figure 8H, K, M). Similarly, photo-inhibition of pSI^{Thy1} neurons reduced the predatory aggression when a socially-housed male was attacking crickets (Figure 8I, L, M). The probability of interruption was similar among these aggressive behaviors blocked by pSI-inhibition (Figure 8N). Silencing pSI^{Thy1} neurons by photo-inhibition also significantly reduced the male-female and female-male aggression (data not shown). Finally, photo-inhibition of pSI^{-PAG} neuronal terminals in the PAG reduced the offensive inter-male aggression (Figure S7M-S).

DISCUSSION

We have identified the pSI as a previously-unappreciated key center for controlling a general aggressive state to drive/promote diverse aggressive behaviors in mice. Upon perception of various social-contextual cues, pSI neurons increased their activity with graded intensity and differential dynamics in a manner that nicely predicted the states and topography of diverse aggressive behaviors. *Via* the projection to the PAG, the pSI is both necessary and sufficient for universally controlling multiple aggressive behaviors in both male and female mice without apparent effects on sexual behaviors (Figure S8).

The pSI Circuit generates a Scalable General Aggressive State

Social behaviors like aggression are believed to be associated with internal states such as arousal, drive, and motivation (Anderson, 2016). Recent studies have suggested that, together with hormones and neuromodulators (Miczek et al., 2007; Pfaff et al., 2005; Tinbergen, 1951), some neural circuits may encode internal states to regulate social behaviors (Anderson, 2016; Asahina et al., 2014; Lee et al., 2014; Manoli et al., 2013; Zelikowsky et al., 2018).

Several lines of evidence indicated that a pSI circuit generates a scalable general aggressive state by integrating various attack-related social-contextual cues, and activity-dependently drives multiple aggressive behaviors. First, the activity of pSI^{Thy1} neurons increased in the following

413 situations: 1. when mice were exposed to aggression-provoking aversive cues, but not with
414 appetitive and neutral stimuli (Figure S2); 2. when mice actively contacted intraspecific and
415 interspecific targets (sniff-attack and rattle-attack; Figures 3 and 4); and 3. before, during, and after
416 the mice executed attacks (Figures 2, 3 and 4). Second, the initiation, termination, and topography
417 of an attack was largely decoded by the dynamics of the pSI^{Thy1} neuronal activity (Figures 2-4,
418 and S1). Third, the increased neuronal activity induced by various cues was graded in intensity
419 and differed in dynamics, depending on the saliency of various attack-related cues, such as the
420 'threat' level of the cues (Figure S2) and the nature of the attacked targets (Figure 4). Finally, the
421 activation of pSI^{-PAG} neurons not only triggered aggression but also increased autonomic arousal
422 (Figure 5), an internal state correlated with aggressive behavior in flies and mice (Anderson, 2016;
423 Asahina et al., 2014), defensive rage in cats (Siegel and Victoroff, 2009), and impulsive aggression
424 in humans (Coccaro, 2012). An increased internal aggressive state may explain our finding that
425 attacks induced by the activation of pSI neurons were directed at a variety of targets within the
426 visual field including a moving glove, crickets, and conspecific male or female mice (Figure 6, 7).
427

428 **The pSI Circuit Governs Multiple Forms of Aggression in a Scalable Manner**

429 Aggression is a complex social behavior and different kinds of aggressive behavior may be evoked
430 by different contextual cues under defined internal states and environmental conditions. Several
431 brain regions including olfactory, amygdalar, and hypothalamic loci have been found to be
432 essential for inter-male aggression in rodents (Chamero et al., 2007; Hong et al., 2014; Leroy et
433 al., 2018; Leypold et al., 2002; Lin et al., 2011; Mandiyan et al., 2005; Stagkourakis et al., 2018;
434 Stowers et al., 2002; Todd et al., 2018). A few identified neural circuits for controlling distinct
435 types of aggression, including predatory aggression (Han et al., 2017; Li et al., 2018; Park et al.,
436 2018; Shang et al., 2019; Zhao et al., 2019), female or maternal aggression (Hashikawa et al., 2017;
437 Unger et al., 2015), and pup-directed aggression (Chen et al., 2019; Isogai et al., 2018; Renier et
438 al., 2016; Trouillet et al., 2019; Tsuneoka et al., 2015) have also been reported recently in mice.
439 These results indicate that aggressive behaviors are regulated at multiple circuit levels, and
440 different types of aggression may have distinct neural mechanisms. Surprisingly, we found here
441 that the pSI-PAG pathway is crucial for controlling all the types of aggressive behavior we
442 examined: male (residents or intruders) aggression, female aggression, object-directed, pup-
443 directed (attempted infanticide), predatory, and defensive aggression (see Figure S8). Our results
444 indicate that pSI^{-PAG} neurons control a general aggressive state or function as a common gating
445 center for various aggressive behaviors. Thus, information for various cues triggering diverse
446 aggressive behaviors converges on pSI neurons, which integrate various threat cues in a scalable
447 and social context-dependent manner and elicit a common set of aggressive behaviors (Figure S8).
448 To our knowledge, the role of the pSI-PAG pathway covers the most extensive scope of aggressive

behaviors than any other brain region reported. Interestingly, different types of aggressions require differential activation levels of pSI neurons (Figure 7 and S2). It should be noted that scalable control of different innate behaviors by differential activity levels of a conmen circuit has been also reported (Chen et al., 2019; Evans et al., 2018; Hong et al., 2014; Lee et al., 2014).

Dedicated circuits for specific forms of aggression usually control attack behavior under defined conditions. For example, activation of progesterone receptor-positive or estrogen receptor 1-positive (Esr1+) neurons in the ventrolateral part of the VMH (VMHvl) initiate male aggression (Lee et al., 2014; Yang et al., 2017), an effect that is influenced by whether residents and intruders are housed singly or in groups prior to testing (Yang et al., 2017). Furthermore, female aggression induced by activation of Esr1+ neurons in the VMHvl is also affected by the genetic background (Swiss Webster or C57B6/N) and reproductive status (virgin or lactating) (Hashikawa et al., 2017). However, we found that the activation of pSI^{-PAG} neurons evoked aggression in both male and female mice irrespective of the social-contextual state, genetic background, or reproductive status of the residents or intruders (Figure 6). Infanticidal behavior is usually committed by adult virgin male, but not by female or sexually-experienced male mice (Isogai et al., 2018; Renier et al., 2016; Tsuneoka et al., 2015). Indeed, activation of GABAergic neurons in the MeA initiates pup-directed aggression in male but hardly seen in female mice (Chen et al., 2019). Our results showing that activation and inactivation of pSI neurons respectively induced attempted infanticide in sexually-experienced adult males and inhibited it in virgin males suggests that pSI neurons also function as a key node in gating infanticidal behavior, bypassing the requirement for vomeronasal signaling (Dulac et al., 2014; Tachikawa et al., 2013).

Animals may respond with different patterns of defensive behavior when encountering a threat, including freezing, flight, or defensive attack, depending on the environmental situation and internal state (Blanchard and Blanchard, 1988; Blanchard et al., 2003). Interestingly, we found that activation of pSI^{-PAG} neurons in a defeated mouse immediately shifted the defensive response pattern of the subordinate mouse to aggressive conspecifics – from defensive flight or freezing to robust attack (Figure 6). It should be noted that the behavior induced in a defensive mouse by stimulation of pSI neurons in the present study, which was characterized by robust attack, is rather different from the active defensive behavior induced by activation of the VMHvl, which is characterized by dashing and jumping away from the aggressor (Wang et al., 2019).

In summary, the activation of pSI^{-PAG} neurons unconditionally controls diverse aggressive behaviors, bypassing factors such as genetic background, reproductive state, social-contextual conditions, or opponent type required for aggression evoked by the activation of the dedicated circuits for controlling specific types of aggressive behaviors reported previously. It is plausible that the pSI-PAG circuit acts further downstream of the aggression-controlling pathway than the dedicated circuits for controlling specific types of attack. Alternatively, pSI neurons may have a

485 more global effect in the brain than other specifically-dedicated circuits so as to override the factors
486 required for evoking aggressive behaviors.
487
488 **Identification of the pSI-Midbrain Circuit Specifically Responsible for Aggression**
489 Aggression is a competitive social behavior that plays essential roles in survival and reproduction.
490 Many reports are consistent with Tinbergen's model (Tinbergen, 1951), which assigns aggression
491 to a "reproductive" behavioral hierarchy (Anderson, 2012; Lee et al., 2014; Lin et al., 2011). It is
492 possible that the correlated social behaviors of aggression and mating or parenting are
493 synergistically regulated by a common neural pathway. Alternatively, they could be separately
494 regulated by distinct neural circuits. Recording neural activity during aggression and mating has
495 revealed that these two behaviors can recruit overlapping neurons in the same brain regions,
496 including the two most intensively studied aggression-associated nuclei, the VMHvl and the MeA
497 (Lin et al., 2011). For example, Esr1+ neurons in the VMHvl (Lee et al., 2014) and vesicular
498 GABA transporter-positive neurons in the MeApd (Hong et al., 2014) have been found to control
499 several social behaviors including attack, social investigation, and mounting in an intensity-
500 dependent manner. Nevertheless, these overlapping neurons in the VMHvl and MeApd may be
501 further dissociated into components for specific social behaviors. In addition, the activity of medial
502 preoptic area neurons (Park et al., 2018; Tsuneoka et al., 2015; Wu et al., 2014) and MeA neurons
503 (Chen et al., 2019) have been correlated with both aggression and parenting behaviors.
504 Interestingly, we found that the pSI^{CaMKII}, pSI^{Thy1}, and pSI^{-PAG} neurons, three anatomically and
505 functionally overlapping populations, specifically regulate various aggressive behaviors but not
506 mating or parenting. Our results are consistent with a previous report that c-Fos expression in SI
507 neurons is much higher after aggression than after mating (Lin et al., 2011). Thus, pSI^{-PAG} neurons
508 specifically regulate aggressive behaviors, without apparent effects on other types of social
509 behavior.
510 The pSI has strongly biased outputs to the midbrain, such as the VL/LPAG, and reciprocal
511 connections with nearby nuclei such as the BNST, both of which have been reported to function
512 as important outputs for aggression (Behbehani, 1995; Gregg and Siegel, 2001; Hashikawa et al.,
513 2017; Lin et al., 2011; Mos et al., 1982; Padilla et al., 2016). Interestingly, our results indicate that
514 the VL/LPAG, but not the BNST or VMH, is a downstream pathway through which the pSI can
515 execute aggression. Since VL/LPAG neurons send strong projections to pre-motor cells, which in
516 turn execute various components of attack (Arber, 2012; Tovote et al., 2016), such a midbrain area
517 may function as a circuit dedicated to the finely-tuned, dynamically-controlled behavioral
518 components of aggression.
519 It should be pointed out that circuits mediating different types of survival behavior like threat-
520 detection (Palmiter, 2018), feeding (Sternson and Eiselt, 2017), anxiety (Tovote et al., 2015), and

521 fear (Mobbs et al., 2019) are also proposed to converge onto some common pathways before
522 diverging again for action selection. Interestingly, many aggression-related hypothalamic nucleus
523 and nearby amygdalar regions directly innervate the pSI according to the neural tracings (Cui et
524 al., 2017; Do et al., 2016; Grove, 1988a; Grove, 1988b) and our unpublished whole-brain mapping
525 of pSI^{-PAG} neurons. We proposed that the pSI-PAG circuit may function as a common aggression
526 pathway receiving convergent aggression-related information from different dedicated circuits
527 (Figure S8). Since various modulating factors (such as sexual-reproductive state and social context)
528 may affect the common downstream pathways, our hypothesis could explains why direct activation
529 of the pSI-PAG circuit unconditionally induced aggressive behaviors, overriding the various
530 factors required for evoking aggressive behaviors through the activation of dedicated upstream
531 circuits.
532
533 **Potential Relevance to Pathological Aggression**
534 An abnormal aggressive arousal and an inability to control aggressive behaviors in an appropriate
535 way such as "Intermittent Explosive Disorder" in humans are serious social problems that still lack
536 efficient interventional approaches (Davidson, 2000; Nelson and Trainor, 2007; Siegel and
537 Victoroff, 2009). Our finding that pSI neurons are sufficient and specific for evoking aggressive
538 arousal and a variety of inappropriate aggressive behaviors suggests that the pSI-induced
539 aggression in mice can serve as an animal model of pathological aggression. Interestingly,
540 abnormalities of the human amygdala are closely associated with pathological aggression (Coccaro,
541 2012; Davidson, 2000; McCloskey et al., 2016; Nelson and Trainor, 2007; Siegel and Victoroff,
542 2009). As a conserved sub-region of the human amygdala (see http://atlas.brain-map.org/) and a
543 necessary node for mouse aggressive behaviors, the pSI circuit may thus provide a therapeutic
544 target for the suppression of human pathological aggression (Davidson, 2000).
545

ACKNOWLEDGMENTS

We thank Xiaohong Xu, Nirao M Shah, Dayu Lin, Weizhe Hong, Bo Li and I.C. Bruce for discussions and reading the manuscript. We thank Hui-Fang Lou, Li-Ya Zhu, Xiaohong Xu, Hao-Ran Wang, Wei-Qian Jiang, and Hai-Shan Yao for technical support. This work was supported by the National Key Research and Development Program (2016YFA0501000 and 2016YFC1306700), the National Natural Science Foundation of China (81527901, 81821091, 31771167, and 31490592), the Non-profit Central Research Institute Fund of the Chinese Academy of Medical Sciences (2018PT31041), Science and Technology Planning Project of Guangdong Province (2018B030331001), and Fundamental Research Funds for the Central Universities (2019FZA7009).

AUTHOR CONTRIBUTIONS

Conceptualization, Z.G., Y.Y.Q., and D.S.; Methodology, Z.G. , Y.Y.Q., and D.S.; Software, Z.G.; Formal Analysis, Z.G., Z.X. , and M.X.; Investigation, Z.G., M.Q., M.L., P.L., L.K., W.J., Y.H., L.S., H.Y., M.W., and H.S.; Visualization, Z.G., M.Q., M.L., P.L., and L.K.; Writing – Original Draft, Z.G., Y.Y.Q., and D.S.; Writing Review & Editing, Z.G., Y.Y.Q., and D.S.; Funding Acquisition, Y.Y.Q., and D.S.; Resources, Y.Y.Q., and D.S.; Supervision, Z.G., Y.Y.Q., and D.S..

DECLARATION OF INTEREST

The authors declare that they have no competing financial interests.

REFERENCES

564 Anderson, D.J. (2012). Optogenetics, sex, and violence in the brain: implications for psychiatry. Biol Psychiatry *71*,
565 1081-1089.
566 Anderson, D.J. (2016). Circuit modules linking internal states and social behaviour in flies and mice. Nat Rev Neurosci
567 *17*, 692-704.
568 Arber, S. (2012). Motor circuits in action: specification, connectivity, and function. Neuron *74*, 975-989.
569 Asahina, K., Watanabe, K., Duistermars, B.J., Hoopfer, E., Gonzalez, C.R., Eyjolfsdottir, E.A., Perona, P., and Anderson,
570 D.J. (2014). Tachykinin-expressing neurons control male-specific aggressive arousal in Drosophila. Cell *156*, 221-235.
571 Autry, A.E., Wu, Z., Kohl, J., Bambah-Mukku, D., Rubinstein, N.D., Marin-Rodriguez, B., Carta, I., Sedwick, V., and Dulac,
572 C. (2019). Perifornical Area Urocortin-3 Neurons Promote Infant-directed Neglect and Aggression. bioRxiv, 697334.
573 Bayless, D.W., Yang, T., Mason, M.M., Susanto, A.A.T., Lobdell, A., and Shah, N.M. (2019). Limbic Neurons Shape Sex
574 Recognition and Social Behavior in Sexually Naive Males. Cell.
575 Behbehani, M.M. (1995). Functional characteristics of the midbrain periaqueductal gray. Progress in Neurobiology
576 *46*, 575-605.
577 Blanchard, D.C., and Blanchard, R.J. (1988). Ethoexperimental approaches to the biology of emotion. Annual review
578 of psychology *39*, 43-68.
579 Blanchard, R.J., Wall, P.M., and Blanchard, D.C. (2003). Problems in the study of rodent aggression. Hormones and
580 Behavior *44*, 161-170.
581 Chamero, P., Marton, T.F., Logan, D.W., Flanagan, K., Cruz, J.R., Saghatelian, A., Cravatt, B.F., and Stowers, L. (2007).
582 Identification of protein pheromones that promote aggressive behaviour. Nature *450*, 899-902.
583 Chen, P., and Hong, W. (2018). Neural Circuit Mechanisms of Social Behavior. Neuron *98*, 16-30.
584 Chen, P.B., Hu, R.K., Wu, Y.E., Pan, L., Huang, S., Micevych, P.E., and Hong, W. (2019). Sexually Dimorphic Control of
585 Parenting Behavior by the Medial Amygdala. Cell *176*, 1206-1221.
586 Coccaro, E.F. (2012). Intermittent explosive disorder as a disorder of impulsive aggression for DSM-5. Am J Psychiatry
587 *169*, 577-588.
588 Coccaro, E.F., McCloskey, M.S., Fitzgerald, D.A., and Phan, K.L. (2007). Amygdala and orbitofrontal reactivity to social
589 threat in individuals with impulsive aggression. Biol Psychiatry *62*, 168-178.
590 Cui, Y., Lv, G., Jin, S., Peng, J., Yuan, J., He, X., Gong, H., Xu, F., Xu, T., and Li, H. (2017). A Central Amygdala-Substantia
591 Innominata Neural Circuitry Encodes Aversive Reinforcement Signals. Cell Rep *21*, 1770-1782.
592 Davidson, R.J. (2000). Dysfunction in the Neural Circuitry of Emotion Regulation--A Possible Prelude to Violence.
593 Science *289*, 591-594.
594 Do, J.P., Xu, M., Lee, S.-H., Chang, W.-C., Zhang, S., Chung, S., Yung, T.J., Fan, J.L., Miyamichi, K., and Luo, L. (2016).
595 Cell type-specific long-range connections of basal forebrain circuit. Elife *5*.
596 Dulac, C., O'Connell, L.A., and Wu, Z. (2014). Neural control of maternal and paternal behaviors. Science *345*, 765-
597 770.
598 Evans, D.A., Stempel, A.V., Vale, R., Ruehle, S., Lefler, Y., and Branco, T. (2018). A synaptic threshold mechanism for

599 computing escape decisions. Nature *558*, 590-594.
600 Gregg, T.R., and Siegel, A. (2001). Brain structures and neurotansmitters regulating aggression in cats: implications
601 for human aggression. Progress in Neuro-Psychopharmacology and Biological Psychiatry *25*, 91-140.
602 Grove, E.A. (1988a). Efferent connections of the substantia innominata in the rat. J Comp Neurol *277*, 347-364.
603 Grove, E.A. (1988b). Neural associations of the substantia innominata in the rat: afferent connections. Journal of
604 Comparative Neurology *277*, 315-346.
605 Han, W., Tellez, L.A., Rangel, M.J., Jr., Motta, S.C., Zhang, X., Perez, I.O., Canteras, N.S., Shammah-Lagnado, S.J., van
606 den Pol, A.N., and de Araujo, I.E. (2017). Integrated Control of Predatory Hunting by the Central Nucleus of the
607 Amygdala. Cell *168*, 311-324 e318.
608 Hashikawa, K., Hashikawa, Y., Lischinsky, J., and Lin, D. (2018). The Neural Mechanisms of Sexually Dimorphic
609 Aggressive Behaviors. Trends Genet *34*, 755-776.
610 Hashikawa, K., Hashikawa, Y., Tremblay, R., Zhang, J., Feng, J.E., Sabol, A., Piper, W.T., Lee, H., Rudy, B., and Lin, D.
611 (2017). Esr1(+) cells in the ventromedial hypothalamus control female aggression. Nat Neurosci *20*, 1580-1590.
612 Heimer, L., Harlan, R.E., Alheid, G.F., Garcia, M.M., and de Olmos, J. (1997). Substantia innominata: a notion which
613 impedes clinical-anatomical correlations in neuropsychiatric disorders. Neuroscience *76*, 957-1006.
614 Hong, W., Kim, D.W., and Anderson, D.J. (2014). Antagonistic control of social versus repetitive self-grooming
615 behaviors by separable amygdala neuronal subsets. Cell *158*, 1348-1361.
616 Isogai, Y., Wu, Z., Love, M.I., Ahn, M.H., Bambah-Mukku, D., Hua, V., Farrell, K., and Dulac, C. (2018). Multisensory
617 Logic of Infant-Directed Aggression by Males. Cell *175*, 1827-1841 e1817.
618 Kim, Y., Venkataraju, K.U., Pradhan, K., Mende, C., Taranda, J., Turaga, S.C., Arganda-Carreras, I., Ng, L., Hawrylycz,
619 M.J., Rockland, K.S.*, et al.* (2015). Mapping social behavior-induced brain activation at cellular resolution in the
620 mouse. Cell Rep *10*, 292-305.
621 Lee, H., Kim, D.W., Remedios, R., Anthony, T.E., Chang, A., Madisen, L., Zeng, H., and Anderson, D.J. (2014). Scalable
622 control of mounting and attack by Esr1+ neurons in the ventromedial hypothalamus. Nature *509*, 627-632.
623 Leroy, F., Park, J., Asok, A., Brann, D.H., Meira, T., Boyle, L.M., Buss, E.W., Kandel, E.R., and Siegelbaum, S.A. (2018). A
624 circuit from hippocampal CA2 to lateral septum disinhibits social aggression. Nature *564*, 213.
625 Leypold, B.G., Yu, C.R., Leinders-Zufall, T., Kim, M.M., Zufall, F., and Axel, R. (2002). Altered sexual and social behaviors
626 in trp2 mutant mice. Proceedings of the National Academy of Sciences *99*, 6376-6381.
627 Li, Y., Zeng, J., Zhang, J., Yue, C., Zhong, W., Liu, Z., Feng, Q., and Luo, M. (2018). Hypothalamic Circuits for Predation
628 and Evasion. Neuron *97*, 911-924 e915.
629 Lin, D., Boyle, M.P., Dollar, P., Lee, H., Lein, E.S., Perona, P., and Anderson, D.J. (2011). Functional identification of an
630 aggression locus in the mouse hypothalamus. Nature *470*, 221-226.
631 Mandiyan, V.S., Coats, J.K., and Shah, N.M. (2005). Deficits in sexual and aggressive behaviors in Cnga2 mutant mice.
632 Nature neuroscience *8*, 1660.
633 Manoli, D.S., Fan, P., Fraser, E.J., and Shah, N.M. (2013). Neural control of sexually dimorphic behaviors. Current
634 opinion in neurobiology *23*, 330-338.

635 McCloskey, M.S., Phan, K.L., Angstadt, M., Fettich, K.C., Keedy, S., and Coccaro, E.F. (2016). Amygdala hyperactivation
636 to angry faces in intermittent explosive disorder. J Psychiatr Res *79*, 34-41.
637 Miczek, K.A., de Almeida, R.M., Kravitz, E.A., Rissman, E.F., de Boer, S.F., and Raine, A. (2007). Neurobiology of
638 escalated aggression and violence. Journal of Neuroscience *27*, 11803-11806.
639 Mobbs, D., Adolphs, R., Fanselow, M.S., Feldman Barrett, L., LeDoux, J.E., Ressler, K., and Tye, K.M. (2019). Viewpoints:
640 Approaches to defining and investigating fear. Nature Neuroscience.
641 Mos, J., Kruk, M., Van Poel, A.D., and Meelis, W. (1982). Aggressive behavior induced by electrical stimulation in the
642 midbrain central gray of male rats. Aggressive Behavior *8*, 261-284.
643 Moyer, K.E. (1968). Kinds of aggression and their physiological basis. Communications in Behavioral Biology *2(2): 65-*
644 *87.*
645 Nelson, R.J., and Trainor, B.C. (2007). Neural mechanisms of aggression. Nat Rev Neurosci *8*, 536-546.
646 Padilla, S.L., Qiu, J., Soden, M.E., Sanz, E., Nestor, C.C., Barker, F.D., Quintana, A., Zweifel, L.S., Ronnekleiv, O.K., Kelly,
647 M.J*., et al.* (2016). Agouti-related peptide neural circuits mediate adaptive behaviors in the starved state. Nat
648 Neurosci *19*, 734-741.
649 Palmiter, R.D. (2018). The Parabrachial Nucleus: CGRP Neurons Function as a General Alarm. Trends Neurosci *41*,
650 280-293.
651 Park, S.G., Jeong, Y.C., Kim, D.G., Lee, M.H., Shin, A., Park, G., Ryoo, J., Hong, J., Bae, S., Kim, C.H*., et al.* (2018). Medial
652 preoptic circuit induces hunting-like actions to target objects and prey. Nat Neurosci *21*, 364-372.
653 Pfaff, D., Westberg, L., and Kow, L.M. (2005). Generalized arousal of mammalian central nervous system. Journal of
654 Comparative Neurology *493*, 86-91.
655 Renier, N., Adams, E.L., Kirst, C., Wu, Z., Azevedo, R., Kohl, J., Autry, A.E., Kadiri, L., Umadevi Venkataraju, K., Zhou, Y*.,*
656 *et al.* (2016). Mapping of Brain Activity by Automated Volume Analysis of Immediate Early Genes. Cell *165*, 1789-
657 1802.
658 Shang, C., Liu, A., Li, D., Xie, Z., Chen, Z., Huang, M., Li, Y., Wang, Y., Shen, W.L., and Cao, P. (2019). A subcortical
659 excitatory circuit for sensory-triggered predatory hunting in mice. Nat Neurosci *22*, 909-920.
660 Siegel, A., and Victoroff, J. (2009). Understanding human aggression: New insights from neuroscience. Int J Law
661 Psychiatry *32*, 209-215.
662 Stagkourakis, S., Spigolon, G., Williams, P., Protzmann, J., Fisone, G., and Broberger, C. (2018). A neural network for
663 intermale aggression to establish social hierarchy. Nat Neurosci *21*, 834-842.
664 Sternson, S.M., and Eiselt, A.K. (2017). Three Pillars for the Neural Control of Appetite. Annu Rev Physiol *79*, 401-423.
665 Stowers, L., Holy, T.E., Meister, M., Dulac, C., and Koentges, G. (2002). Loss of sex discrimination and male-male
666 aggression in mice deficient for TRP2. Science *295*, 1493-1500.
667 Tachikawa, K.S., Yoshihara, Y., and Kuroda, K.O. (2013). Behavioral transition from attack to parenting in male mice:
668 a crucial role of the vomeronasal system. Journal of Neuroscience *33*, 5120-5126.
669 Tinbergen, N. (1951). The study of instinct.
670 Todd, W.D., Fenselau, H., Wang, J.L., Zhang, R., Machado, N.L., Venner, A., Broadhurst, R.Y., Kaur, S., Lynagh, T., Olson,

671 D.P.*, et al.* (2018). A hypothalamic circuit for the circadian control of aggression. Nat Neurosci *21*, 717-724.
672 Tovote, P., Esposito, M.S., Botta, P., Chaudun, F., Fadok, J.P., Markovic, M., Wolff, S.B., Ramakrishnan, C., Fenno, L.,
673 Deisseroth, K.*, et al.* (2016). Midbrain circuits for defensive behaviour. Nature *534*, 206-212.
674 Tovote, P., Fadok, J.P., and Luthi, A. (2015). Neuronal circuits for fear and anxiety. Nat Rev Neurosci *16*, 317-331.
675 Trouillet, A.C., Keller, M., Weiss, J., Leinders-Zufall, T., Birnbaumer, L., Zufall, F., and Chamero, P. (2019). Central role
676 of G protein Galphai2 and Galphai2(+) vomeronasal neurons in balancing territorial and infant-directed aggression
677 of male mice. Proc Natl Acad Sci U S A.
678 Tsuneoka, Y., Tokita, K., Yoshihara, C., Amano, T., Esposito, G., Huang, A.J., Yu, L.M., Odaka, Y., Shinozuka, K., McHugh,
679 T.J.*, et al.* (2015). Distinct preoptic-BST nuclei dissociate paternal and infanticidal behavior in mice. EMBO J *34*, 2652-
680 2670.
681 Unger, E.K., Burke, K.J., Jr., Yang, C.F., Bender, K.J., Fuller, P.M., and Shah, N.M. (2015). Medial amygdalar aromatase
682 neurons regulate aggression in both sexes. Cell Rep *10*, 453-462.
683 Wang, L., Chen, I.Z., and Lin, D. (2015). Collateral pathways from the ventromedial hypothalamus mediate defensive
684 behaviors. Neuron *85*, 1344-1358.
685 Wang, L., Talwar, V., Osakada, T., Kuang, A., Guo, Z., Yamaguchi, T., and Lin, D. (2019). Hypothalamic Control of
686 Conspecific Self-Defense. Cell Reports *26*, 1747-1758.e1745.
687 Wu, Z., Autry, A.E., Bergan, J.F., Watabe-Uchida, M., and Dulac, C.G. (2014). Galanin neurons in the medial preoptic
688 area govern parental behaviour. Nature *509*, 325-330.
689 Yang, C.F., Chiang, M.C., Gray, D.C., Prabhakaran, M., Alvarado, M., Juntti, S.A., Unger, E.K., Wells, J.A., and Shah, N.M.
690 (2013). Sexually dimorphic neurons in the ventromedial hypothalamus govern mating in both sexes and aggression
691 in males. Cell *153*, 896-909.
692 Yang, T., Yang, C.F., Chizari, M.D., Maheswaranathan, N., Burke, K.J., Jr., Borius, M., Inoue, S., Chiang, M.C., Bender,
693 K.J., Ganguli, S.*, et al.* (2017). Social Control of Hypothalamus-Mediated Male Aggression. Neuron *95*, 955-970 e954.
694 Yu, K., Ahrens, S., Zhang, X., Schiff, H., Ramakrishnan, C., Fenno, L., Deisseroth, K., Zhao, F., Luo, M.-H., Gong, L.*, et al.*
695 (2017). The central amygdala controls learning in the lateral amygdala. Nature Neuroscience *20*, 1680-1685.
696 Zelikowsky, M., Hui, M., Karigo, T., Choe, A., Yang, B., Blanco, M.R., Beadle, K., Gradinaru, V., Deverman, B.E., and
697 Anderson, D.J. (2018). The Neuropeptide Tac2 Controls a Distributed Brain State Induced by Chronic Social Isolation
698 Stress. Cell *173*, 1265-1279 e1219.
699 Zhao, Z.D., Chen, Z., Xiang, X., Hu, M., Xie, H., Jia, X., Cai, F., Cui, Y., Chen, Z., Qian, L.*, et al.* (2019). Zona incerta
700 GABAergic neurons integrate prey-related sensory signals and induce an appetitive drive to promote hunting. Nat
701 Neurosci *22*, 921-932.

MAIN FIGURES, FIGURE LEGENDS

Figure Legends

Figure 1. Elevated Neuronal Activity in the pSI during Inter-male Aggression

(A) Schematic of c-Fos analysis after sniff (without attack) or after attack.

(B) c-Fos+ neurons per slice in the pSI (*P = 0.0285; n = 7/7 mice), aSI (P = 0.500; n = 3/3 mice), central amygdala (CeA) (P = 0.500; n = 3/3 mice), and globus pallidus (GP) (P = 0.743; n = 3/4 mice). Two-tailed unpaired t-test and Mann-Whitney test.

(C) Example images of c-Fos+ neurons (green) in the pSI after sniff (middle) or attack (bottom) (scale bars, 100 μm). CeM, central amygdaloid nucleus, medial division.

(D) Upper panel, example image of c-Fos+ (magenta) and Thy1+ (green) neurons (two weeks previously, AAV-DIO-EYFP virus was injected into the pSI in Thy1-Cre mice) in the pSI examined after aggression (scale bars, 100 μm); Lower panel, magnified image of the boxed area in the upper panel (scale bars, 20 μm).

(E) Left, percentage of c-Fos+ neurons co-localized with Thy1 (n = 6 mice), CaMKIIα (n = 5), ChAT (n = 3), or GAD67 (n = 5) after an attack. Unpaired Kruskal-Wallis test, ***P < 0.001. Right, percentage of Thy1+ neurons expressing c-Fos (n = 6 mice), or CaMKIIα+ neurons expressing c-Fos (n = 5 mice) after an attack. Unpaired t test, P = 0.2349.

(F) Schematics of *in vivo* recording of pSI neuronal activity during non-aggressive and aggressive behaviors.

(G) Representative image of electrode placement (upper, scale bar, 100 μm) and overlay of electrode placements in the pSI (lower).

(H) Relative proportions of neurons excited (red), inhibited (blue), or unaffected (gray) while contacting an object (n = 110 neurons), sniffing a male mouse without attack (n = 110 neurons), or attacking a male mouse (n = 113 neurons).

(I) Heatmap of normalized firing rates of pSI neurons related to aggression (left). Time = 0 s denotes the time when the attack started. Bars (right) indicate the relative proportions of neurons excited (red) or inhibited (blue) during an attack.

(J) Mean population activity (area under the z-score curve) before, during, and after an attack for all recorded neurons in all attacks examined. Two-tailed paired t-test and Wilcoxon matched-pairs signed rank test; from left to right, P = 0.1566, ***P < 0.001, *P = 0.0458.

(K) Z-score of firing rate of the neurons excited by aggression.

(L) Mean population activity per second before, during, and after an attack for neurons excited by aggression. Two-tailed paired t-test and Wilcoxon matched-pairs signed rank test, ***P < 0.001 between the two groups indicated.

(M) Relative proportions of 'attack-active' neurons excited (red), inhibited (blue), or unaffected (gray) while sniffing an object (n = 37 neurons, left), Z-score of firing rate of the 'attack-active'

neurons excited by sniffing object (middle), and mean population activity per second before, during, and after sniffing object for the 'attack-active' neurons (right). P = 0.8913, One-way ANOVA.

(N) Relative proportions of 'attack-active' neurons excited (red), inhibited (blue), or unaffected (gray) while sniffing a male (n = 37 neurons, left), Z-score of firing rate of the 'attack-active' neurons excited by sniffing a male (middle), and mean population activity per second before, during, and after sniffing a male for the 'attack-active' neurons (right). *P = 0.0273, Friedman test.

(O) Z-score of firing rate of the 'object sniff-active' neurons excited by sniffing an object.

(P) Relative proportions of 'object sniff-active' neurons excited (red), inhibited (blue), or unaffected (gray) by aggression (n = 37 neurons, left), mean population activity per second before, during, and after an attack for 'object sniff-active' neurons (right). P = 0.2134, Friedman test.

(Q) Z-score of firing rate of the 'male sniff-active' neurons excited by sniffing a male.

(R) Relative proportions of 'male sniff-active' neurons excited (red), inhibited (blue), or unaffected (gray) by aggression (n = 37 neurons, left), mean population activity per second before, during, and after an attack for 'male sniff-active' neurons (right). P = 0.2090, Friedman test.

(S) Relative proportions of pSI neurons excited during three distinct behavioral activities.

(T) Proportion of neurons excited in three distinct behaviors among pSI 'attack-active' neurons.

ns, not significant.

Data are presented as the mean ± SEM.

Figure 2. Correlation of pSI^{Thy1} Neuronal Ca^{2+} Dynamics with Attack Patterns

(A) Setup for fiber photometric recording in pSI^{Thy1} neurons during inter-male aggression.

(B) Overlay of EGFP (left) and GCaMP6m (middle) expression in the pSI. Right panel, a representative image (scale bar, 100 μm) of GCaMP6m (green) and the optical fiber track.

(C) An example raster plot of single attack distribution from 11 mice.

(D) Summarized distribution of attack episodes plotted by percentage of trials showing attack at different time points (n = 458 attacks).

(E) Heatmap of GCaMP6m Δ*F/F* signals from pSI neurons in aggression (n = 458 attack trials).

(F) Representative Δ*F/F* of GCaMP6m (magenta) and EYFP (gray) signals before, during, and after an attack. Note that the elevation of Ca^{2+} signaling (t = –1.2 s) preceded the attack behavior (onset at t = 0 s).

(G) Time windows of pSI^{Thy1} neuronal activation before, during, and after attacks.

(H) Area under the curve (AUC) per second (left) and peak Δ*F/F* (right) of GCaMP6m and EYFP signals before, during, and after an attack. Mann-Whitney test and Wilcoxon matched-pairs signed rank test; ***$P < 0.001$ between the groups indicated. '#' and '&' above each bar indicate that the AUC per second (left) or peak Δ*F/F* (right) during each behavior period was ($P < 0.001$) and wasn't ($P > 0.05$) significantly changed compared with EYFP group, determined by Mann-Whitney test.

(I) Distribution of the incidence of single attacks and continuous attacks with different episode orders.

(J) Representative GCaMP6m signals during a single attack (upper) and continuous attacks with different episode orders (lower). Green bars, episodes of attack.

(K-M) From top to bottom: distribution of attack behavior episodes, heatmaps of GCaMP6m Δ*F/F* signals from pSI^{Thy1} neurons, time windows of pSI^{Thy1} neuronal activation, and Δ*F/F* of the EYFP and GCaMP6m signals from pSI^{Thy1} neurons before, during, and after single attacks (K, n = 165 trials) and the first (L, n = 99 trials) and last (M, n = 99 trials) episodes of continuous attacks.

(N) Peak Δ*F/F* of EYFP and GCaMP6m signals before, during, and after single attacks (left) and the first (middle) and last (right) episodes of continuous attacks. The EYFP and GCaMP6m signals in each type of attack behavior were compared using the Mann-Whitney test, Wilcoxon matched-pairs signed rank test, and two-tailed paired t-test; from left to right, ***$P < 0.001$, ***$P < 0.001$, **$P = 0.0049$, ***$P < 0.001$, ***$P < 0.001$, $P = 0.5349$. The GCaMP6m signals in the three types of attack behavior were compared using the Mann-Whitney test; ***$P < 0.001$. '#' above each bar indicate that peak ΔF/F (right) during each behavior period was significantly (**$P < 0.01$) changed compared with EYFP group, determined by Mann-Whitney test.

(O) Averaged Δ*F/F* of GCaMP6m dynamic signaling of continuous attacks with different episode orders.

(P) Peak $\Delta F/F$ of GCaMP6m signals before, during, and after continuous attacks with different episode orders. Mann-Whitney test, unpaired t-test, and Kruskal-Wallis test; from left to right, ***$P < 0.001$, ***$P < 0.001$, $P = 0.2623$, $P = 0.9688$, $P = 0.9867$, *$P = 0.0189$, **$P = 0.005$. ns, not significant.

Data are presented as the mean ± SEM.

See also **Figure S1**.

Figure 3. Graded Ca^{2+} Responses in pSI^{Thy1} Neurons under Different Aggressive States

(A) Setup for fiber photometric recording in pSI^{Thy1} neurons during aggressive or non-aggressive social behaviors.

(B) Representative GCaMP6m signals during several aggressive or non-aggressive social behaviors when a male mouse intruded into the home cage of the tested mouse.

(C, D) Distribution of episodes of behavior (upper), heatmaps of GCaMP6m $\Delta F/F$ signals from pSI^{Thy1} neurons, time windows of pSI^{Thy1} neuronal activation, and $\Delta F/F$ of the EYFP and GCaMP6m signals (lower) before, during, and after a sniff without attack (C, n = 343 trials) and a sniff preceding an attack (D, n = 236 trials).

(E) Peak $\Delta F/F$ of GCaMP6m and EYFP signals during a sniff with and without a subsequent attack. Mann-Whitney test, ***$P < 0.001$.

(F) Peak $\Delta F/F$ of GCaMP6m signals before, during, and after a sniff with or without a subsequent attack. Mann-Whitney test, ***$P < 0.001$.

(G) Sample decoding accuracy (SVM classifier) of pSI^{Thy1} neuronal activity in the sniff/sniff (attack) trials under shuffled (black) and recording (red) conditions.

(H) Averaged sample decoding accuracy of pSI neuronal activity in sniff/sniff (attack) trials under shuffled and recording conditions. Decoding accuracy in recording differences before, during, and after sniff trials was determined by the Mann-Whitney test. From left to right, ***P <0.001, ***P <0.001. '#' above each bar indicates that decoding accuracy during each behavior period was significantly (P <0.05) increased compared with decoding accuracy in the shuffled period, determined by the Mann-Whitney test.

(I-K) Distribution of episodes of behavior (upper), heatmaps of GCaMP6m $\Delta F/F$ signals from pSI^{Thy1} neurons (middle), and $\Delta F/F$ of GCaMP6m signals (lower) before, during, and after a rattle without an attack (I, n = 26 trials), a rattle preceding an attack (J, n = 26 trials), and threat behavior (K, n = 49 trials).

(L) Peak $\Delta F/F$ of GCaMP6m signals before, during, and after a rattle without a subsequent attack, a rattle preceding an attack, and threat behavior. Wilcoxon matched-pairs signed rank test, Mann-Whitney test, two-tailed unpaired and paired t-tests; from left to right, $P = 0.1814$, *$P = 0.0129$, **$P = 0.0094$, $P = 0.9432$, **$P = 0.002$.

(M) Sample decoding accuracy of the pSI^{Thy1} neuronal activity in rattle/rattle (attack) trials.

(N) Averaged sample decoding accuracy of pSI neuronal activity before, during, and after a rattle under shuffled and recording conditions. Mann-Whitney test, from left to right, ***P <0.001, ***P <0.001.

(O) Peak $\Delta F/F$ (upper), and AUC/s (lower) of GCaMP6m signals during non-aggressive states, aggressive states, and aggressive attacks. '#' and '&' above each bar indicate that peak $\Delta F/F$ (upper) or AUC per second (lower) during each behavior period was ($P < 0.05$) and wasn't ($P > 0.05$)

837 significantly increased compared with baseline pre-behavior, determined by Wilcoxon matched-
838 pairs signed rank test and two-tailed paired t-test. Significance of peak $\Delta F/F$ differences was
839 determined by the Mann-Whitney and Kruskal-Wallis tests: from left to right, $P = 0.0775$, ***$P <$
840 0.001, $P = 0.5532$, *$P = 0.0193$. Significance of AUC/s differences was determined by the Mann-
841 Whitney and Kruskal-Wallis tests; from left to right, $P = 0.3028$, ***$P < 0.001$, $P = 0.4294$, ***P
842 < 0.001.
843 (P) Three-class sample decoding accuracy of the pSI^{Thy1} neuronal activity in three social behavior
844 trials (sniff *vs* sniff (attack) *vs* attack).
845 (Q) Averaged sample decoding accuracy of pSI neuronal activity before, during, and after the three
846 social behaviors under shuffled and recording conditions. Mann-Whitney test, from left to right,
847 ***P <0.001, ***P <0.001.
848 ns, not significant.
849 Data are presented as the mean ± SEM.
850 See also **Figure S1**.

Figure 4. Graded Ca^{2+} Responses in pSI^{Thy1} Neurons under Diverse Aggressive Behaviors

(A) Setup for fiber photometric recording of pSI^{Thy1} neuronal activity during male-female, defensive, predatory, pup-directed, and female-male aggression.

(B) Distribution of attack episodes (upper, n = 60 attacks) and heatmap of GCaMP6m $\Delta F/F$ signals from pSI neurons (lower, n = 60 attack trials) in male-female aggression.

(C) Time window of the pSI^{Thy1} neuronal activation (upper) and $\Delta F/F$ of GCaMP6m signals (lower) before, during, and after a male-female attack.

(D) Peak $\Delta F/F$ of GCaMP6m signals before, during, and after male-male and male-female attacks. Mann-Whitney test and Wilcoxon matched-pairs signed rank test; from left to right, $P = 0.4071$, $***P < 0.001$.

(E) Distribution of attack episodes (upper, n = 680 attacks) and heatmap of GCaMP6m $\Delta F/F$ signals from pSI neurons (lower, n = 680 attack trials) in defensive aggression.

(F) Time window of pSI^{Thy1} neuronal activation (upper) and $\Delta F/F$ of GCaMP6m signals (lower) before, during, and after a defensive attack.

(G) Peak $\Delta F/F$ of GCaMP6m signals before, during, and after male-male offensive and defensive attacks. Mann-Whitney and Wilcoxon matched-pairs signed rank tests; $***P < 0.001$.

(H-J) From top to bottom: distribution of episodes of behavior, heatmaps of GCaMP6m $\Delta F/F$ signals from pSI neurons, time window of pSI^{Thy1} neuronal activation, and $\Delta F/F$ of GCaMP6m signals before, during, and after an approach without attack (H), approach preceding attack (I), and attack (J) in predatory aggression.

(K) Left, three-class sample decoding accuracy of pSI neuronal Ca^{2+} signals in the cricket-directed approach, approach (attack), and attack trials under shuffled and recording conditions. Right, averaged sample decoding accuracy of pSI neuronal activity under recording conditions; '#' above each bar indicates that the decoding accuracy during each period was significantly increased ($P < 0.05$) compared with the decoding accuracy in the shuffled period, determined by Mann-Whitney test.

(L) Peak $\Delta F/F$ of GCaMP6m signals before, during, and after a male-male attack and a predatory attack. Mann-Whitney test, $***P < 0.001$.

(M-O) From top to bottom: distribution of episodes of behavior, heatmaps of GCaMP6m $\Delta F/F$ signals from pSI neurons, time windows of pSI^{Thy1} neuronal activation, and $\Delta F/F$ of GCaMP6m signals before, during, and after approach without attack (M), approach preceding attack (N), and attack (O) in pup-directed aggression.

(P) Left, sample decoding accuracy of the pSI neuronal Ca^{2+} signals in pup-directed approach, approach (attack), and attack trials under shuffled and recording conditions. Right, averaged sample decoding accuracy of pSI neuronal activity under recording conditions.

(Q) Peak $\Delta F/F$ of GCaMP6m signals before, during, and after male-male attacks and pup-directed

attacks. Mann-Whitney test; from left to right, $^{**}P = 0.0031$, $^{***}P < 0.001$.

(R-T) From top to bottom: distribution of episodes of behavior, heatmaps of GCaMP6m $\Delta F/F$ signals from pSI neurons, time windows of pSI^{Thy1} neuronal activation, and $\Delta F/F$ of GCaMP6m signals before, during, and after a sniff without attack (R), sniff preceding attack (S), and attack (T) in female-male aggression.

(U) Left, sample decoding accuracy of the pSI neuronal Ca^{2+} signals in the female sniff, female sniff (attack), and attack trials under shuffled and recording conditions. Right, averaged sample decoding accuracy of pSI neuronal activity under recording conditions.

(V) Peak $\Delta F/F$ of GCaMP6m signals before, during, and after male-male and female-male attacks. Mann-Whitney test; from left to right, $^{***}P < 0.001$, $^{***}P < 0.001$.

(W) Peak $\Delta F/F$ (upper), and AUC/s (lower) of GCaMP6m signals during diverse aggressive behaviors. '#' and '&' above each bar indicate that peak $\Delta F/F$ (upper) or AUC per second (lower) during each behavior period was ($P < 0.05$) and wasn't ($P > 0.05$) significantly increased compared with baseline pre-behavior, determined by Wilcoxon matched-pairs signed rank test and two-tailed paired t-test. Significance of peak $\Delta F/F$ differences was determined by the Kruskal-Wallis and Mann-Whitney tests; from left to right, $^{***}P < 0.001$, $^{***}P < 0.001$, $P = 0.1017$, $^{***}P < 0.001$, $^{***}P < 0.001$, $P = 0.4071$, $^{***}P < 0.001$. Significance of differences in AUC/s was determined by the Mann-Whitney and Kruskal-Wallis tests; from left to right, $^{*}P = 0.0213$, $^{***}P < 0.001$, $^{***}P < 0.001$, $^{***}P < 0.001$, $^{***}P < 0.001$, $P = 0.8884$, $^{***}P < 0.001$.

ns, not significant.

Data are presented as the mean ± SEM.

See also **Figures S1, S2**.

Figure 5. Activation of pSI^{Thy1} or pSI^{-PAG} Neurons Promotes Inter-male Aggression and Autonomic Arousal

(A) Experimental design and schematic of the viral injection strategy.

(B) Overlay of DIO-hM3Dq-mCherry expression in pSI.

(C) Percentage of animals showing aggressive or mating behaviors (left most panel), total latency to attack, attack duration, and attack events tested before (pre-) and after injection with saline or CNO in the control and hM3Dq groups (n = 6/7 mice). Pre-CNO *vs* CNO in hM3D group; from left to right, $*P = 0.0156$, $*P = 0.0156$, $*P = 0.0156$; saline *vs* CNO in hM3D group: from left to right, $*P = 0.0156$, $*P = 0.0156$, $*P = 0.0156$; Wilcoxon matched-pairs signed rank test.

(D) Representative images of retrograde AAV-retro-EGFP infection (green) in the PAG (left) and pSI (right) (scale bars, 100 μm). Aq, aqueduct; DRL, dorsal raphe nucleus, lateral part.

(E) Proportion of retrogradely-labelled SI^{-PAG} neurons distributed in the SI.

(F) Strategy for photoactivation of pSI^{-PAG} neurons in male mice.

(G) Behavioral paradigm of aggression test.

(H) Distribution of attack episodes during photostimulation (n = 13/6 mice in the ChR2 and control groups).

(I) Percentage of trials, latency, duration, and events of light-induced attacks in the ChR2 and control groups (n = 13/6 mice) during the pre-laser, laser, and post-laser phases. Pre *vs* Laser *vs* Post in ChR2 Group, $***P < 0.001$, Friedman test; Laser in EYFP and ChR2 group; from left to right, $***P < 0.001$, $***P < 0.001$, $***P < 0.001$, $***P < 0.001$, Mann-Whitney test.

(J) Schematic of physiological state assessment by video-recording and computer-assist detection of pupil diameter and heart rate in head-fixed mice with photostimulation of pSI^{-PAG} neurons.

(K) Schematic for eye and pupil size measurements.

(L) Representative images of computer-detected pupil (red circle) and eye (green outline) before, during, and after photostimulation.

(M, N) Left panels, peristimulus time histograms of normalized pupil size (M) and computer-detected eye outline (N) aligned with light onset in the laser and sham stimulation groups (n = 9/8 mice). Right panels, normalized pupil size (M, $***P < 0.001$, Friedman test) and computer-detected eye outline (N, $*P = 0.0357$, repeated one-way ANOVA) before, during, and after photostimulation (n = 9 mice).

(O-Q) Normalized breathing rate (O, $*P = 0.0136$), normalized heart rate (P, $*P = 0.0447$), and duration of body trembling (Q, $**P = 0.0019$) before, during, and after photostimulation (n = 9/8/9 mice, repeated one-way ANOVA).

(R) Cartoon of correlation of the increased arousal state and aggressiveness before and during the activation of pSI^{-PAG} neurons.

ns, not significant.

946 Data are presented as the mean ± SEM.

947 See also **Figures S3**, **S4**, and **Movies S1**, **S2**.

948

Figure 6. Activation of pSI^{-PAG} Neurons Promotes Diverse Aggressive Behaviors

(A) Schematic of the behavioral design to test aggression induced by photostimulation of pSI^{-PAG} neurons under various conditions.

(B) Left, schematic of female aggression with photostimulation of pSI^{-PAG} neurons when a socially-housed female encountered a singly-housed male in its home cage. Right, distribution of attack episodes during photostimulation.

(C) Summary of female aggression induced by photostimulation of pSI^{-PAG} neurons: percentage of trials showing attacks, latency to attack onset, attack duration, and attack events in pre-laser, laser, and post-laser phases. ***$P < 0.001$; n = 10 mice, Friedman test.

(D) Schematic of the behavioral paradigm in which a singly-housed male mouse in its home cage encountered a pup.

(E) Summary of pup-directed attack induced by photostimulation of pSI^{-PAG} neurons (left, ***$P < 0.001$; right, ***$P < 0.001$; n = 14 mice, Friedman test).

(F) Left, schematic of the behavioral paradigm in which a singly-housed male mouse encountered a moving glove in its home cage. Right, distribution of attacks.

(G) Summary of the object-directed attack induced by photostimulation of pSI^{-PAG} neurons (from left to right, **$P = 0.0041$, **$P = 0.0021$, **$P = 0.0041$, **$P = 0.0041$, n = 6 mice, Friedman test).

(H) Left, schematic of the defensive aggression test when a socially-housed male encountered a CD-1 mouse in the latter's cage during photostimulation. Right, distribution of attacks.

(I) Summary of the defensive aggression induced by photostimulation of pSI^{-PAG} neurons (from left to right, *$P = 0.0123$, ***$P = 0.0009$, *$P = 0.0180$, *$P = 0.0140$, n = 5 mice, Friedman test).

(J) Probability of light-induced aggression in various aggression paradigms (n = 13, 7, 7, 6, 5, 5, 11, 10, 5, 14, 6, 5, and 12 mice). Values for columns 1-13 during laser stimulation: 93.9 ± 3.5 *vs* 85.7 ± 5.1 *vs* 70.8 ± 7.6 *vs* 86.1 ± 5.9 *vs* 84.0 ± 16.0 *vs* 80.0 ± 6.3 *vs* 98.2 ± 1.8 *vs* 79.0 ± 9.7 *vs* 88.0 ± 12.0 *vs* 70.7 ± 8.2 *vs* 73.3 ± 14.3 *vs* 89.1 ± 4.6 *vs* 92.8 ± 2.4 (%). ♂ *vs* ♂, socially-housed male mouse in its home cage encounters a male mouse; ♂ *vs* ♂ (novel), socially-housed male in a novel cage encounters a male; ♂ *vs* ♂ (resident), socially-housed male in a residents' cage encounters a male; single ♂ *vs* ♂, singly-housed male in its home cage encounters a male; ♀ *vs* ♂, socially-housed male in its home cage encounters a male. ns, no significant difference among various groups for light-induced aggression ($P = 0.1170$, repeated one-way ANOVA).

ns, not significant.

Data are presented as the mean ± SEM.

See also **Figures S5**, **S6**, and **Movies S3**, **S4**.

982 **Figure 7. Intensity-Response Relationships of Photostimulation of pSI^{-PAG} Neurons and**
983 **Success Rate of Evoked Attacks for Different Aggressive Behaviors**
984 (A) Schematic for testing the relationship between the activation levels of pSI^{-PAG} neurons and the
985 success rates of the evoked attacks for different types of aggression.
986 (B) Behavioral paradigm of the inter-male aggression test during photoactivation of pSI^{-PAG}
987 neurons at different stimulation intensities.
988 (C) Distribution of attack episodes during photoactivation of pSI^{-PAG} neurons at 13 graded
989 stimulation intensities (each intensity of laser power is illustrated as a different colored line).
990 (D) Correlation (sigmoidal curve with nonlinear regression) of the probabilities of evoked inter-
991 male aggression with different intensities of photostimulation, before (–15-0 s, gray point)s and
992 during (0-15 s, blue points) laser stimulation. Lines are non-linear fits (pooled across all mice and
993 binned light intensities).
994 (E) Behavioral paradigm of diverse aggressive behaviors during photoactivation of pSI^{-PAG}
995 neurons at different stimulation intensities tested in male and female mice.
996 (F, G) Nonlinear regression of the probabilities of trials showing attack (F) and latency to attack
997 onset (G) for the five types of induced aggression with different intensity of photostimulation
998 before and during laser stimulation. Different colored lines are non-linear fits before or during
999 different aggressive behaviors (pooled across all mice and binned light intensities).
1000 (H) Probabilities of trials showing attack (left) and latency to attack onset (right) of the five types
1001 of induced aggression during laser stimulation with a lower intensity (0.1 mW). Comparisons of
1002 the probabilities of attack and latency to attack onset in diverse aggressive behaviors were assessed
1003 by the Kruskal-Wallis test. ***P <0.001.
1004 (I) Threshold model for the relationship between the activation level of pSI^{-PAG} neurons and evoked
1005 attacks for diverse aggressive behaviors.
1006 Data are presented as the mean ± SEM.
1007

1008 **Figure 8. Inactivation of pSI^{Thy1} Neurons Interrupts Diverse Aggressive Behaviors but not**
1009 **Mating**
1010 (A) Upper panel, experimental design and viral injection strategy for the expression of hM4Di-
1011 mCherry in pSI^{Thy1} neurons in male Thy1-Cre mice. Lower panel, behavioral paradigm.
1012 (B) Schematic of virus injection (upper panel) and representative histological image (lower panel)
1013 showing the expression of hM4Di-mCherry (red) in pSI^{Thy1} neurons in a Thy1-Cre mouse (scale
1014 bar, 100 μm).
1015 (C) Latency to attack (left), attack duration (middle), and attack events (right) before and after
1016 injection of saline or CNO in the control and hM4Di groups (n = 6/6 mice). Pre-CNO *vs* CNO in
1017 the hM4D group; from left to right, ***$P < 0.001$, *$P = 0.0174$, *$P = 0.0154$; saline *vs* CNO in the
1018 hM4D group; from left to right, ***$P < 0.001$, *$P = 0.0313$, *$P = 0.011$, Wilcoxon matched-pairs
1019 signed rank test and two-tailed paired t-test.
1020 (D) Mating behavioral paradigm.
1021 (E) Latency to mounting onset, mounting duration, and mounting events before and after injection
1022 of saline or CNO in the hM4Di groups (n = 6 mice). Pre-CNO *vs* CNO in the hM4D group; from
1023 left to right, $P = 0.5014$, $P = 0.4764$, $P = 0.603$, two-tailed paired t-test.
1024 (F) Upper, schematic of bilateral injection of DIO-GtACR1-GFP virus into the pSI in male Thy1-
1025 Cre mice. Lower, co-localization ratio of GFP expression with CaMKIIα in the pSI.
1026 (G-I) Left, behavioral paradigms to assess the effects of optogenetic inhibition of pSI^{Thy1} neurons
1027 on offensive inter-male aggression (G, n = 8 mice), pup-directed aggression (H, n = 6 mice), and
1028 predatory aggression (I, n = 4 mice). Right, example raster plots showing the time-locked
1029 interruption of the three types of aggressive behaviors by optogenetic inhibition of pSI^{Thy1} neurons.
1030 (J-L) Distribution of attack episodes interrupted by optogenetic inhibition of pSI^{Thy1} neurons in
1031 inter-male aggression (J), pup-directed aggression (K), and predatory aggression (L).
1032 (M) Attack duration in the pre-laser, laser, and post-laser phases by optogenetic inhibition of
1033 aggressive behaviors; from left to right, *$P = 0.0179$, *$P = 0.0120$, **$P = 0.0046$, Friedman test.
1034 (N) Percentage of attack trials interrupted within 3 s during the laser phase by optogenetic
1035 inhibition in aggressive behaviors (n = 8/6/4 mice). 98.4±1.6 *vs* 94.9±5.1 *vs* 92.9±7.1 (from left to
1036 right), $P = 0.8824$, Kruskal-Wallis test.
1037 ns, not significant.
1038 Data are presented as the mean ± SEM.
1039 See also **Figure S7**, and **Movie S5**.
1040

1041 **Supplemental Figure Legends**

1042 **Figure. S1. Correlation of Different Aggressive Behaviors with the Differential Calcium**
1043 **Activity Levels in pSI^{Thy1} Neurons, Related to Figures 2-4**

1044 (A) Distribution of attack episodes (n = 458 attacks, upper) and representative Δ*F/F* of GCaMP6m
1045 signals before and during attacks (n = 458 attacks, lower). Note that elevation of the Ca^{2+} signal (t
1046 = –1.2 s) preceded the attack behavior (onset at t = 0 s).

1047 (B) Linear regression of the AUC per second of GCaMP6m signals prior to the attack behavior
1048 and probability of attack (n = 458 attacks).

1049 (C) Distribution of last attack episodes (n = 99 attacks, upper) and representative Δ*F/F* of
1050 GCaMP6m signals before, during, and after the last episode of continuous attacks (n = 99 attacks,
1051 lower).

1052 (D) Linear regression of the AUC per second of GCaMP6m signals prior to the last attack episode
1053 and probability of attack (n = 99 attacks).

1054 (E) Peak Δ*F/F* of GCaMP6m in all attack behavior, single attack behavior, and the first and last
1055 episodes of attack behavior. $P = 0.1270$, Kruskal-Wallis test.

1056 (F) Sample decoding accuracy of the pSI neuronal Ca^{2+} signals in single and the first episode of
1057 continuous attack trials.

1058 (G) Averaged decoding accuracy of pSI neuronal activity before, during, and after attack trials
1059 under recording and shuffled conditions. '#' above each bar indicates that the decoding accuracy
1060 during each behavior period was significantly increased ($P < 0.05$) compared with that in the
1061 shuffled period, assessed by the Mann-Whitney test. Decoding accuracy in recording differences
1062 before, during, and after attack trials was assessed by the Mann-Whitney test. From left to right,
1063 ***$P < 0.001$, ***$P < 0.001$.

1064 (H) Sample decoding accuracy of pSI neuronal Ca^{2+} signals in single and the last episode of
1065 continuous attack trials.

1066 (I) Averaged decoding accuracy of pSI neuronal activity before, during, and after attack trials under
1067 recording and shuffled conditions. Decoding accuracy in recording differences before, during and
1068 after attack trials was assessed by the Mann-Whitney test. From left to right, ***$P < 0.001$, ***P
1069 < 0.001.

1070 (J) Averaged ΔF/F of Ca^{2+} signals in pSI neurons before, during, and after male-male, female-male,
1071 predatory, and pup-directed attacks.

1072 (K) Peak ΔF/F of Ca^{2+} signals during diverse attacks. Comparison of diverse attacks was
1073 determined by Monte Carlo simulation with a subset of the male-male data 2000 times. *P*-value of
1074 comparison of subset of Ca^{2+} data associated with the diverse attacks was determined by the
1075 Wilcoxon rank sum test. 'ns (96.95%)' indicates that these two samples were not significantly
1076 different ($P > 0.05$). Monte Carlo simulation showed that 96.95% of the 2000 comparisons were

from populations with identical distributions. '*** (0.20%)' indicates that these two samples was significantly different (P <0.001), and Monte Carlo simulation showed that 0% of 2000 comparisons were from populations with identical distributions.

(L-Q) Sample decoding accuracy of the pSI neuronal Ca^{2+} signals and averaged sample decoding accuracy of pSI neuronal activity under recording and shuffled conditions compared between the cricket-directed approach and predatory attack trials (L, M), the pup-directed approach and pup-directed attack trials (N, O), and the female-male sniff and female-male attack trials (P, Q). '#' above each bar indicates that decoding accuracy during each behavior period was significantly higher (P <0.05) than that in the shuffles period, determined by the Mann-Whitney test. Decoding accuracy in recording differences before, during, and after attack trials was determined by the Mann-Whitney test. From left to right, ***P <0.001, ***P <0.001.

(R-W) Sample decoding accuracy of the pSI neuronal Ca^{2+} signals and averaged sample decoding accuracy of pSI neuronal activity under recording and shuffled conditions compared between the cricket-directed approach and approach (attack) trials (R, S), the pup-directed approach and approach (attack) trials (T, U), and the female-male sniff and sniff (attack) trials (V, W). From left to right, ***P <0.001, ***P <0.001.

(X) Sample decoding accuracy of the pSI neuronal Ca^{2+} signals and averaged sample decoding accuracy of pSI neuronal activity under recording and shuffled conditions in cricket-directed, pup-directed, female-male, and inter-male approaches or sniffs (left), approaches or sniffs preceding an attack (middle), and attack trials (right).

(Y) Averaged sample decoding accuracy in four types of approaches/sniffs, approaches/sniffs preceding attacks, and attacks under recording conditions as shown in (AB). '#' or '&' above each bar indicates that the decoding accuracy during each behavior period was (P <0.05) or was not (P >0.05) significantly higher than that before each behavior period, determined by the Mann-Whitney test. Decoding accuracy in recording differences in the three behaviors was determined by the Mann-Whitney test. From left to right, ***P <0.001, ***P <0.001.

(Z) Sample decoding accuracy of the pSI neuronal Ca^{2+} signals under recording and shuffled conditions in predatory, pup-directed, female-male, inter-male, male-female, and inter-male defensive attack trials).

(AA) Averaged sample decoding accuracy under recording and shuffled conditions. '#' above each bar indicates that the decoding accuracy during each behavior period was significantly (P <0.05) higher than that before each behavior period, determined by the Mann-Whitney test. Decoding accuracy in recording differences was determined by the Mann-Whitney test. From left to right, ***P <0.001, ***P <0.001.

ns, not significant.

Data are presented as the mean ± SEM.

Figure. S2. pSI^{Thy1} Neurons Are Differently Modulated by Non-social and Social Contextual Cues, Related to Figure 4

(A) Setup for aggressive behaviors recording in response to diverse non-social and social stimuli.

(B) Distribution of episodes of attack behavior during water consumption (n = 52 trials), food consumption (n = 260 trials), approach a cotton ball (n = 23 trials), during detection of DMSO (n = 30 trials), approach a urine cotton ball (n = 36 trials), object entry (n = 39 trials), female C57 entry (n = 39 trials), and approach a TMT cotton ball (n = 57 trials).

(C) Distribution of episodes of attack behavior in response to air puff (n = 322 trials), the threat of a flying glove (n = 567 trials), tail suspension (n = 142 trials), male CD-1 entry (n = 119 trials), and male C57 entry (n = 108 trials).

(D) Possibilities of behavior trials showing attack during diverse stimuli as shown in (B) and (C).

(E) Setup for fiber photometric recording in pSI^{Thy1} neurons in response to diverse non-social and social stimuli.

(F) Distribution of episodes of behavior and heatmaps of GCaMP6m $\Delta F/F$ signals from pSI neurons during water consumption (upper, n = 52 trials), food consumption (middle, n = 260 trials), and approach a cotton ball (lower, n = 23 trials).

(G) Distribution of episodes of behavior and heatmaps of GCaMP6m $\Delta F/F$ signals from pSI neurons during detection of DMSO (upper, n = 30 trials), urine (middle, n = 36 trials), and TMT (lower, n = 57 trials) by approach.

(H) Distribution of episodes of behavior and heatmaps of GCaMP6m $\Delta F/F$ signals from pSI neurons in response to air puff (upper, n = 40 trials), the threat of a flying glove (middle, n = 40 trials), and tail suspension (lower, n = 40 trials).

(I) AUC/s (left) and Peak $\Delta F/F$ (right) of GCaMP6m signals during diverse stimuli. '#' and '&' above each bar indicate that AUC per second (left) or peak $\Delta F/F$ (right) during each behavior period was ($P < 0.05$) and wasn't ($P > 0.05$) significantly increased compared with baseline pre-behavior, determined by Wilcoxon matched-pairs signed rank test and two-tailed paired t-test.

(J-N) Distribution of episodes of behavior, heatmaps of GCaMP6m $\Delta F/F$ signals, and $\Delta F/F$ of GCaMP6m (magenta) signals from pSI neurons with object entry (J, n = 53 trials in female entry (K, n = 39 trials), male C57 entry (L, n = 39 trials), male CD-1 entry (M, n = 58 trials), and male C57 entry preceding an attack (N, n = 28 trials).

(O) Peak $\Delta F/F$ (upper), and AUC/s (lower) of GCaMP6m signals during different entries. '#' above each bar indicate that peak $\Delta F/F$ (upper) or AUC per second (lower) during each behavior period was significantly ($P < 0.001$) increased compared with baseline pre-behavior, determined by Wilcoxon matched-pairs signed rank test and two-tailed paired t-test. The significance of differences in peak $\Delta F/F$ was determined by the Mann-Whitney and Kruskal-Wallis tests, unpaired t-test, and paired t-test; from left to right, $^{**}P = 0.005$, $^{***}P < 0.001$, $^{**}P = 0.004$, $^{*}P = 0.0131$.

Significance of differences in the AUC/s was determined by the Mann-Whitney and Kruskal-Wallis tests, unpaired t-test, and paired t-test; from left to right, $^{**}P = 0.007$, $^{**}P = 0.0083$, $^{***}P < 0.001$, $^{*}P = 0.0239$.

ns, not significant.

Data are presented as the mean ± SEM.

1155 **Figure S3. Anterograde Virus Tracing of the pSI-PAG Connection, and Pharmacogenetic**
1156 **Activation of pSI^{Thy1} or pSI^{-PAG} Neurons Promoted Inter-male Aggression, Related to Figure**
1157 **5**
1158 (A) Schematic for injection of anterograde trans-synaptic virus into the pSI to trace pSI-PAG
1159 connections in Ai14 male mice.
1160 (B) Representative images of pSI (left) and VL/LPAG (right) neurons infected with anterograde
1161 trans-synaptic AAV1-CMV-Cre Tdtomato (scale bars, 50 μm).
1162 (C) Schematic of the strategy for anterograde virus tracing.
1163 (D) Representative images showing the expression of trans-synaptic anterograde AAV1-CMV-Cre
1164 and AAV-DIO-mCherry (red) in the pSI (left, scale bar, 50 μm) and the VL/LPAG (right, scale bar,
1165 100 μm). Aq, aqueduct; DRL, dorsal raphe nucleus, lateral part.
1166 (E) Schematic showing injection of retrograde tracing virus into the PAG and
1167 immunostaining/imaging of pSI^{-PAG} neurons.
1168 (F) Example images showing overlap of retrogradely-labeled pSI^{-PAG} neurons (green) with staining
1169 for DAPI (blue) and CaMKIIα (left, red) or GAD67 (right, red). Scale bars, 50 μm.
1170 (G) Left panels, example images showing overlap of retrogradely-labeled pSI^{-PAG} neurons (green)
1171 with staining for Thy1 (red). Scale bars, 100 μm. Right panels, magnified images of the boxed
1172 areas in the left panels; Scale bars, 10 μm. Arrowheads indicate retrogradely-labeled neurons co-
1173 localized with mCherry.
1174 (H) Percentage overlap of EGFP-expressing neurons with Thy1, CaMKIIα or GAD67 (KW =
1175 11.65, ***$P < 0.001$; Kruskal-Wallis test, n = 5/5/6 mice).
1176 (I) Schematic of the strategy for retrograde tracing from the PAG and Cre-dependent
1177 pharmacogenetic activation of pSI^{-PAG} neurons.
1178 (J) Left, overlay of EGFP and mCherry expression from mice unilaterally injected with retrograde
1179 AAV-Retro-Cre-EGFP virus into the PAG and anterograde AAV-DIO-mCherry virus into the pSI.
1180 Right, overlay of EGFP and hM3D-mCherry expression from mice unilaterally injected with
1181 retrograde AAV-Retro-Cre-EGFP virus into the PAG and anterograde AAV-DIO-hM3D-mCherry
1182 virus into the pSI.
1183 (K) Representative image of the PAG showing neurons infected with retrograde AAV-Retro-Cre-
1184 EGFP (green) and mCherry terminals (red) projected from the pSI (scale bar, 100 μm).
1185 (L) Upper, schematic of whole-cell electrophysiological recordings from hM3D-expressing pSI
1186 neurons in slice preparations. Lower, sample recording trace from an hM3D-expressing pSI neuron
1187 in response to perfusion with CNO.
1188 (M) Timing for the examination of c-Fos expression in the pSI after intraperitoneal injection of
1189 CNO.
1190 (N) Middle, schematic showing unilateral injection of hM3Dq-mCherry virus into the pSI. Left,

representative histological image showing c-Fos expression (yellow) on the uninjected side. Right, representative histological image of c-Fos expression on the side of the pSI injected with hM3Dq-mCherry virus (red). Scale bars, 100 μm.

(O) High-magnification images of the boxed area in (N) (scale bar, 10 μm; arrowheads indicate pSI neurons immunopositive for c-Fos antibody).

(P) Behavioral paradigm of aggression test.

(Q) Raster plots of attack behavior recorded during 15-min encounters.

(R) Summary of aggression during the pre- and post-injection phases in the control and hM3Dq groups (n = 7/10 mice) with saline or CNO injection. Red blocks indicate duration of attack episodes. Pre-CNO *vs* CNO in the hM3D group; from left to right, $^{**}P = 0.002$, $^{**}P = 0.002$, $^{**}P = 0.002$; saline *vs* CNO in the hM3D group; from left to right, $^{**}P = 0.002$, $^{**}P = 0.002$, $^{**}P = 0.002$, Wilcoxon matched-pairs signed rank test.

(S) Raster plots of attack behavior recorded during 15-min encounters.

ns, not significant.

Data are presented as the mean ± SEM.

Figure S4. Photoactivation of pSI^{-PAG} Neurons or pSI$^{CaMKII\alpha}$ Neurons Time-locked to Evoked Inter-male Aggression and Autonomic Arousal, but not Anxiety, Related to Figure 5

(A) Strategy for virus injection and photoactivation of pSI^{-PAG} neurons in male mice.

(B) Schematics and representative images of AAV-Retro-Cre-EGFP expression in the PAG (left, scale bar, 100 μm) and AAV-DIO-ChR2-EYFP expression in upstream pSI neurons (right, scale bars, 50 μm).

(C) Left, overlay of EGFP expression from mice unilaterally injected with retrograde AAV-Retro-Cre-EGFP virus into the PAG and anterograde AAV-DIO- EGFP virus into the pSI. Right, overlay of EGFP and ChR2-EGFP expression from mice unilaterally injected with retrograde AAV-Retro-Cre-EGFP virus into the PAG and anterograde AAV-DIO-ChR2-EGFP virus into the pSI.

(D) Left, schematic of whole-cell recordings from ChR2-expressing pSI^{-PAG} neurons in slice preparations. Middle, light-induced inward current recorded in a ChR2+ pSI neuron (blue bar, application of a LED-generated blue light pulse). Right, action potentials recorded from a ChR2-expressing pSI neuron induced by 5, 10, 20, and 40 Hz light stimulation.

(E) Behavioral paradigm of inter-male aggression test.

(F) Success rates of light-induced attacks in response to different frequencies of light stimulation at a fixed intensity (2.7 mW). 5 Hz *vs* 10 Hz *vs* 20 Hz *vs* 40 Hz in the ChR2 group; 0.0 ± 0.0 *vs* 6.7 ± 3.3 *vs* 34.4 ± 11.7 *vs* 90.0 ± 6.7 (%), ***$P < 0.001$, n = 9 trials, Friedman test.

(G) An example of behavioral output during photostimulation in the ChR2 and control groups.

(H) Left, peristimulus time histogram of relative pupil size (pupil size/eye size) aligned with light onset in the laser or sham stimulation group (n = 9/8 mice). Right, relative pupil size before, during, and after photostimulation (***$P < 0.001$, n = 9 mice, Friedman test).

(I) Average percentage of time in the open arms of the elevated plus maze before, during, and after photostimulation of pSI^{-PAG} neurons (Friedman test, FM = 0.7429, $P = 0.7407$, n = 9 mice). (J) Average percentage of time in the center of the open field before, during, and after photostimulation of pSI^{-PAG} neurons (one-way ANOVA, F (1.608, 12.87) = 0.2183, $P = 0.7599$, n = 9 mice).

(K) Behavioral paradigm of open field test with photoactivation of pSI^{-PAG} neurons in socially-housed male C57 mice (n = 6 mice), with a shield cover (nest) inside the open field box.

(L-N) Latency to the nest (L, $P = 0.0721$, Friedman test), averaged velocity in each photostimulation period (M, from -15 s to 30 s), and velocity in the pre (1), during (2), and post-laser (3) period (N, $P = 0.3379$, one-way ANOVA).

(O) Averaged velocity during period 1, 2, and 3 ($P = 0.0875$, one-way ANOVA).

(P) Schematic of the timing and behavioral paradigm with optical activation of pSI$^{CaMKII\alpha}$ neurons in male mice.

(Q) Left, schematic of pSI injection of virus carrying AAV-CaMKIIα-ChR2-mCherry or AAV-

CaMKIIα-mCherry and light stimulation of pSI$^{CaMKII\alpha}$ neurons. Right, representative histological images of light-induced c-Fos expression (green) in neurons expressing AAV-CaMKIIα-ChR2-mCherry (magenta). Arrowheads indicate neurons co-expressing AAV-CaMKIIα-ChR2-mCherry and c-Fos.

(R) Overlay of CaMKIIα-ChR2-mCherry expression in pSI (-1.06 mm from bregma).

(S) Behavioral paradigm of a socially-housed male mouse in its home cage attacking a singly-housed male intruder.

(T) Percentage of trials with attacks, total latency to attack, attack duration, and number of attack events in response to pSI photostimulation in the ChR2 group and controls (mCherry group) (Wilcoxon matched-pairs signed rank test and two-tailed unpaired t-test; from left to right, ***$P < 0.001$, ***$P < 0.001$, *$P = 0.0313$, ***$P < 0.001$, n = 15/6 mice) during the pre-laser, laser, and post-laser phases when a socially-housed male mouse initiated an attack in its home cage on a singly-housed male intruder (Friedman test, from left to right, ***$P < 0.001$, ***$P < 0.001$,***$P < 0.001$, ***$P < 0.001$, n = 15 mice).

ns, not significant.

Data are presented as the mean ± SEM.

Figure S5. Optical Activation of pSI$^{CaMKII\alpha}$ Neurons or Pharmacogenetic Activation of pSI^{Thy1} Neurons Evoked Aggressive Behaviors under Various Conditions, Related to Figure 6

(A) Upper left, schematic of pSI injection of virus carrying AAV-CaMKIIα-ChR2-mCherry and optical activation of pSI$^{CaMKII\alpha}$ neurons. Upper right, schematic of the timing and behavioral paradigm with optical activation of pSI$^{CaMKII\alpha}$ neurons in male or female mice. Lower, overlay of CaMKIIα-ChR2-mCherry expression in the pSI (–1.06 mm from bregma) of female mice.

(B) Behavioral paradigm of a socially-housed mouse in its home cage attacking a singly-housed intruder induced by optical activation of pSI$^{CaMKII\alpha}$ neurons.

(C-E) Percentage of trials with attacks, latency to attack onset, attack duration, and attack events with photostimulation of pSI$^{CaMKII\alpha}$ neurons in the pre-laser, laser, and post-laser phases. A socially-housed male mouse in its home cage initiated an attack on a socially-housed female intruder (C, from left to right, ***$P < 0.001$, ***$P < 0.001$, **$P = 0.0092$, **$P = 0.0022$, n = 6 mice), and a socially-housed female in its home cage initiated an attack on a socially-housed male (D, from left to right, ***$P < 0.001$, ***$P < 0.001$, **$P = 0.0046$, **$P = 0.0047$, n = 6 mice) or female intruder (E, from left to right, *$P = 0.0168$, ***$P < 0.001$, **$P = 0.005$, **$P = 0.0063$, n = 5 mice). Significance was determined by one-way ANOVA.

(F) Upper, schematic of the timing and behavioral paradigm with pharmacogenetic activation of pSI^{Thy1} neurons through Cre-dependent expression of AAV-DIO-hM3d-mCherry in Thy1-Cre male and female mice. Lower, overlay of hM3d-mCherry expression in pSI (-1.06 mm from bregma) of the female Thy1-Cre mice.

(G) Behavioral paradigm in which the pharmacogenetic activation of pSI^{Thy1} neurons in a socially-housed Thy1-Cre male mouse in a novel cage promoted attacks on a socially-housed female.

(H-J) Latency to attack, attack duration, and attack events during the pre- and post-injection phases of the pharmacogenetic activation of pSI^{Thy1} neurons. A socially-housed male mouse encountered a socially-housed female (H, from left to right, *$P = 0.0313$, ***$P < 0.001$, **$P = 0.001$, n = 6 mice) and a socially-housed female encountered a socially-housed male (I, from left to right, ***$P < 0.001$, *$P = 0.0176$, *$P = 0.0264$, n = 5 mice) or female (J, from left to right, $P = 0.0625$, *$P = 0.0378$, $P = 0.0625$, n = 5 mice) in a novel cage. Significance was determined by the Wilcoxon matched-pairs signed rank test and two-tailed paired t-test.

ns, not significant.

Data are presented as the mean ± SEM.

Figure S6. The Projection from pSI$^{CaMKII\alpha}$ Neurons to the PAG, but not to the BNST or VMH, Universally Drove Diverse Aggressive Behaviors, Related to Figure 6

(A) Strategy for virus injection and optical activation of the terminals of pSI^{-PAG} neurons in the PAG and BNST in male mice.

1296 (B) Schematics and representative images of AAV-Retro-Cre-EGFP expression in the VL/LPAG
1297 (left; scale bar, 100 μm) and AAV-DIO-ChR2-EYFP expression (green) upstream from pSI
1298 neurons (right; scale bar, 100 μm).
1299 (C) Behavioral paradigm of the attack test of a socially-housed male in its home cage towards a
1300 singly-housed male intruder.
1301 (D) Upper, schematic of c-Fos examination of PAG neural activation induced by light stimulation
1302 of pSI^{-PAG} terminals in male mice. Lower, representative histological images of the PAG stained
1303 with c-Fos (red) after photostimulation of pSI^{-PAG} terminals expressing ChR2-EGFP (green) on the
1304 stimulated and unstimulated sides (scale bars, 50 μm).
1305 (E) Left, percentage of animals showing attacks by photostimulation of the pSI-BNST, pSI-VMH
1306 and pSI-PAG projection in male mice. Right, distribution of attack episodes during
1307 photostimulation of the pSI-PAG projection (magenta, ChR2 group; gray, EYFP group; n = 5 mice).
1308 (F) Percentage of trials, latency to attack, attack duration, and attack events in the photostimulation
1309 (ChR2) and control (EYFP) groups during the pre-laser, laser, and post-laser phases. Pre *vs* Laser
1310 *vs* Post in the ChR2 group, $P = 0.123$, ***$P < 0.001$, *$P = 0.0271$, $P = 0.123$, one-way ANOVA or
1311 Friedman test, n = 5 mice; Laser in EYFP and the ChR2 group, **$P = 0.0022$, ***$P < 0.001$, **P
1312 $= 0.0044$, **$P = 0.0022$, two-tailed unpaired t-test and Mann-Whitney test, n = 5/6 mice.
1313 (G) Schematic of the behavioral design to test various forms of aggression induced by
1314 photostimulation of pSI^{-PAG} projection terminals in the PAG under various conditions.
1315 (H-K) Aggression probability (H), latency to attack onset (I), duration (J), and events (K) of
1316 various forms of aggression induced by photostimulation of pSI^{-PAG} projection terminals in the
1317 PAG. '(E)' and '(N)' under the x-axis indicate that the aggression during photostimulation was
1318 significantly increased (E) or not changed (N), determined by one-way ANOVA or the Friedman
1319 test. 'NT' under the x-axis indicates that this index of aggression was not tested under this
1320 condition.

1321 (L) Left, schematic of Cre-dependent expression of ChR2-mCherry or mCherry in $pSI^{CaMKII\alpha}$
1322 neurons and optogenetic activation of the terminals of $pSI^{CaMKII\alpha}$ neurons projecting to the PAG or
1323 BNST. Middle, schematic and example images of c-Fos expression (green) in the PAG induced by
1324 local light stimulation of $pSI^{CaMKII\alpha}$ neuronal terminals in the PAG. Right, example image of
1325 $pSI^{CaMKII\alpha}$ neuronal terminals in the BNST.

1326 (M) Schematic of the timing and behavioral paradigm with optical activation of $pSI^{CaMKII\alpha}$ neuron
1327 terminals in a socially-housed mouse in its home cage encountering a male intruder.

1328 (N) Behavioral paradigm of a socially-housed mouse in its home cage attacking a singly-housed
1329 intruder induced by optical activation of $pSI^{CaMKII\alpha}$ neuronal terminals.

(O) Summary data showing attacks were induced by optogenetic activation of $pSI^{CaMKII\alpha}$ terminals in the PAG but not in the BNST in socially-housed male mice.

(P) Summary data showing socially-housed male mice in their home cages initiated attacks on singly-housed male intruders during optical activation of the $pSI^{CaMKII\alpha}$ -PAG projection. Percentage of trials with attacks, latency to attack, attack duration, and attack events induced by optogenetics during the pre-laser, laser, and post-laser phases in the control mCherry group (n = 6 mice) and in the ChR2 group (n = 8 mice). Pre *vs* Laser *vs* Post in the ChR2 group, ***$P < 0.001$, ***$P < 0.001$, ***$P < 0.001$, ***$P < 0.001$, Friedman test, n = 8 mice; Laser in the mCherry and ChR2 groups, ***$P < 0.001$, ***$P < 0.001$, ***$P < 0.001$, ***$P < 0.001$, two-tailed unpaired t-test, n = 6/8 mice. Significance was determined by the Friedman test and unpaired t-test.

(Q) Summary data showing socially-housed female mice in their home cages initiated attacks on singly-housed male intruders during optical activation of the $pSI^{CaMKII\alpha}$-PAG projection (**P = 0.007, **P = 0.0056, *P = 0.0451, *P = 0.0182, n = 3 mice, significance determined by one-way ANOVA).

(R) Overlays of CaMKIIα-ChR2-mCherry (left) and CaMKIIα-mCherry (middle) expression in pSI (-1.06 mm from bregma) in male mice, Right, overlay of CaMKIIα-ChR2-mCherry expression in pSI (–1.06 mm from bregma) of female mice.

ns, not significant.

Data are presented as the mean ± SEM.

Figure S7. pSI^{-PAG} and pSI^{Thy1} Neurons or the pSI-PAG Circuit Are Necessary for Inter-male Aggression, Related to Figure 8

(A) Schematic of the expression of AAV-Retro-Cre-EGFP in the PAG to drive Cre-dependent expression of AAV-DIO-hM4Di-mCherry in pSI^{-PAG} neurons.

(B) Left, schematic and representative image showing the expression of retrograde AAV-Retro-Cre-EGFP (green) in the PAG (scale bar, 100 μm). Right, schematic and representative image showing Cre-dependent expression of AAV-DIO-hM4Di-mCherry (red) in pSI^{-PAG} neurons infected with AAV-Retro-Cre-EGFP (green, arrowheads) (scale bars, 100 μm; inset, 10 μm).

(C) Schematic of the timing (upper) and behavioral paradigm (lower) for pharmacogenetic inhibition of pSI^{-PAG} neurons of a singly-housed male mouse in its home cage encountering a socially-housed male intruder (lower).

(D) Example raster plots of behavioral recordings from mice during 15-min encounters in the control group (mCherry, n = 6 mice) and the hM4Di group (n = 8 mice) (red marks, episodes of aggression).

(E) Latency to attack (left), attack duration (middle), and attack events (right) during the pre- and post-injection phases in control and hM4Di groups after saline or CNO injection. Latency, W = 13.00, $^{**}P < 0.01$; duration, W = –36.00, $^{**}P < 0.01$; and events, W = –36.00, $^{**}P < 0.01$ in the hM4Di group (Wilcoxon matched-pairs signed rank test and two-tailed paired t-test, n = 8 mice).

(F) Overlays of EGFP and mCherry expression from mice bilaterally injected with retrograde AAV-Retro-Cre-EGFP virus into the PAG and anterograde AAV-DIO-mCherry virus into the pSI.

(G) Overlays of EGFP and hM4D-mCherry expression from mice bilaterally injected with retrograde AAV-Retro-Cre-EGFP virus into the PAG and anterograde AAV-DIO-hM4D-mCherry virus into the pSI.

(H) Left, representative whole-cell current clamp recordings from a pSI neuron （upper）in response to intracellular current injection of a pulse train from 0 pA to 120 pA in a step of 20 pA (lower) before, during, and after 5 μM CNO perfusion. Right, red traces indicate the minimal current to induce action potentials.

(I) Summarized response curves showing number of induced action potentials at different injected current steps in CNO and control group. Paired t test, $^{**}P = 0.003$, n = 8 neurons.

(J) Minimal injected current to induce action potential (APs) in CNO and control group. Paired t test, $^{**}P = 0.002$, n = 8 neurons.

(K) Overlays of mCherry (left) and hM4d-mCherry expression (right) in male Thy1-Cre mice with AAV-DIO-mCherry and AAV-DIO-hM4D-mCherry virus bilaterally injected into the pSI.

(L) Left, aggression behavioral paradigm. Right, example raster plots of attack behavior recorded during 15-min encounters.

(M) Schematic of Cre-dependent expression of DIO-GtACR1-GFP in pSI^{Thy1} neurons and

optogenetic inhibition of the terminals of pSI^{Thy1} neurons projecting to the PAG in male Thy1-Cre mice.

(N) Left panel, example image showing the expression of DIO-GtACR1-GFP in pSI^{Thy1} neurons, scale bar, 50 μm. Right panel, light-induced inhibition of action potentials (upper green trace) evoked by intracellular current injection (lower black trace) in a GtACR1-expressing pSI^{Thy1} neurons (blue bar, application of a LED-generated blue light pulse; n=8 neurons).

(O) Upper panel, representative image of the PAG showing GtACR1-GFP expressing terminals (green) from pSI^{Thy1} neurons; scale bar, 50 μm. Lower panel, magnified image of the boxed area; scale bar, 10 μm.

(P) Schematic of the timing (upper) and behavioral paradigm (lower) for optogenetic inhibition of pSI^{Thy1} neuronal terminals in the PAG of a singly-housed male mouse in its home cage encountering a socially-housed male intruder (n = 5 mice).

(Q) Two example raster plots showing that optogenetic inhibition of pSI^{Thy1} neuronal terminals in the PAG time-locked interrupted inter-male aggressive behavior (red, episodes of aggression; blue, stimulation episodes).

(R) Percentage of attack trials interrupted within 3 s and latency to attack offset during the laser phase by optogenetic inhibition of the pSI^{Thy1} neuronal projection to the PAG.

(S) Distribution of attack episodes interrupted by optogenetic inhibition in inter-male aggression. ns, not significant.

Data are presented as the mean ± SEM.

1407 **Figure S8. Schematic for a pSI-controlled General Aggressive State**

1408 The hypothesis that aggression-related cue processing and the general aggressive state are encoded
1409 and generated by the pSI. The activation of pSI^{-PAG} neurons increases aggressive arousal, then
1410 robustly and gradually initiates diverse aggressive behaviors, bypassing various requirements for
1411 natural aggressive behaviors.

1412

1413 **Supplemental Movies S1-S5**

1414 **Movie S1. Optogenetic activation of pSI^{-PAG} neurons in a C57 male mouse in its home cage**
1415 **evokes attacks on a singly-housed male intruder, Related to Figure 5**.
1416 The male mouse (black) transfected with ChR2 in pSI^{-PAG} neurons and implanted with a fiber-
1417 optic cable in the pSI was photostimulated during the period indicated by "Light on".
1418

1419 **Movie S2. Optogenetic activation of pSI^{-PAG} neurons evokes arousal responses including**
1420 **an enlarged pupil in a head-fixed C57 male mouse, Related to Figure 5**.
1421 The male mouse (black) transfected with ChR2 in pSI^{-PAG} neurons and implanted with a fiber-
1422 optic cable in the pSI was photostimulated during the period indicated by "Light on".
1423

1424 **Movie S3. Optogenetic activation of pSI^{-PAG} neurons in a C57 female mouse in its home**
1425 **cage evokes attack on a socially-housed male intruder, Related to Figure 6**.
1426 The female mouse (black) transfected with ChR2 in pSI^{-PAG} neurons and implanted with a fiber-
1427 optic cable in pSI was photostimulated during the period indicated by "Light on".
1428

1429 **Movie S4. Optogenetic activation of pSI^{-PAG} neurons in a C57 male mouse evokes defensive**
1430 **attack on a male CD-1 mouse in the latter's cage, Related to Figure 6**.
1431 The male mouse (black) transfected with ChR2 in pSI^{-PAG} neurons and implanted with a fiber-
1432 optic cable in pSI was photostimulated during the period indicated by "Light on".
1433

1434 **Movie S5. Optogenetic silencing of pSI^{Thy1} neurons in a male Thy1-Cre mouse interrupts a**
1435 **naturally-occurring attack on a socially-housed mouse in a time-locked manner, Related to**
1436 **Figure 8**.
1437 The Thy1-Cre male mouse (white) transfected with GtACR1 in pSI^{Thy1} neurons and implanted
1438 with a fiber-optic cable in pSI was photostimulated during the period indicated by "Light on".

Table S1. Statistical data for all Figures

Fig	Comparison	Analysis	Statistic value	P value, F/T/W/U value	N
1B	c-Fos+ neurons per slice in the Control (sniff) vs Attack group	Unpaired t-test; Mann-Whitney test	pSI: 2.952±0.4402 *vs* 10.12±2.847; aSI: 0.9056±0.7605 *vs* 1.623±0.8423; CeA: 0.7083±0.1816 *vs* 1.250±0.3819; GP: 0.1467±0.0769 *vs* 0.1675±0.0698;	pSI: P = 0.0285; t=2.488, df=12; aSI: P = 0.5000; U=2.500; CeA: P = 0.5000; U=2.000; GP: P = 0.7429; U=5.000	7/7/3/3/3/3/4 mice
1E	Thy1 *vs* CaMKIIα *vs* ChAT *vs* GAD67	Kruskal-Wallis test	80.76±3.979 *vs* 76.82±9.086 *vs* 2.778±2.778 *vs* 2.5±2.5	P = 0.0002; KW=13.67	6/5/3/5 mice
1E	Thy1 *vs* CaMKIIα	Unpaired t-test	24.5 ± 3.6 *vs* 33.7 ± 6.7	P = 0.2349; t=1.273, df=9	6/5 mice
1J	Mean population activity per second (area under z-score curve); All neurons	Paired t-test; Wilcoxon matched-pairs signed rank test; Friedman test	6 columns (-2 s to 4 s): 0.00085±0.0001 *vs* 0.1127±0.07825 *vs* 0.3322±0.09643 *vs* 0.3049±0.08694 *vs* 0.1607±0.08520 *vs* 0.1920±0.08485	[-1s *vs* -2s]: P = 0.1566, t=1.426, df=112; [1s *vs* -2s]: P < 0.001, W=2391; 6 columns: P = 0.0458, FM=11.30	113/ 113 neurons
1L	Mean population activity per second (area under z-score curve); 'attack-active' neurons	Paired t-test; Wilcoxon matched-pairs signed rank test; Friedman test	6 columns (-2 s to 4 s): -0.00028±0.0013 *vs* 0.5620±0.1416 *vs* 1.202±0.1457 *vs* 0.9873±0.1383 *vs* 0.6930±0.1345 *vs* 0.6567±0.1531	[-1 s *vs* -2 s]: P < 0.001, t=3.959, df=43; [1 s *vs* -2 s]: P < 0.001, W=990; 6 columns: P < 0.001, FM=75.84	44/44 neurons
1M	Mean population activity per second (area under z-score curve); 'attack-active' neurons	Repeated one-way ANOVA	6 columns (-2 s to 4 s): -0.00029±0.0013 *vs* -0.043±0.1009 *vs* 0.0055±0.1379 *vs* 0.04501±0.1349 *vs* -0.06792±0.1565 *vs* -0.06651±0.1137	6 columns: P = 0.8913, F (3.732, 134.3) = 0.2613	37 neurons
1N	Mean population activity per second (area under z-score curve); 'attack-active' neurons	Friedman test	6 columns (-2 s to 4 s): -0.001834±0.0012 *vs* -0.09239±0.1349 *vs* 0.2831±0.2179 *vs* 0.3748±0.2179 *vs* 0.1418±0.1846 *vs* -0.02886±0.1559	6 columns: P = 0.0273, FM=12.61	37 neurons
1P	Mean population activity per second (area under z-score curve); 'Object sniff-active' neurons.	Friedman test	6 columns (-2 s to 4 s): -0.00094±0.0016 *vs* -0.1966±0.1336 *vs* 0.2948±0.1252 *vs* 0.3180±0.1368 *vs* 0.2804±0.1555 *vs* 0.09248±0.1323	6 columns: P = 0.2134, FM=7.099	26 neurons
1R	Mean population activity per second (area under z-score curve); 'Male sniff-active' neurons.	Friedman test	6 columns (-2 s to 4 s): 0.002916±0.001471 *vs* 0.2613±0.1824 *vs* 0.4357±0.2319 *vs* 0.4139±0.1918 *vs* 0.1320±0.1646 *vs* 0.1367±0.1933	6 columns: P = 0.2090, FM=7.161	32 neurons
2H	EYFP and GCamp6m Group, Area under curve per s	Mann-Whitney test; Wilcoxon matched-pairs signed rank test	0.0008±0.0012 *vs* 0.00153±0.0029 *vs* -0.0027±0.0048 vs 0.02327±0.004659 *vs* 0.1632±0.01011 *vs* 0.04729±0.008616	GCamp6m *vs* EYFP (pre: P = 0.0626, U=12132; attack: P < 0.001, U=3936; post: P < 0.001, U=9756); GCamp6m: pre *vs* attack, P < 0.001, W=94597; pre *vs* post, P < 0.001, W=20517	62/ 458 trials
2H	EYFP and GCamp6m Group, Peak value	Mann-Whitney test; Wilcoxon matched-pairs signed rank test	2.000±0.2249 *vs* 2.523±0.5819 *vs* 3.672±0.6622 *vs* 15.63±0.9487 *vs* 23.43±1.143 *vs* 22.28±1.194	GCamp6m *vs* EYFP (pre: P < 0.001, U=4460; attack: P < 0.001, U=3593; post: P < 0.001, U=4659); GCamp6m: pre vs attack, P < 0.001, W=63625; pre *vs* post, P < 0.001, W=41623	62/ 458 trials
2N	EYFP and GCamp6m Group, Peak value in single attacks	Mann-Whitney test; Wilcoxon matched-pairs signed rank test	2.183±0.3090 *vs* 3.482±0.9341 *vs* 4.347±0.9432 *vs* 15.27±2.071 *vs* 28.07±2.483 *vs* 22.30±2.491	GCamp6m *vs* EYFP (pre: P < 0.001, U=918; attack: P < 0.001, U=629; post: P < 0.001, U=1353); GCamp6m: pre *vs* attack, P < 0.001, W=12001	41 /165 trials
2N	EYFP and GCamp6m Group, Peak value in first attacks	Unpaired t-test; Mann-Whitney test; Paired t test	1.299±0.3873 *vs* 0.9214±0.3131 *vs* 2.472±0.7287 *vs* 8.419±1.111 *vs* 23.23±1.761 *vs* 29.26±1.931	GCamp6m *vs* EYFP (pre: P = 0.0451, t=2.027 df=107; attack: P < 0.001, t=4.009 df=107; post: P < 0.001, U=57); GCamp6m: pre *vs* attack, P < 0.001, t=11.64 df=98	10 /99 trials
2N	EYFP and GCamp6m Group, Peak value in last attacks	Mann-Whitney test; Wilcoxon matched-pairs signed rank test	1.935±0.4055 *vs* 2.026±0.7418 *vs* 2.100±0.6013 *vs* 19.53±1.657 *vs* 20.07±2.030 *vs* 16.21±1.971	GCamp6m *vs* EYFP (pre: P < 0.001, U=136; attack: P < 0.001, U=142; post: P < 0.001, U=177); GCamp6m: pre *vs* attack, P = 0.4835, W=404	10 /99 trials
2N	EYFP and GCamp6m Group, Peak value in single, first and last attacks	Mann-Whitney test	Peak value in post- single vs last attacks, P < 0.001, U=5774; Peak value in pre- first *vs* last attacks, P < 0.001, U=2881; Peak value in post- single *vs* last attacks, P < 0.001, U=3121		165 /99/99 trials
2P	GCamp6m Group of continuous attacks, Peak value in pre-attack	Kruskal-Wallis test; Mann-Whitney test	8.454±0.8678 *vs* 21.67±2.306 *vs* 23.34±3.593 *vs* 25.22±4.103 *vs* 21.01±4.794 *vs* 23.26±4.088 *vs* 19.18±1.667	1-7 continuous attacks, P < 0.001, KW=53.00; First *vs* second, P < 0.001, U=930.5; Last *vs* second, P = 0.2623, U=1875	99/43/24 /13/8/4/9 9 trials
2P	GCamp6m Group of continuous attacks, Peak value in attack	Kruskal-Wallis test	25.00±1.567 *vs* 26.60±2.651 *vs* 25.62±3.512 *vs* 23.79±3.984 *vs* 22.77±3.824 *vs* 28.98±4.508 *vs* 24.04±1.976	1-7 continuous attacks, P = 0.9688, KW=1.351	99/43/24 /13/8/4/9 9 trials
2P	GCamp6m Group of continuous attacks, Peak value in post-attack	Kruskal-Wallis test; Unpaired t test	29.50±1.783 *vs* 29.56±3.012 *vs* 28.64±3.686 *vs* 23.39±5.809 *vs* 27.37±4.707 *vs* 30.42±5.473 *vs* 19.45±1.933	1-7 continuous attacks, P = 0.0189, KW=15.18; First *vs* second, P = 0.9867, t= 0.01671 df=140; Last *vs* second, P = 0.005, t=2.854 df=140	99/43/24 /13/8/4/9 9 trials
3E	EYFP and GCamp6m Group in sniff and sniff (attack)	Mann-Whitney test	2.276±0.6475 *vs* 9.902±0.8186 *vs* 1.848±0.5129 *vs* 21.23±1.811	GCamp6m *vs* EYFP in sniff, P < 0.001, U=5415; GCamp6m *vs* EYFP in sniff (attack), P < 0.001, U=949.0	55/343/2 9/236 trials
3F	GCamp6m Group in sniff and sniff (attack), Peak value of pre-sniff, sniff and post-sniff	Mann-Whitney test	8.923±0.6919 *vs* 9.902±0.8186 *vs* 8.210±0.8686 *vs* 14.42±1.504 *vs* 21.23±1.811 *vs* 28.09±1.965	sniff *vs* sniff (attack): pre-sniff, P < 0.001, U=32851; sniff, P < 0.001, U=25656; post-sniff, P < 0.001, U=17216	343/236 trials
3H	Sniff/sniff (attack) decoding accuracy in shuffle and recoding	Mann-Whitney test; Wilcoxon matched-pairs signed rank test	50.25±0.4583 *vs* 50.06±0.4483 *vs* 50.85±0.4598 *vs* 54.45±0.4369 *vs* 69.02±0.4278 *vs* 64.80±0.4514	Shuffle *vs* recoding: Pre, P < 0.001, U=417829; sniff, P < 0.001, U=170821; Post, P < 0.001, U=250602. Recoding: Pre *vs* sniff, P < 0.001, W=273731; Pre *vs* post, P < 0.001, W=198811	1000/ 1000
3L	GCamp6m Group in sniff, sniff (attack), and threat, Peak value	Wilcoxon matched-pairs signed rank	9.113±2.548 *vs* 7.032±3.543 *vs* 8.816±3.204 *vs* 7.723±2.115 *vs*	Pre_ rattle *vs* rattle, P = 0.1814, W=-107; Pre_ rattle *vs* rattle (attack), P = 0.0094,	26/26/49 trials

	of pre-behavior, behavior and post-behavior	test; Paired t test; Mann-Whitney test	17.37±3.290 *vs* 17.88±3.513 *vs* 12.70±1.997 *vs* 17.06±2.609 *vs* 20.60±2.753	W=201; Pre_threat *vs* threat, $P = 0.002$, t=3.261 df=48; rattle *vs* rattle (attack), $P = 0.0129$, U=203; rattle (attack) *vs* threat, $P = 0.9432$, t= 0.07152 df=73	
3N	Rattle/rattle (attack) decoding accuracy in shuffle and recoding	Mann-Whitney test; Wilcoxon matched-pairs signed rank test	50.19±0.4471 *vs* 50.35±0.4554 *vs* 50.30±0.4781 *vs* 58.00±0.4646 *vs* 66.08±0.4327 *vs* 63.31±0.4821	Shuffle *vs* recoding: Pre, $P < 0.001$, U=352170; rattle, $P < 0.001$, U=218929; Post, $P < 0.001$, U=272458. Recoding: Pre *vs* rattle, $P < 0.001$, W=156413; Pre *vs* post, $P < 0.001$, W=103151	1000/ 1000
3O	GCamp6m Group in 6 types of social behaviors, Peak value during social behaviors	Mann-Whitney test; Kruskal-Wallis test	7.032±3.543 *vs* 9.902±0.8186 *vs* 17.37±3.290 *vs* 21.23±1.811 *vs* 17.06±2.609 *vs* 23.43±1.143	rattle *vs* sniff, $P = 0.0775$, U=3534; rattle (attack) *vs* sniff (attack) *vs* threat, $P = 0.5532$, KW=1.184; sniff *vs* sniff (attack), $P < 0.001$, U=25656; attack *vs* sniff (attack), $P = 0.0193$, U=48187	26/343/26/236/49/458 trials

3O	GCamp6m Group in 6 types of social behaviors, Peak value during social behaviors	Mann-Whitney test; Kruskal-Wallis test		rattle, $P = 0.1814$, W=-107;
				sniff, $P = 0.0404$, W=7536;
				rattle (attack), $P = 0.0094$, W=201;
				sniff (attack), $P < 0.001$, W=11552;
				threat, $P < 0.001$, t=3.261 df=48;
				attack, $P < 0.001$, W=63625	

3O	GCamp6m Group in 6 types of social behaviors, Area under curve per s	Mann-Whitney test; Kruskal-Wallis test	0.02494±0.03053 *vs* 0.03004±0.00646 *vs* 0.08252±0.02238 *vs* 0.1237±0.0159 *vs* 0.1342±0.02293 *vs* 0.1632±0.01011	rattle *vs* sniff, $P = 0.3028$, U=3917; rattle (attack) *vs* sniff (attack) *vs* threat, $P = 0.4294$, KW=1.691; sniff *vs* sniff (attack), $P < 0.001$, U=24892; attack *vs* sniff (attack), $P < 0.001$, U=43684	

3O	GCamp6m Group in each 6 types of social behaviors, Area under curve per s of pre-behavior and during behavior	Mann-Whitney test; Paired t test; Wilcoxon matched-pairs signed rank test		rattle, $P = 0.5317$, U=-51;
				sniff, $P = 0.0610$, W=6888;
				rattle (attack), $P = 0.0032$, W=225;
				sniff (attack), $P < 0.001$, W=20204;
				threat, $P < 0.001$, t=6.305 df=48;
				attack, $P < 0.001$, W=94597	

3Q	Rattle/rattle (attack) /attack decoding accuracy in shuffle and recoding	Mann-Whitney test; Wilcoxon matched-pairs signed rank test	33.04±0.3517 *vs* 33.64±0.3405 *vs* 33.95±0.3632 *vs* 41.55±0.3789 *vs* 54.69±0.3811 *vs* 44.93±0.3632	Shuffle *vs* recoding: Pre, $P < 0.001$, U=304214; Beh, $P < 0.001$, U=100653; Post, $P < 0.001$, U=255098. Recoding: Pre *vs* Beh, $P < 0.001$, W=300581; Pre *vs* post, $P < 0.001$, W=94099	1000/ 1000
4D	Peak value of male-male attack and male-female attack in GCamp6m Group	Wilcoxon matched-pairs signed rank test; Mann-Whitney test	15.63±0.9487 *vs* 23.43±1.143 *vs* 22.28±1.194 *vs* 14.99±2.329 *vs* 25.62±2.329 *vs* 20.91±2.625	GCamp6m of pre-attack *vs* attack in male-female aggression, $P < 0.001$, W=1616; male-female attack *vs* male-female attack, $P = 0.4071$, U=12834	458/60 trials
4G	Peak value of male-male attack and male-male defensive attack in GCamp6m Group	Wilcoxon matched-pairs signed rank test; Mann-Whitney test	15.63±0.9487 *vs* 23.43±1.143 *vs* 22.28±1.194 *vs* 24.56±0.7408 *vs* 30.23±0.7896 *vs* 30.59±0.8752	GCamp6m of pre-attack vs attack in inter-male defensive aggression, $P < 0.001$, W=103264; male-male attack *vs* inter-male defensive attack, $P < 0.001$, U=121345	458/680 trials
4K	Approach/ approach (attack) /predatory attack decoding accuracy in shuffle and recoding	Mann-Whitney test; Wilcoxon matched-pairs signed rank test	33.18±0.3709 *vs* 32.49±0.3791 *vs* 33.61±0.3811 *vs* 43.59±0.4010 *vs* 46.39±0.3972 *vs* 40.39±0.38889	Shuffle *vs* recoding: Pre, $P < 0.001$, U=277581; Beh, $P < 0.001$, U=214523; Post, $P < 0.001$, U=348929. Recoding: Pre *vs* Beh, $P = 0.001$, W=70681; Pre *vs* post, $P < 0.001$, W=-80243	1000/ 1000
4L	Peak value of male-male attack and predatory attack in GCamp6m Group	Mann-Whitney test	15.63±0.9487 *vs* 23.43±1.143 *vs* 22.28±1.194 *vs* 6.553±0.4438 *vs* 8.406±0.4702 *vs* 9.018±0.5822	GCamp6m of pre-attack in male-male attack *vs* predatory attack, $P < 0.001$, U=26345; GCamp6m of attack period in male-male attack *vs* predatory attack, $P < 0.001$, U=18607	458/186 trials
4P	Approach/ approach (attack) /pup-directed attack decoding accuracy in shuffle and recoding	Mann-Whitney test; Wilcoxon matched-pairs signed rank test	33.38±0.3756 *vs* 32.91±0.3479 *vs* 33.74±0.3918 *vs* 52.81±0.4142 *vs* 52.57±0.4253 *vs* 50.19±0.3986	Shuffle *vs* recoding: Pre, $P < 0.001$, U=139754; Beh, $P < 0.001$, U=133330; Post, $P < 0.001$, U=179120. Recoding: Pre *vs* Beh, $P = 0.8169$, W=-3405; Pre *vs* post, $P < 0.001$, W=-61577	1000/ 1000
4Q	Peak value of male-male attack and pup-directed attack in GCamp6m Group	Mann-Whitney test	15.63±0.9487 *vs* 23.43±1.143 *vs* 22.28±1.194 *vs* 8.804±0.7489 *vs* 9.496±0.8951 *vs* 7.116±0.8026	GCamp6m of pre-attack in male-male attack *vs* attack in pup-directed aggression, $P = 0.0031$, U=9140; male-male attack *vs* pup-directed attack, $P < 0.001$, U=5786	458/53 trials
4U	Sniff/ sniff (attack) /female-male attack decoding accuracy in shuffle and recoding	Mann-Whitney test; Wilcoxon matched-pairs signed rank test	33.53±0.3569 *vs* 32.93±0.3262 *vs* 33.08±0.3596 *vs* 37.41±0.3755 *vs* 43.35±0.3773 *vs* 39.87±0.3682	Shuffle *vs* recoding: Pre, $P < 0.001$, U=411334; Beh, $P < 0.001$, U=257635; Post, $P < 0.001$, U=341973. Recoding: Pre *vs* Beh, $P < 0.001$, W=154324; Pre *vs* post, $P < 0.001$, W=62653	1000/ 1000
4V	Peak value of male-male attack and female-male attack in GCamp6m Group	Mann-Whitney test	15.63±0.9487 *vs* 23.43±1.143 *vs* 22.28±1.194 *vs* 9.437±0.4577 *vs* 8.758±0.5132 *vs* 12.73±0.6120	GCamp6m of pre-attack in male-male attack *vs* attack in female-male aggression, $P < 0.001$, U=77784; male-male attack *vs* female-male attack, $P < 0.001$, U=49660	458/454 trials
4W	GCamp6m Group in 14 types of social behaviors, Peak value of pre-behavior and during behavior	Wilcoxon matched-pairs signed rank test	6.354±1.259 *vs* 4.923±0.5329 *vs* 8.406±0.4702 *vs* 4.496±1.583 *vs* 7.808±0.8946 *vs* 9.496±0.8951 *vs* 7.033±0.7578 *vs* 7.477±0.8170 *vs* 8.758±0.5132 *vs* 9.902±0.8186 *vs* 21.23±1.811 *vs* 23.43±1.143 *vs* 25.62±2.329 *vs* 30.23±0.7896	1-14th: $P = 0.7768$, W=62; $P = 0.0673$, W=-2290; $P < 0.001$, W=7191; $P = 0.0228$, W=-556; $P = 0.0015$, W=664; $P = 0.1355$, W=339; $P = 0.0759$, W=1893; $P = 0.1258$, W=-1749; $P = 0.0052$, W=-15649; $P = 0.0404$, W=7536; $P < 0.001$, W=11552; $P < 0.001$, W=63625; $P < 0.001$, W=1616; $P < 0.001$, W=103264	51/167/186/56/51/53/150/157/454/343/236/458/60/680 trials
4W	GCamp6m Group in 14 types of social behaviors, Peak value during social behaviors	Kruskal-Wallis test; Mann-Whitney test		1st-3rd, $P < 0.001$, KW=26.49; 4th-6th, $P < 0.001$, KW=18.17; 7th-9th, $P = 0.1017$, KW=4.572; 10th-12nd, $P < 0.001$, KW=131.8; 12nd *vs* 13rd, $P = 0.4071$, U=12834; 12nd *vs* 14th, $P < 0.001$, U=121345; 12nd *vs* 9th, $P < 0.001$, U=49660	
4W	GCamp6m Group in 14 types of social behaviors, Area under curve per s of pre-behavior and during behavior	Wilcoxon matched-pairs signed rank test; Paired t test;	0.02711±0.01149 *vs* 0.01926±0.0049 *vs* 0.03484±0.0043 *vs* 0.011±0.01398 *vs* 0.049±0.008 *vs* 0.053±0.0075 *vs* 0.02559±0.0065 *vs* 0.0517±0.00739 *vs* 0.06606±0.00472 *vs* 0.03±0.00646 *vs*	1-14th: $P = 0.004$, W=606; $P < 0.001$, W=7744; $P < 0.001$, W=13603; $P = 0.4783$, W=176; $P < 0.001$, W=1254; $P < 0.001$, t=4.498 df=52; $P = 0.008$, W=2815; $P < 0.001$, W=6779; $P < 0.001$, W=16219; $P = 0.0610$, W=6888; $P <$	

			0.1237±0.0159 *vs* 0.1632±0.01011 *vs* 0.1624±0.0191 *vs* 0.2231±0.006856	0.001, W=20204; $P < 0.001$, W=94597; $P < 0.001$, W=1754; $P < 0.001$, W=1664	
4W	GCamp6m Group in 14 types of social behaviors, Area under curve per s	Mann-Whitney test; Kruskal-Wallis test		1st-3rd, $P = 0.0213$, KW=7.696; 4th-6th, $P < 0.001$, KW=18.15; 7th-9th, $P < 0.001$, KW=25.88; 10th-12nd, $P < 0.001$, KW=171.5; 12nd *vs* 13rd, $P = 0.8884$, U=13587; 12nd *vs* 14th, $P < 0.001$, U=120984; 12nd *vs* 9th, $P < 0.001$, U=60271	
5C	Pre-CNO vs CNO in mCherry Group, Latency(L), Duration(D), Events(E)	Wilcoxon matched-pairs signed rank test	L: 770.3±86.62 *vs* 619.2±158.8; D: 0.38±0.3453 *vs* 1.595±1.003; E: 0.3333±0.2108 *vs* 0.8333±0.4773.	L: $P = 0.2500$; W=-6.0; D: $P = 0.2500$; W=6.0; E: $P = 0.5000$; W=3;	6/6 mice
5C	Saline *vs* CNO in mCherry Group, Latency(L), Duration(D), Events(E)	Paired t-test	L: 585.2±149.6 *vs* 619.2±158.8; D: 2.783±1.676 *vs* 1.595±1.003; E: 1.5±0.9574 *vs* 0.8333±0.4773.	L: $P = 0.7571$; t= 0.3268, df=5; D: $P = 0.1858$; t=1.533 df=5; E: $P = 0.2856$; t=1.195 df=5;	6/6 mice
5C	Pre-CNO vs CNO in HM3D Group, Latency(L), Duration(D), Events(E)	Wilcoxon matched-pairs signed rank test	L: 791±109 *vs* 53.26±12.63; D: 1.034±1.034 *vs* 33.99±9.798; E: 0.5714±0.5714 *vs* 21.14±4.93.	L: $P = 0.0156$; W=-28.0; D: $P = 0.0156$; W=28.0; E: $P = 0.0156$; W=28.0;	7/7 mice
5C	Saline *vs* CNO in HM3D Group, Latency(L), Duration(D), Events(E)	Wilcoxon matched-pairs signed rank test	L: 797.1±102.9 *vs* 53.26±12.63; D: 1.927±1.927 *vs* 33.99±9.798; E: 1.286±1.286 *vs* 21.14±4.93.	L: $P = 0.0156$; W=-28.0; D: $P = 0.0156$; W=28.0; E: $P = 0.0156$; W=28.0;	7/7 mice
5I	Pre *vs* Laser *vs* Post in ChR2 Group, Possibility of trials showing aggression(P), Latency(L), Duration(D), Events(E)	Friedman test	P: 0±0 *vs* 93.85±3.497 *vs* 1.538±1.538; L: 15±0 *vs* 2.512±0.5046 *vs* 14.84±0.1611; D: 0±0 *vs* 3.695±0.5748 *vs* 0.018±0.018; E: 0±0 *vs* 1.498±0.1956 *vs* 0.01538±0.01538	P: $P < 0.001$; FM= 25.40; L: $P < 0.001$; FM= 25.40; D: $P < 0.001$; FM= 25.40; E: $P < 0.001$; FM= 25.40;	13 mice
5I	Laser in EYFP and ChR2 Group, Possibility of trials showing aggression(P), Latency(L), Duration(D), Events(E)	Mann-Whitney test	P: 0±0 *vs* 93.85±3.497; L: 15±0 *vs* 2.512±0.5046; D: 0±0 *vs* 3.695±0.5748; E: 0±0 *vs* 1.498±0.1956	P: $P < 0.001$; U= 0; L: $P < 0.001$; U= 0; D: $P < 0.001$; U= 0; E: $P < 0.001$; U= 0	6/13 mice
5M	Pre *vs* Laser *vs* Post in ChR2 Group, Normalized pupil size	Friedman test	0.9953±0.003685 *vs* 1.286±0.071 *vs* 1.151±0.05884	$P < 0.001$; FM= 16.22	9 mice
5N	Pre *vs* Laser *vs* Post in ChR2 Group, Normalized eye size	Repeated one-way ANOVA	1±0 *vs* 1.037±0.0172 *vs* 0.999±0.01009	$P = 0.0357$; F (1.398, 11.19) = 5.102	9 mice
5O	Pre *vs* Laser *vs* Post in ChR2 Group, Normalized breathing rate	Repeated one-way ANOVA	1±0 *vs* 1.076±0.02183 *vs* 1.028±0.007836	$P = 0.0136$; F (1.186, 9.490) = 8.515	9 mice
5P	Pre *vs* Laser *vs* Post in ChR2 Group, Normalized heart rate	Repeated one-way ANOVA	1±0 *vs* 1.068±0.01586 *vs* 1.006±0.02477	$P = 0.0447$; F (1.426, 9.979) = 4.744	8 mice
5Q	Pre *vs* Laser *vs* Post in ChR2 Group, trembling time	Repeated one-way ANOVA	0.4078±0.1478 *vs* 2.427±0.4445 *vs* 0.4171±0.1638	$P = 0.0019$; F (1.201, 9.608) = 16.21	9 mice
6C	Pre *vs* Laser *vs* Post in ChR2 Group, Possibility of trials showing aggression(P), Latency(L), Duration(D), Events(E)	Friedman test	P: 1.154±1.154 *vs* 79.00±9.713 *vs* 0.7692±0.7692; L: 14.93±0.0686 *vs* 4.404±1.449 *vs* 15±0; D: 0.0188±0.0188 *vs* 2.884±0.9603 *vs* 0.00±0.00; E: 0.02±0.02 *vs* 1.845±0.2477 *vs* 0.00±0.00	P: $P < 0.001$; FM= 19.42; L: $P < 0.001$; FM= 19.42; D: $P < 0.001$; FM= 19.42; E: $P < 0.001$; FM= 19.42	10 mice
6E	Pre *vs* Laser *vs* Post in ChR2 Group, Possibility of trials showing aggression(P), Latency(L)	Friedman test	P: 4.286±2.276 *vs* 70.71±8.151 *vs* 10.0±4.06; L: 14.62±0.2072 *vs* 6.526±1.197 *vs* 14.18±0.3291	P: $P < 0.001$; FM= 26.53; L: $P < 0.001$; FM= 25.40	14 mice
6G	Pre *vs* Laser *vs* Post in ChR2 Group, Possibility of trials showing aggression(P), Latency(L), Duration(D), Events(E)	Friedman test	P: 0±0 *vs* 73.33±14.3 *vs* 4.762±4.762; L: 15±0 *vs* 5.611±1.793 *vs* 14.67±0.2147; D: 0.00±0.00 *vs* 3.255±0.9358 *vs* 0.06214±0.06214; E: 0.00±0.00 *vs* 1.377±0.3448 *vs* 0.04762±0.04762	P: $P = 0.0041$; FM= 11.47; L: $P = 0.0021$; FM= 11.20; D: $P = 0.0041$; FM= 11.47; E: $P = 0.0041$; FM= 11.47.	6 mice
6I	Pre *vs* Laser *vs* Post in ChR2 Group, Possibility of trials showing aggression(P), Latency(L), Duration(D), Events(E)	Friedman test; Repeated one-way ANOVA	P:17.57±8.118 *vs* 89.14±4.554 *vs* 11.67±7.265; L: 12.07±1.369 *vs* 2.498±0.7538 *vs* 13.69±0.9331; D: 0.0765±0.03467 *vs* 2.904±0.8344 *vs* 0.1625±0.1545; E:0.25±0.1118 *vs* 2.633±0.6217 *vs* 0.25±0.1936	P: $P = 0.0123$; FM= 8.444; L: $P = 0.0009$; F (1.677, 6.707) = 25.61; D: $P = 0.0180$; F (1.007, 5.033) = 11.89; E: $P = 0.0140$; F (1.199, 4.798) = 13.53.	5 mice
6J	Pre *vs* Laser *vs* Post in ChR2 Group, Possibility of trials showing aggression	Repeated one-way ANOVA	Value of the 1-13 column: 93.9 ± 3.5 *vs* 85.7 ± 5.1 *vs* 70.8 ± 7.6 *vs* 86.1 ± 5.9 *vs* 84.0 ± 16.0 *vs* 80.0 ± 6.3 *vs* 98.2 ± 1.8 *vs* 79.0 ± 9.7 *vs* 88.0 ± 12.0 *vs* 70.7 ± 8.2 *vs* 73.3 ± 14.3 *vs* 89.1 ± 4.6 *vs* 92.8 ± 2.4 (%). P: $P = 0.1170$; F (12, 93) = 1.664		13/7/7/6/5/5/11/10/5/14/6/5/12 mice
6J. 2nd	Pre *vs* Laser *vs* Post in ChR2 Group, Possibility of inter-male aggression in novel cage	Friedman test	1.786±1.786 *vs* 85.71±5.050 *vs* 8.929±5.923	$P = 0.0007$; FM= 13.13	7 mice
6J. 3rd	Pre *vs* Laser *vs* Post in ChR2 Group, Possibility of inter-male aggression in residents' cage	Friedman test	0.00±0.00 *vs* 70.83±7.553 *vs* 1.786±7.786	$P = 0.0014$; FM= 13.45	7 mice
6J. 4th	Pre *vs* Laser *vs* Post in ChR2 Group, Possibility of inter-male aggression versus cage mate	Friedman test	0.00±0.00 *vs* 86.11±5.927 *vs* 0.00±0.00	$P = 0.0041$; FM= 12.00	6 mice
6J.	Pre *vs* Laser *vs* Post in ChR2	Friedman test	6.19±3.81 *vs* 84.0±16.0 *vs* 5.714±5.714	$P = 0.0123$; FM= 8.824	5 mice

5th	Group, Possibility of inter-male aggression in singly mice				
6J. 6th	Pre *vs* Laser *vs* Post in ChR2 Group, Possibility of inter-male aggression in singly mice, in novel cage	Friedman test	0±0 *vs* 80±6.325 *vs* 3.333±3.333	*P* = 0.0123; FM= 9.500	5 mice
6J. 7th	Pre *vs* Laser *vs* Post in ChR2 Group, Possibility of male-female aggression	Friedman test	1.299±1.299 *vs* 98.2±1.8 *vs* 1.299±1.299	*P* < 0.001; FM= 22.00	11 mice
6J. 9th	Pre *vs* Laser *vs* Post in ChR2 Group, Possibility of female-female aggression	Friedman test	0±0 *vs* 88±12 *vs* 0±0	*P* = 0.0123; FM= 10.00	5 mice
6J. 13rd	Pre *vs* Laser *vs* Post in ChR2 Group, Possibility of predatory aggression	Friedman test	0.00±0.00 *vs* 92.81±2.412 *vs* 22.76±4.482	*P* < 0.001; FM= 23.13	12 mice
7D	Possibility of inter-male aggression during 14 intensities of laser stimulation	Non-Linear regression: Sigmoidal fit, X is log (laser power)	0, 0.03, 0.10, 0.17, 0.26, 0.34, 0.40, 0.68, 1.17, 1.58, 1.98, 2.24, 2.70, and 2.98 mW laser power were used in inter-male aggression;	Goodness of Fit: R^2 (during stimulation) = 0.7442, R^2 (before stimulation) = 1; Slope (during stimulation) = 0.7977	84 trials, 6 mice
7F	Possibility of 5 types of aggression during 14 intensities of laser stimulation	Non-Linear regression: Sigmoidal fit, X is log (laser power)	Slope (inter-male) = 0.7977; Slope (male-female) = 0.7940; Slope (female-male) = 1.987; Slope (infanticide) = 6.439; Slope (predation) = 23.69	R^2 (inter-male) = 0.7442; R^2 (male-female) = 0.7280; R^2 (female-male) = 0.4105; R^2 (infanticide) = 0.8195; R^2 (predation) = 0.9295	84/84/70 /84/84 trials
7G	Latency to attack onset of 5 types of aggression during 14 intensities of laser stimulation	Non-Linear regression: Sigmoidal fit, X is log (laser power)	Slope (inter-male) = 0.7420; Slope (male-female) = 0.6737; Slope (female-male) = 1.832; Slope (infanticide) = 6.007; Slope (predation) =6.334	R^2 (inter-male) = 0.7372; R^2 (male-female) = 0.7652; R^2 (female-male) = 0.4252; R^2 (infanticide) = 0.7804; R^2 (predation) = 0.8963	84/84/70 /84/84 trials
7H	Possibility of 5 types of aggression during 0.1 mW laser stimulation	Kruskal-Wallis test	6.667±6.667 *vs* 43.33±10.85 *vs* 44.00±16.00 *vs* 85.55±5.209 *vs* 96.67±3.333 (%)	*P* < 0.001, KW=21.59	6/6/5/6/6 mice
7H	Latency to attack onset of 5 types of aggression during 0.1 mW laser stimulation	Kruskal-Wallis test	14.073±0.927 *vs* 9.076±1.525 *vs* 9.125±2.231 *vs* 3.720±0.895 *vs* 2.158±0.428 (s)	*P* < 0.001, KW=19.74	6/6/5/6/6 mice
8C	mCherry Group, Latency to attack	Wilcoxon matched-pairs signed rank test and Paired t-test	Pre-saline vs Saline *vs* Pre-CNO vs CNO: 209.3±53.75 *vs* 83.69±36.81 *vs* 285.6±79.49 *vs* 126.2±53.31	Pre-saline vs Saline: *P* = 0.0625 W=-19.0; Pre-CNO vs CNO: *P* = 0.0836 t=2.156 df=5; Saline *vs* CNO: *P* = 0.4814 t= 0.7603 df=5;	6/6/6/6 mice
8C	HM4D Group, Latency to attack	Wilcoxon matched-pairs signed rank test and Paired t-test	Pre-saline vs Saline *vs* Pre-CNO vs CNO: 56.91±38.25 *vs* 187±89.83 *vs* 118.2±68.1 *vs* 900±0	Pre-saline vs Saline: *P* = 0.0313 W=21.0; Pre-CNO vs CNO: *P* < 0.001 t=11.48 df=5; Saline *vs* CNO: *P* < 0.001 t=7.937 df=5;	6/6/6/6 mice
8C	mCherry Group, Duration of attack	Wilcoxon matched-pairs signed rank test	Pre-saline vs Saline *vs* Pre-CNO vs CNO: 21.23±15.03 *vs* 15.96±10.84 *vs* 21.02±11.57 *vs* 11.61±5.644	Pre-saline vs Saline: *P* = 0.2188 W=-13; Pre-CNO vs CNO: *P* = 0.4375 W=-9.000; Saline *vs* CNO: *P* = 0.3125 W=-11.00;	6/6/6/6 mice
8C	HM4D Group, Duration of attack	Wilcoxon matched-pairs signed rank test and Paired t-test	Pre-saline vs Saline *vs* Pre-CNO vs CNO: 39.19±13.11 *vs* 26.75±10.78 *vs* 25.83±7.395 *vs* 0±0	Pre-saline vs Saline: *P* = 0.2188 W=-13.00; Pre-CNO vs CNO: *P* = 0.0174 t=3.493 df=5; Saline *vs* CNO: *P* = 0.0313 W=-21.00;	6/6/6/6 mice
8C	mCherry Group, Events of attack	Wilcoxon matched-pairs signed rank test and Paired t-test	Pre-saline vs Saline *vs* Pre-CNO vs CNO: 19±3.464 *vs* 17±3.54 *vs* 23.17±8.784 *vs* 20.17±4.086	Pre-saline vs Saline: *P* = 0.5907 t= 0.5742 df=5; Pre-CNO vs CNO: *P* = 0.999 W=1.000; Saline *vs* CNO: *P* = 0.5931 t= 0.5703 df=5;	6/6/6/6 mice
8C	HM4D Group, Events of attack	Paired t-test	Pre-saline vs Saline *vs* Pre-CNO vs CNO: 16.83±5.712 *vs* 8.167±2.072 *vs*18.67±5.175 *vs* 0±0	Pre-saline vs Saline: *P* = 0.0978 t=2.033 df=5; Pre-CNO vs CNO: *P* = 0.0154 t=3.607 df=5; Saline *vs* CNO: *P* = 0.011 t=3.941 df=5;	6/6/6/6 mice
8E	HM4D Group, Latency to mount onset	Paired t-test	Pre-saline vs Saline *vs* Pre-CNO vs CNO: 156.5±12.88 *vs* 106.8±26.11*vs* 109.3±24.49 *vs* 131±40.03	Pre-saline vs Saline: *P* = 0.1658 t=1.621 df=5; Pre-CNO vs CNO: *P* = 0.5014 t=11.48 df=5; Saline *vs* CNO: *P* = 0.325 t=1.091 df=5;	6/6/6/6 mice
8E	HM4D Group, mount duration	Paired t-test	Pre-saline vs Saline *vs* Pre-CNO vs CNO: 37.75±16.56 *vs* 45.17±19.36 *vs*49.67±12.46 *vs* 45±15.62	Pre-saline vs Saline: *P* = 0.509 t= 0.7107 df=5; Pre-CNO vs CNO: *P* = 0.4764 t= 0.7695 df=5; Saline *vs* CNO: *P* = 0.9901 t= 0.01310 df=5;	6/6/6/6 mice
8E	HM4D Group, mount events	Paired t-test	Pre-saline vs Saline *vs* Pre-CNO vs CNO: 11.67±4.529 *vs* 10.5±3.085 *vs*15±3.044 *vs* 13.67±3.721	Pre-saline vs Saline: *P* = 0.6598 t= 0.4675 df=5; Pre-CNO vs CNO: *P* = 0.603 t= 0.5547 df=5; Saline *vs* CNO: *P* = 0.2858 t=1.195 df=5;	6/6/6/6 mice
8M	*vs* social male, Attack duration of the pre-laser, laser and post-laser phase	Friedman test	3.394±0.4378 *vs* 1.356±0.2270 *vs* 0.8136±0.4251	*P* = 0.0179; FM = 7.750	8 mice
8M	*vs* pups, Attack duration of the pre-laser, laser and post-laser phase	Friedman test	3.626±1.025 *vs* 1.575±0.3004 *vs* 1.084±0.6395	*P* = 0.0120; FM=8.333	6 mice
8M	*vs* crickets, Attack duration of the pre-laser, laser and post-laser phase	Friedman test	11.70±0.8476 *vs* 5.383±0.7261 *vs* 10.14±0.7384	*P* = 0.0046; FM=8	4 mice
8N	Possibility of attack trials interrupted within 3 s	Kruskal-Wallis test	98.44±1.563 *vs* 94.87±5.128 *vs* 92.86±7.143	*P* = 0.8824; KW= 0.3672	8/6/4 mice
S1B	Linear regression of the AUC per second of GCaMP6m signals and possibilities of attacks prior to the attack behavior	Linear regression	Y = 0.001644*X + 0.01182	R^2 = 0.03025; *P* = 0.2832	40 trials
S1D	Linear regression of the AUC per second of GCaMP6m signals and possibilities of attacks prior to the attack behavior	Linear regression	Y = -0.002264*X + 0.08717	R^2 = 0.3545; *P* < *0*.0001	40 trials
S1E	The Peak ΔF/F of GCaMP6m in attack behaviors	Kruskal-Wallis test	18.36±1.058 *vs* 21.47±2.229 *vs* 19.50±1.697 *vs* 21.80±1.663	*P* = 0.1270; KW=5.704	458/165/ 99/99 trials

S1G	Single/first (attack) decoding accuracy in shuffle and recoding	Mann-Whitney test; Wilcoxon matched-pairs signed rank test	49.74±0.4551 *vs* 49.95±0.4038 *vs* 49.57±0.4643 *vs* 55.80±0.4628 *vs* 57.89±0.4574 *vs* 66.32±0.4410	Shuffle *vs* recoding: Pre, $P < 0.001$, U=385461; Beh, $P < 0.001$, U=340263; Post, $P < 0.001$, U=207572. Recoding: Pre *vs* Beh, $P = 0.0019$, W=40899; Pre *vs* post, $P < 0.001$, W=199251	1000/ 1000
S1I	Single/last (attack) decoding accuracy in shuffle and recoding	Mann-Whitney test; Wilcoxon matched-pairs signed rank test	49.16±0.4791 *vs* 49.74±0.4235 *vs* 49.46±0.4599 *vs* 62.77±0.4398 *vs* 53.16±0.4350 *vs* 55.11±0.4624	Shuffle *vs* recoding: Pre, $P < 0.001$, U=259307; Beh, $P < 0.001$, U=427698; Post, $P < 0.001$, U=389430. Recoding: Pre *vs* Beh, $P < 0.001$, W=-79639; Pre *vs* post, $P < 0.001$, W=-145607	1000/ 1000
S1M	Approach/predatory (attack) decoding accuracy in shuffle and recoding	Mann-Whitney test; Wilcoxon matched-pairs signed rank test	49.75±0.5053 *vs* 50.35±0.4804 *vs* 48.74±0.4686 *vs* 60.29±0.4891 *vs* 56.11±0.4872 *vs* 53.88±0.4814	Shuffle *vs* recoding: Pre, $P < 0.001$, U=320836; Beh, $P < 0.001$, U=394073; Post, $P < 0.001$, U=400667. Recoding: Pre *vs* Beh, $P < 0.001$, W=299829; Pre *vs* post, $P < 0.001$, W=-120570	1000/ 1000
S1O	Approach/pup-directed (attack) decoding accuracy in shuffle and recoding	Mann-Whitney test; Wilcoxon matched-pairs signed rank test	50.81±0.4755 *vs* 49.95±0.4939 *vs* 50.66±0.4858 *vs* 72.97±0.4410 *vs* 68.12±0.4780 *vs* 64.73±0.5095	Shuffle *vs* recoding: Pre, $P < 0.001$, U=147955; Beh, $P < 0.001$, U=209369; Post, $P < 0.001$, U=265718. Recoding: Pre *vs* Beh, $P < 0.001$, W=-101899; Pre *vs* post, $P < 0.001$, W=-154832	1000/ 1000
S1Q	Female-male sniff/female-male attack decoding accuracy in shuffle and recoding	Mann-Whitney test; Wilcoxon matched-pairs signed rank test	50.29±0.4550 *vs* 49.33±0.4550 *vs* 50.18±0.4510 *vs* 54.13±0.4421 *vs* 57.40±0.4557 *vs* 54.11±0.4261	Shuffle *vs* recoding: Pre, $P < 0.001$, U=423148; Beh, $P < 0.001$, U=348253; Post, $P < 0.001$, U=420140. Recoding: Pre *vs* Beh, $P < 0.001$, W=66857; Pre *vs* post, $P < 0.001$, W=-4625	1000/ 1000
S1S	Approach/ approach (attack) decoding accuracy in shuffle and recoding	Mann-Whitney test; Wilcoxon matched-pairs signed rank test	50.69±14.77 *vs* 50.46±0.4563 *vs* 49.32±0.4833 *vs* 56.09±0.4983 *vs* 67.42±0.4823 *vs* 59.95±0.4991	Shuffle *vs* recoding: Pre, $P < 0.001$, U=402551; Beh, $P < 0.001$, U=215285; Post, $P < 0.001$, U=317394. Recoding: Pre *vs* Beh, $P < 0.001$, W=210500; Pre *vs* post, $P < 0.001$, W=74759	1000/ 1000
S1U	Pup-directed approach/approach (attack) decoding accuracy in shuffle and recoding	Mann-Whitney test; Wilcoxon matched-pairs signed rank test	49.02±0.4784 *vs* 49.58±0.4345 *vs* 49.13±0.4954 *vs* 61.31±0.4875 *vs* 64.98±0.4767 *vs* 71.45±0.4550	Shuffle *vs* recoding: Pre, $P < 0.001$, U=288077; Beh, $P < 0.001$, U=228883; Post, $P < 0.001$, U=153610. Recoding: Pre *vs* Beh, $P < 0.001$, W=74342; Pre *vs* post, $P < 0.001$, W=191828	1000/ 1000
S1W	Female-male sniff/sniff(attack) decoding accuracy in shuffle and recoding	Mann-Whitney test; Wilcoxon matched-pairs signed rank test	49.28±0.438 *vs* 50.28±0.459 *vs* 49.54±0.461 *vs* 53.21±0.462 *vs* 69.69±0.430 *vs* 59.28±0.4524	Shuffle *vs* recoding: Pre, $P < 0.001$, U=426905; Beh, $P < 0.001$, U=295332; Post, $P < 0.001$, U=368411. Recoding: Pre *vs* Beh, $P < 0.001$, W=169026; Pre *vs* post, $P < 0.001$, W=99728	1000/ 1000
S1Y	Four types of approach/approach (attack)/ aggression decoding accuracy in shuffle and recoding	Wilcoxon matched-pairs signed rank test; Mann-Whitney test	32.14±0.3121 *vs* 28.73±0.2895 *vs* 33.33±0.3439 *vs* 32.25±0.3133 *vs* 36.11±0.3128 *vs* 37.48±0.3372 *vs* 37.94±0.3342 *vs* 40.06±0.3119 *vs* 37.47±0.3275	Pre *vs* Beh, approach, $P < 0.001$, W=-112561; approach (attack), $P < 0.001$, W=122698; attack, $P < 0.001$, W=71717; Beh, approach *vs* approach (attack): $P < 0.001$, U=293364; approach *vs* attack: $P < 0.001$, U=389620	1000/ 1000
S1AA	Six types of aggression decoding accuracy in shuffle and recoding	Mann-Whitney test; Wilcoxon matched-pairs signed rank test	16.89±0.2094 *vs* 16.91±0.1726 *vs* 16.48±0.1975 *vs* 30.06±0.2411 *vs* 31.49±0.2483 *vs* 29.53±0.2447	Shuffle *vs* recoding: Pre, $P < 0.001$, U=98544; Beh, $P < 0.001$, U=61998; Post, $P < 0.001$, U=95592. Recoding: Pre *vs* Beh, $P < 0.001$, W=63543; Pre *vs* post, $P < 0.001$, W=-27648	1000/ 1000
S2I	The Peak ΔF/F of GCaMP6m in various stimuli	Wilcoxon matched-pairs signed rank test; Paired t-test	5.886±0.9575 *vs* 2.931±0.2572 *vs* 4.023±0.7258 *vs* 5.218±0.8725 *vs* 6.156±0.9221 *vs* 5.472±0.7139 *vs* 14.29±1.119 *vs* 28.86±2.026 *vs* 26.08±2.221	$P = 0.0089$, t=2.718 df=51; $P = 0.1174$,W=-2379; $P = 0.0028$, t=3.371 df=22; $P = 0.0128$, W=239; $P = 0.0044$, W=356; $P < 0.001$, t=6.689 df=56; $P < 0.001$, W=794; $P < 0.001$, W=820; $P < 0.001$, t=9.605 df=39	52/260/2 3/30/36/ 57/40/40 /40 trials
S2I	AUC per second of GCaMP6m in various stimuli	Wilcoxon matched-pairs signed rank test; Paired t-test	0.02068±0.00835 *vs* 0.00561±0.0021*vs* 0.01227±0.00637 *vs* 0.01569±0.0076 *vs* 0.02665±0.0080 *vs* 0.0323±0.0060 *vs* 0.0651±0.0099 *vs* 0.1915±0.0201 *vs* 0.2002±0.01385	$P = 0.5122$,W=-146; $P = 0.0329$,W=-522; $P = 0.8124$, t= 0.2402 df=22; $P = 0.1057$, W=-753; $P = 0.0363$, W=266; $P = 0.1089$, W=405; $P < 0.001$, W=794; $P < 0.001$, W=820; $P < 0.001$, t=4.645, df=39	52/260/2 3/30/36/ 57/40/40 /40 trials
S2O	The Peak ΔF/F of GCaMP6m in various threats	Wilcoxon matched-pairs signed rank test; Paired t-test; Mann-Whitney test	1.831±0.4328 *vs* 6.403±1.025 *vs* 3.031±0.5995 *vs* 10.49±1.193 *vs* 5.142±1.067 *vs* 19.34±1.814 *vs* 6.119±1.420 *vs* 28.77±2.060 *vs* 3.530±0.6563 *vs* 27.10±2.553	Versus baseline ($P < 0.001$, W=931; $P < 0.001$, W=752; $P < 0.001$, W=726; $P < 0.001$, W=1711; $P < 0.001$, t=8.744, df=27); female *vs* object: $P = 0.005$, U=681; male *vs* female: $P < 0.001$, U=377; male CD-1 *vs* male: $P = 0.004$, U=743; male attack *vs* male: $P = 0.0203$, U=364	53/53/39 /39/39/3 9/58/58/ 28/28 trials
S2O	AUC per second of GCaMP6m in various threats	Wilcoxon matched-pairs signed rank test; Paired t-test; Mann-Whitney test	-0.00078±0.00347 *vs* 0.02357±0.0069 *vs* 0.00204±0.0051 *vs* 0.05571±0.00819 *vs* 0.01166±0.0074 *vs* 0.0936±0.0107 *vs* 0.02065±0.00653 *vs* 0.1813±0.01490 *vs* 0.00253±0.00512 *vs* 0.1310±0.01195	Versus baseline ($P < 0.001$, W=951; $P < 0.001$, t=7.672, df=38; $P < 0.001$, W=676; $P < 0.001$, W=1711; $P < 0.001$, t=10.59 df=27); female *vs* object: $P = 0.007$, U=694; male *vs* female: $P = 0.0083$, U=498; male CD-1 *vs* male: $P = 0.0001$, U=613; male attack *vs* male: $P = 0.0337$, U=379	53/53/39 /39/39/3 9/58/58/ 28/28 trials
S3H	Thy1 *vs* CaMKIIα *vs* GAD67	Kruskal-Wallis test	87.39±3.924 *vs* 74.63±6.663 *vs* 3.668±1.687	$P = 0.0001$; KW=11.65	5/5/6 mice
S3R	Pre-CNO vs CNO in mCherry Group, Latency(L), Duration(D), Events(E)	Paired t-test	L: 618.2±116.3 *vs* 547.1±140.4; D: 1.727±0.7234 *vs* 1.537±0.6903; E: 5.429±2.543 *vs* 3.857±1.752.	L: $P = 0.7146$; t= 0.3835 df=6; D: $P = 0.829$; t= 0.2256 df=6; E: $P = 0.5908$ t= 0.5678 df=6;	7/7 mice
S3R	Saline *vs* CNO in mCherry Group, Latency(L), Duration(D), Events(E)	Wilcoxon matched-pairs signed rank test	L: 672.9±146.6 *vs* 547.1±140.4; D: 0.9843±0.9497 *vs* 1.537±0.6903; E: 2±1.839 *vs* 3.857±1.752.	L: $P = 0.6250$; W=-5; D: $P = 0.6250$; W=5; E: $P = 0.6250$; W=5;	7/7 mice
S3R	Pre-CNO vs CNO in HM3D Group, Latency(L), Duration(D), Events(E)	Wilcoxon matched-pairs signed rank test	L: 827.7±63.13 *vs* 45.45±13.96; D: 0.076±0.05538 *vs* 11.09±3.925; E: 0.2±0.1333 *vs* 14.2±1.843.	L: $P = 0.0020$; W=-55; D: $P = 0.0020$; W=55; E: $P = 0.0020$; W=55;	10/10 mice
S3R	Saline *vs* CNO in HM3D Group, Latency(L), Duration(D), Events(E)	Wilcoxon matched-pairs signed rank test	L: 689.2±108.2 *vs* 45.45±13.96; D: 1.09±0.8137 *vs* 11.09±3.925; E: 1±0.5578 *vs* 14.2±1.843.	L: $P = 0.0020$; W=-55; D: $P = 0.0020$; W=45; E: $P = 0.0020$; W=55;	10/10 mice
S4F	5 Hz *vs* 10 Hz *vs* 20 Hz *vs* 40 Hz in ChR2 Group	Friedman test	0±0 *vs* 6.667±3.333 *vs* 34.44±11.68 *vs* 90±6.667	$P < 0.001$; FM= 23.80	9 mice
S4H	Pre *vs* Laser *vs* Post in ChR2 Group, Relative pupil size	Friedman test	1±0 *vs* 1.262±0.0666 *vs* 1.163±0.05992	$P < 0.001$; FM= 16.22	9 mice
S4I	Pre vs Laser vs Post in ChR2	Friedman test	15.41±6.22 *vs* 16.06±6.82 *vs*	$P = 0.7407$; FM= 0.7429	9 mice

	Group, Time in open arm		14.07±5.382		
S4J	Pre vs Laser vs Post in ChR2 Group, Time in center	Repeated one-way ANOVA	10.73±1.742 *vs* 11.16±3.204 *vs* 13.61±4.572	P = 0.7599; F (1.608, 12.87) = 0.2183	9 mice
S4L	Latency to the nest	Friedman test	12.34±1.016 *vs* 13.65±0.658 *vs* 10.34±1.031	P = 0.0721; FM=5.333	6 mice
S4N	averaged velocity in each photostimulation period	Repeated one-way ANOVA	0.034±0.004 *vs* 0.02467±0.004 *vs* 0.028±0.003	P = 0.3379; F (1.379, 6.896) = 1.181	6 mice
S4O	velocity in the pre, during, post-laser period	Repeated one-way ANOVA	0.03532±0.0035 *vs* 0.02898±0.0015 *vs* 0.026±0.003	P = 0.0875; F (1.557, 7.783) = 3.539	6 mice
S4T	Pre *vs* Laser *vs* Post in ChR2 Group, Possibility of trials showing aggression(P), Latency(L), Duration(D), Events(E)	Friedman test	P: 0±0 *vs* 65.33±4.802 *vs* 0±0; L: 15±0 *vs* 4.179±2.351 *vs* 15±0; D: 0±0 *vs* 3.755±0.7100 *vs* 0±0; E: 0±0 *vs* 2.670±0.3224 *vs* 0±0	P: P < 0.001; FM=29.39; L: P < 0.001; FM=29.39; D: P < 0.001; FM=29.39; E: P < 0.001; FM=29.39.	15 mice
S4T	Laser in mCherry and ChR2 Group, Possibility of trials showing aggression(P), Latency(L), Duration(D), Events(E)	Unpaired t-test; Wilcoxon matched-pairs signed rank test	P: 0±0 *vs* 65.33±4.802; L: 15±0 *vs* 4.179±2.351; D: 0±0 *vs* 3.755±0.7100; E: 0±0 *vs* 2.670±0.3224	P: P < 0.001; t=8.473, df=19; L: P < 0.001; t=11.10, df=19; D: P = 0.0313; W=21.00; E: P < 0.001; t=5.158, df=19.	15/6 mice
S5C	Pre *vs* Laser *vs* Post in ChR2 Group, Possibility of trials showing aggression(P), Latency(L), Duration(D), Events(E)	Repeated one-way ANOVA	P: 0±0 *vs* 76.58±7.523 *vs* 0±0; L: 15±0 *vs* 4.493±0.6313 *vs* 15±0; D: 0±0 *vs* 3.416±0.8304 *vs* 0±0; E: 0±0 *vs* 3.842±0.6689 *vs* 0±0	P: P < 0.001 F (1.000, 5.000) = 103.6; L: P < 0.001 F (1.000, 5.000) = 277.0; D: P = 0.0092 F (1.000, 5.000) = 16.92; E: P = 0.0022 F (1.000, 5.000) = 32.99	6 mice
S5D	Pre *vs* Laser *vs* Post in ChR2 Group, Possibility of trials showing aggression(P), Latency(L), Duration(D), Events(E)	Repeated one-way ANOVA	P: 0±0 *vs* 73.27±5.153 *vs* 0±0; L: 15±0 *vs*2.490±0.4068 *vs* 15±0; D: 0±0 *vs* 1.717±0.3525 *vs* 0±0; E: 0±0 *vs* 4.498±0.9287 *vs* 0±0	P: P < 0.001 F (1.000, 5.000) = 202.2; L: P < 0.001 F (1.000, 5.000) = 945.9; D: P = 0.0046 F (1.000, 5.000) = 23.71; E: P = 0.0047 F (1.000, 5.000) = 23.46	6 mice
S5E	Pre *vs* Laser *vs* Post in ChR2 Group, Possibility of trials showing aggression(P), Latency(L), Duration(D), Events(E)	Repeated one-way ANOVA	P: 0±0 *vs* 66.67±37.71 *vs* 0±0; L: 15±0 *vs*2.446±0.7965 *vs* 15±0; D: 0±0 *vs* 2.018±0.3606 *vs* 0±0; E: 0±0 *vs* 5.263±1.002 *vs* 0±0	P: P = 0.0168 F (1.000, 4.000) = 15.63; L: P < 0.001 F (1.000, 4.000) = 248.4; D: P = 0.0050 F (1.000, 4.000) = 31.31; E: P = 0.0063 F (1.000, 4.000) = 27.59	5 mice
S5H	Pre-CNO *vs* CNO in HM3D Group, Latency(L), Duration(D), Events(E)	Wilcoxon matched-pairs signed rank test and Paired t-test	L: 900±0 *vs* 174.0±124.9; D: 0±0 *vs* 38.17±5.125; E: 0±0 *vs* 28.33±4.153;	L: P = 0.0313 W=-21; D: P < 0.001 t=7.447, df=5; E: P = 0.001 t=6.823, df=5	6/6 mice
S5I	Pre- CNO *vs* CNO in HM3D Group, Latency(L), Duration(D), Events(E)	Paired t-test	L: 900±0 *vs* 204.4±62.88; D: 0±0 *vs* 7.403±1.901; E: 0±0 *vs* 12.25±3.564;	L: P < 0.001 t=11.06 df=4; D: P = 0.0176 t=3.895 df=4; E: P = 0.0264 t=3.437, df=4	5/5 mice
S5J	Pre- CNO *vs* CNO in HM3D Group, Latency(L), Duration(D), Events(E)	Wilcoxon matched-pairs signed rank test and Paired t-test	L: 900±0 *vs* 171.4±108.5; D: 0±0 *vs* 8.995±2.944; E: 0±0 *vs* 10.28±2.092;	L: P = 0.0625 W=-15; D: P = 0.0378 t=3.056, df=4; E: P = 0.0625 W=15;	5/5 mice
S6F	Pre *vs* Laser *vs* Post in ChR2 Group, Possibility of trials showing aggression(P), Latency(L), Duration(D), Events(E)	Friedman test; Repeated one-way ANOVA	P: 0±0 *vs* 90.00±10.00 *vs* 0±0; L: 15±0 *vs* 2.347±0.2823 *vs* 15±0; D: 0±0 *vs* 3.672±1.078 *vs* 0±0; E: 0±0 *vs* 1.200±0.200 *vs* 0±0	P: P = 0.123; FM=10; L: P < 0.001; F (1.000, 4.000) = 2009; D: P = 0.0271; F (1.000, 4.000) = 11.61; E: P = 0.123; FM=10.	5 mice
S6F	Laser in mCherry and ChR2 Group, Possibility of trials showing aggression(P), Latency(L), Duration(D), Events(E)	Mann-Whitney test; Unpaired t-test	P: 0±0 *vs* 90.00±10.00; L:15±0 *vs* 2.347±0.2823; D:0±0 *vs* 3.672±1.078; E: 0±0 *vs* 1.200±0.200	P: P = 0.0022; U= 0; L: P < 0.001; t=49.65, df=9; D:P = 0.0044; t=3.774, df=9; E: P = 0.0022; U= 0.	6/5 mice
S6H	Pre *vs* Laser *vs* Post in ChR2 Group, Possibility of trials showing aggression	Repeated one-way ANOVA or Friedman test	Values of the 1st-12nd column: 90±10 *vs* 83.33±4.167 *vs* 76.39±6.056 *vs* 80±12.65 *vs* 44±11.66 *vs* 92±8 *vs* 77.33±9.333 *vs* 80±12.65 *vs* 61.91±12.28 *vs* 76.00±14.70 *vs* 60.67±16.94 *vs* 88.75±4.146		5/3/3/5/5 /5/5/5/6/ 5/5/4 mice
S6I	Pre *vs* Laser *vs* Post in ChR2 Group, Latency to attack onset	Repeated one-way ANOVA or Friedman test	Values of the 1st-12nd column: 2.347±0.2823 *vs* 5.423±0.8551 *vs* 4.632±1.041 *vs* 2.256±10.5129 *vs* 4.849±1.699 *vs* 2.566±0.3001 *vs* 1.801±0.3906 *vs* 3.011±0.5467 *vs* 8.169±1.244 *vs* 2.917±0.2879 *vs* 3.564±0.7097 *vs* 4.008±1.028		5/3/3/5/5 /5/5/5/6/ 5/5/4 mice
S6J	Pre *vs* Laser *vs* Post in ChR2 Group, Attack duration	Repeated one-way ANOVA or Friedman test	Values of the 1st-12nd column: 3.672±1.078 *vs* 5.806±1.689 *vs* 5.511±2.350 *vs* 4.038±0.9196 *vs* 2.524±0.7988 *vs* 5.086±1.072 *vs* 3.233±1.815 *vs* 3.281±1.085 *vs* NT *vs* 3.403±2.160 *vs* 1.759±0.6263 *vs* 4.676±1.085		5/3/3/5/5 /5/5/5/6/ 5/5/4 mice
S6K	Pre *vs* Laser *vs* Post in ChR2 Group, Attack events	Repeated one-way ANOVA or Friedman test	Values of the 1st-12nd column: 1.200±0.2000 *vs* 1.292±0.1816 *vs* 1.278±0.3100 *vs* 1.240±0.1939 *vs* 1.000±0.00 *vs* 1.478±0.2655 *vs* 1.333±0.1430 *vs* 1.197±0.05753 *vs* NT *vs* 1.400±0.1716 *vs* 1.520±0.2871 *vs* 1.725±0.09735		5/5/5/5/5 /5/5/5/6/ 5/5/4 mice
S6P	Pre *vs* Laser *vs* Post in ChR2 Group, Possibility of trials showing aggression(P), Latency(L), Duration(D), Events(E)	Friedman test	P: 2.418±1.876 *vs* 46.24±5.130 *vs* 3.462±1.985; L: 14.90±0.09516 *vs* 4.676±0.7076 *vs* 14.64±0.1831; D: 0.1008±0.08410 *vs* 3.930±0.3019 *vs* 0.1199±0.06707; E: 0.04551±0.03419 *vs* 1.188±0.04542 *vs* 0.06291±0.03510	P: P = 0.0002; FM=15.08; L: P = 0.0001; FM=14.89; D: P = 0.0005; FM=14.30; E: P = 0.123; FM=10.	8 mice
S6P	Laser in mCherry and ChR2 Group, Possibility of trials showing aggression(P), Latency(L), Duration(D), Events(E)	Unpaired t-test	P: 0±0 *vs* 46.24±5.130; L: 15±0 *vs* 4.676±0.7076; D: 0±0 *vs* 3.930±0.3019; E: 0±0 *vs* 1.188±0.04542	P: P < 0.001; t=7.726, df=12; L: P < 0.001; t=12.50, df=12; D: P < 0.001; t=11.16, df=12; E: P < 0.001; t=22.41, df=12	6/8 mice
S6Q	Pre *vs* Laser *vs* Post in ChR2 Group, Possibility of trials showing aggression(P), Latency(L), Duration(D), Events(E)	Repeated one-way ANOVA	P: 0±0 *vs* 57.64±4.861 *vs* 0±0; L: 15±0 *vs* 3.944±0.8333 *vs* 15±0; D: 0±0 *vs* 6.861±2.613 *vs* 0±0; E: 0±0 *vs* 1.494±0.2042 *vs* 0±0	P: P = 0.0070; F (1.000, 2.000) = 140.6; L: P = 0.0056; F (1.000, 2.000) = 176.0; D: P = 0.0451; F (1.000, 2.000) = 20.68; E: P = 0.0182; F (1.000, 2.000) = 53.56.	3 mice

S7E	mCherry Group, Latency to attack	Wilcoxon matched-pairs signed rank test and Paired t-test	Pre-saline *vs* Saline *vs* Pre-CNO *vs* CNO: 76.83±29.76 *vs* 21.23±10.42 *vs* 7.017±4.198 *vs* 34.13±12.96	Pre-saline vs Saline: *P* = 0.1212 t=1.865, df=5; Pre-CNO vs CNO: *P* = 0.1250 W=13.00; Saline *vs* CNO: *P* = 0.4063 W=9.000;	6/6/6/6 mice
S7E	HM4D Group, Latency to attack	Wilcoxon matched-pairs signed rank test and Paired t-test	Pre-saline *vs* Saline *vs* Pre-CNO *vs* CNO: 112.3±57.78 *vs* 32.48±8.039 *vs* 22.91±7.128 *vs* 696.9±112.3	Pre-saline vs Saline: *P* = 0.171 t=1.525, df=7; Pre-CNO vs CNO: *P* = 0.0078 W=36.00; Saline *vs* CNO: *P* = 0.0078 W=36.00;	8/8/8/8 mice
S7E	mCherry Group, Duration of attack	Wilcoxon matched-pairs signed rank test and Paired t-test	Pre-saline *vs* Saline *vs* Pre-CNO *vs* CNO: 38.74±22.36 *vs* 40.26±21.74 *vs* 40.08±15.55 *vs* 26.06±10.31	Pre-saline vs Saline: *P* = 0.6004 t= 0.5589, df=5; Pre-CNO vs CNO: *P* = 0.1563 W=-15.00; Saline *vs* CNO: *P* = 0.5625 W=-7.000;	6/6/6/6 mice
S7E	HM4D Group, Duration of attack	Wilcoxon matched-pairs signed rank test and Paired t-test	Pre-saline *vs* Saline *vs* Pre-CNO *vs* CNO: 25.02±9.786 *vs* 13.29±3.847 *vs*20.4±5.443 *vs* 0.6363±0.3349	Pre-saline vs Saline: *P* = 0.1209 t=1.765, df=7; Pre-CNO vs CNO: *P* = 0.0078 W=-36.00; Saline *vs* CNO: *P* = 0.0078 W=-36.00;	8/8/8/8 mice
S7E	mCherry Group, Events of attack	Wilcoxon matched-pairs signed rank test and Paired t-test	Pre-saline *vs* Saline *vs* Pre-CNO *vs* CNO: 25.17±13.02 *vs* 32.83±15.61 *vs* 40.83±8.412 *vs* 30.83±8.976	Pre-saline vs Saline: *P* = 0.999 W=1; Pre-CNO vs CNO: *P* = 0.2662 t=1.251, df=5; Saline *vs* CNO: *P* = 0.9118 t= 0.1165, df=5;	6/6/6/6 mice
S7E	HM4D Group, Events of attack	Wilcoxon matched-pairs signed rank test and Paired t-test	Pre-saline *vs* Saline *vs* Pre-CNO *vs* CNO: 33.75±5.314 *vs* 21.75±4.225 *vs* 28.75±7.362 *vs* 1.625±0.9051	Pre-saline vs Saline: *P* = 0.0589 t=2.253, df=7; Pre-CNO vs CNO: *P* = 0.0078 W=-36.00; Saline *vs* CNO: *P* = 0.0078 W=-36.00;	8/8/8/8 mice
S7I	Number of induced action potentials at different injected current steps in CNO and control group	Paired t-test	Control *vs* CNO: 23±5.97216 *vs* 0.5±0.5; 34.5±6.98212 *vs* 1.75±1.03078; 44.5±7.55535 *vs* 4.5±2.02073; 49.25±7.40917 *vs* 10.75±3.19831; 54.75±6.93271 *vs* 14.5±3.52373; 58.5±7.35414 *vs* 22.75±5.006; 57.25±8.23989 *vs* 25.5±5.63471	*P* = 0.035, t=3.67016, df=3; *P* = 0.01968, t=4.56822, df=3; *P* = 0.01561, t=4.97416, df=3; *P* = 0.01299, t=5.31773, df=3; *P* = 0.0341, t=8.50516, df=3; *P* = 0.01502, t=5.04427, df=3; *P* = 0.02032, t=4.51379, df=3	8/8 neurons
S7J	Minimal injected current to induce action potential (APs) induced in CNO and control group	Paired t-test	control *vs* CNO: 60±7.55929 *vs* 110±11.33893	*P* = 0.002, t=5.3513, df=7	8/8 neurons

Figures 1-8

Figure 1

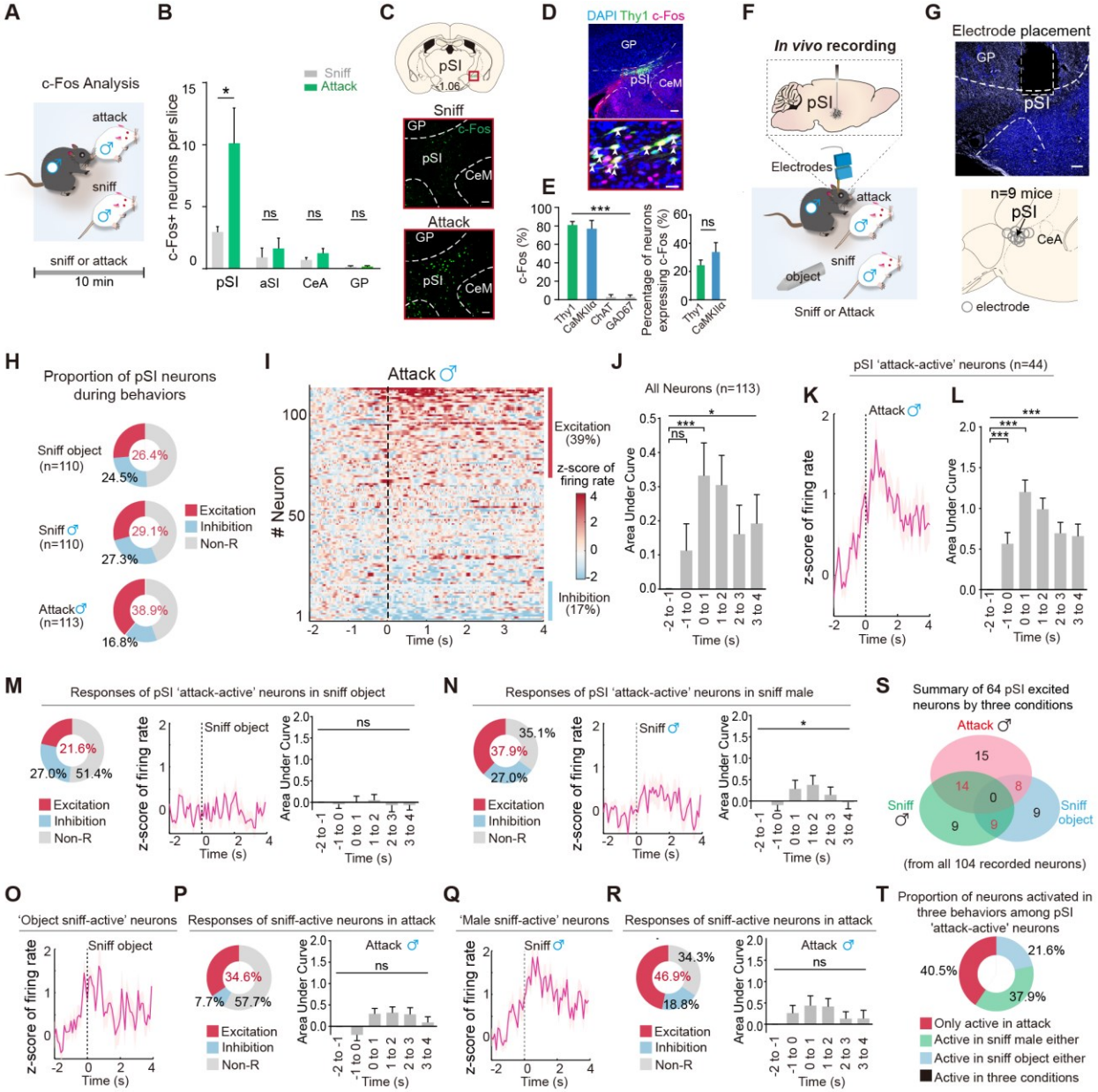

Figure 2

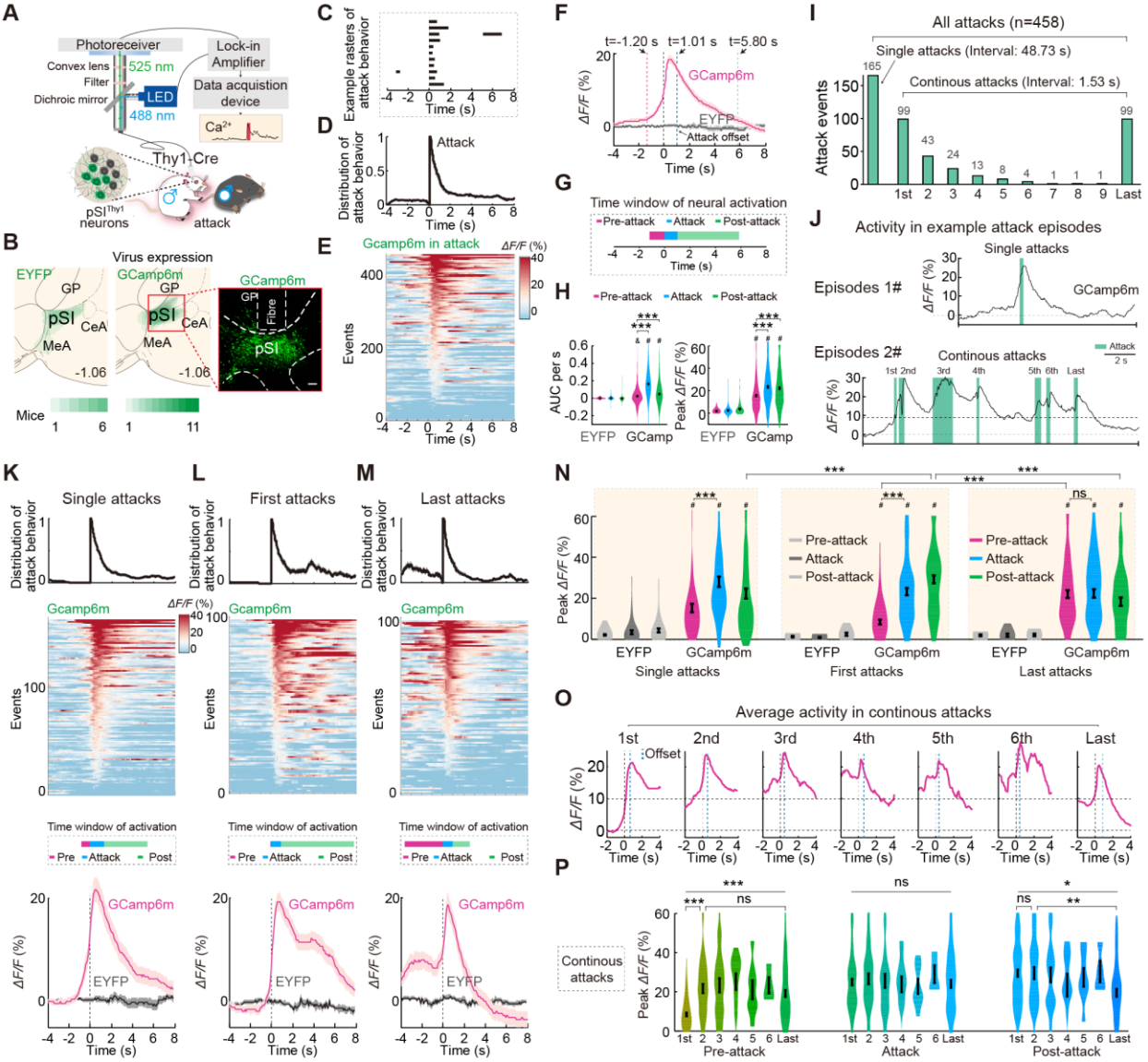

A
Photoreceiver
Convex lens
Filter
Dichroic mirror
525 nm
LED
488 nm
Lock-in Amplifier
Data acquistion device
Ca2+
Thy1-Cre
pSI Thy1 neurons
attack
B
Virus expression
EYFP
GCamp6m
GP
pSI
CeA
MeA
-1.06
Fibre
Mice
C
Example rasters of attack behavior
Time (s)
D
Distribution of attack behavior
Attack
E
Gcamp6m in attack
ΔF/F (%)
Events
F
t=-1.20 s
t=1.01 s
t=5.80 s
GCamp6m
EYFP
Attack offset
ΔF/F (%)
G
Time window of neural activation
Pre-attack
Attack
Post-attack
H
AUC per s
Peak ΔF/F (%)
EYFP
GCamp
I
All attacks (n=458)
Single attacks (Interval: 48.73 s)
Continous attacks (Interval: 1.53 s)
Attack events
1st
Last
J
Activity in example attack episodes
Single attacks
Episodes 1#
Episodes 2#
Continous attacks
Attack
2 s
K
Single attacks
L
First attacks
M
Last attacks
Distribution of attack behavior
Time window of activation
Pre
Post
N
Peak ΔF/F (%)
Single attacks
First attacks
Last attacks
O
Average activity in continous attacks
Offset
P
Continous attacks
Pre-attack
Attack
Post-attack

Figure 3

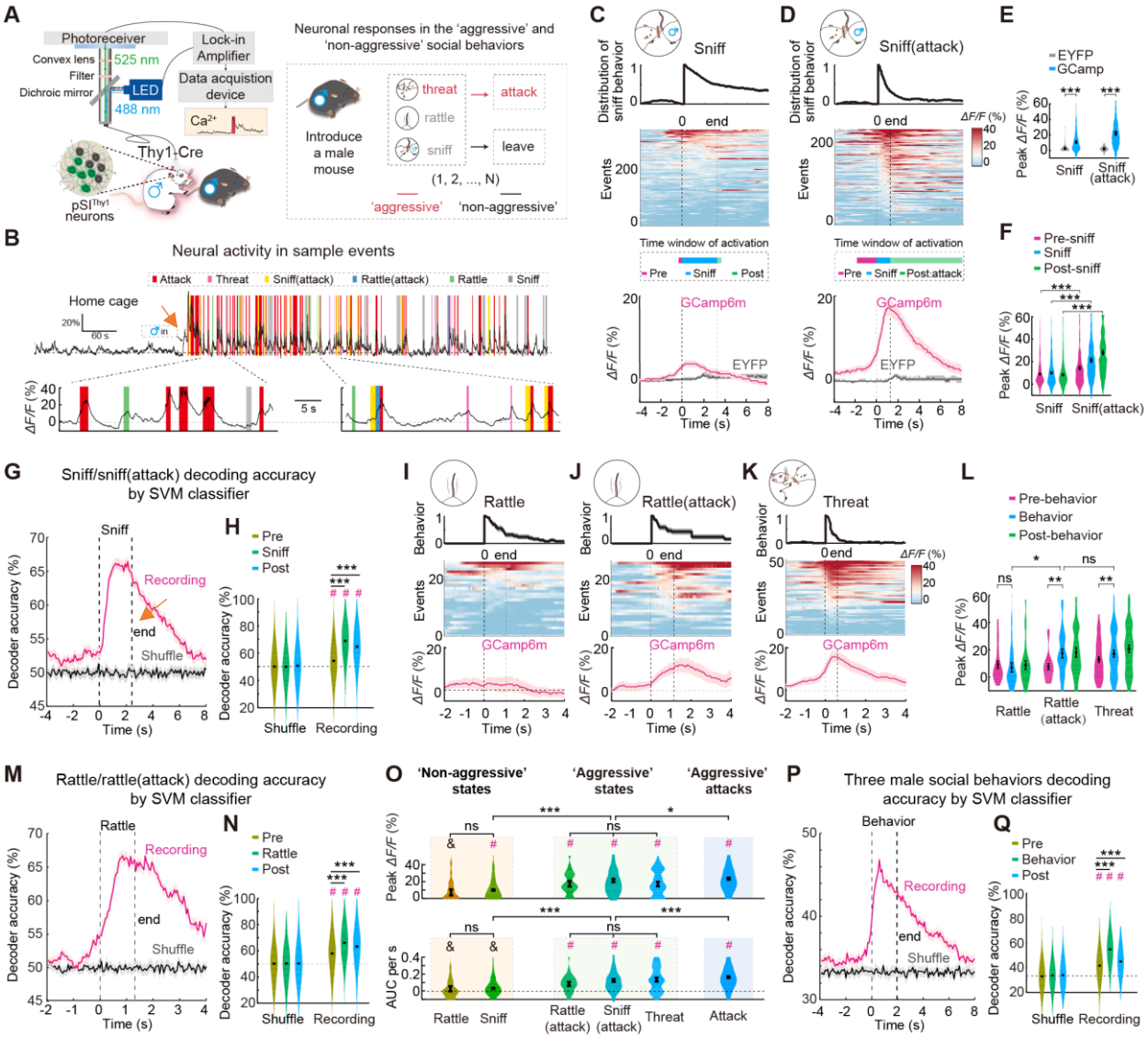
A
Photoreceiver
Convex lens
Filter
Dichroic mirror
525 nm
LED
488 nm
Lock-in Amplifier
Data acquistion device
Ca2+
Thy1-Cre
pSI Thy1 neurons
Neuronal responses in the 'aggressive' and 'non-aggressive' social behaviors
Introduce a male mouse
threat
rattle
sniff
attack
leave
(1, 2, ..., N)
'aggressive'
'non-aggressive'
B
Neural activity in sample events
Attack
Threat
Sniff(attack)
Rattle(attack)
Rattle
Sniff
Home cage
20%
60 s
in
ΔF/F (%)
5 s
C
Sniff
Distribution of sniff behavior
0 end
Events
Time window of activation
Pre
Sniff
Post
GCamp6m
EYFP
ΔF/F (%)
Time (s)
D
Sniff(attack)
Post-attack
ΔF/F (%)
E
EYFP
GCamp
Peak ΔF/F (%)
Sniff
Sniff (attack)
F
Pre-sniff
Sniff
Post-sniff
Sniff(attack)
G
Sniff/sniff(attack) decoding accuracy by SVM classifier
Decoder accuracy (%)
Recording
Shuffle
end
H
Pre
Sniff
Post
Shuffle
Recording
I
Rattle
Behavior
J
Rattle(attack)
K
Threat
L
Pre-behavior
Behavior
Post-behavior
ns
Rattle
Rattle (attack)
Threat
M
Rattle/rattle(attack) decoding accuracy by SVM classifier
N
Pre
Rattle
Post
O
'Non-aggressive' states
'Aggressive' states
'Aggressive' attacks
Peak ΔF/F (%)
AUC per s
Rattle
Sniff
Rattle (attack)
Sniff (attack)
Threat
Attack
P
Three male social behaviors decoding accuracy by SVM classifier
Behavior
Q
Pre
Behavior
Post
Shuffle
Recording

Figure 4

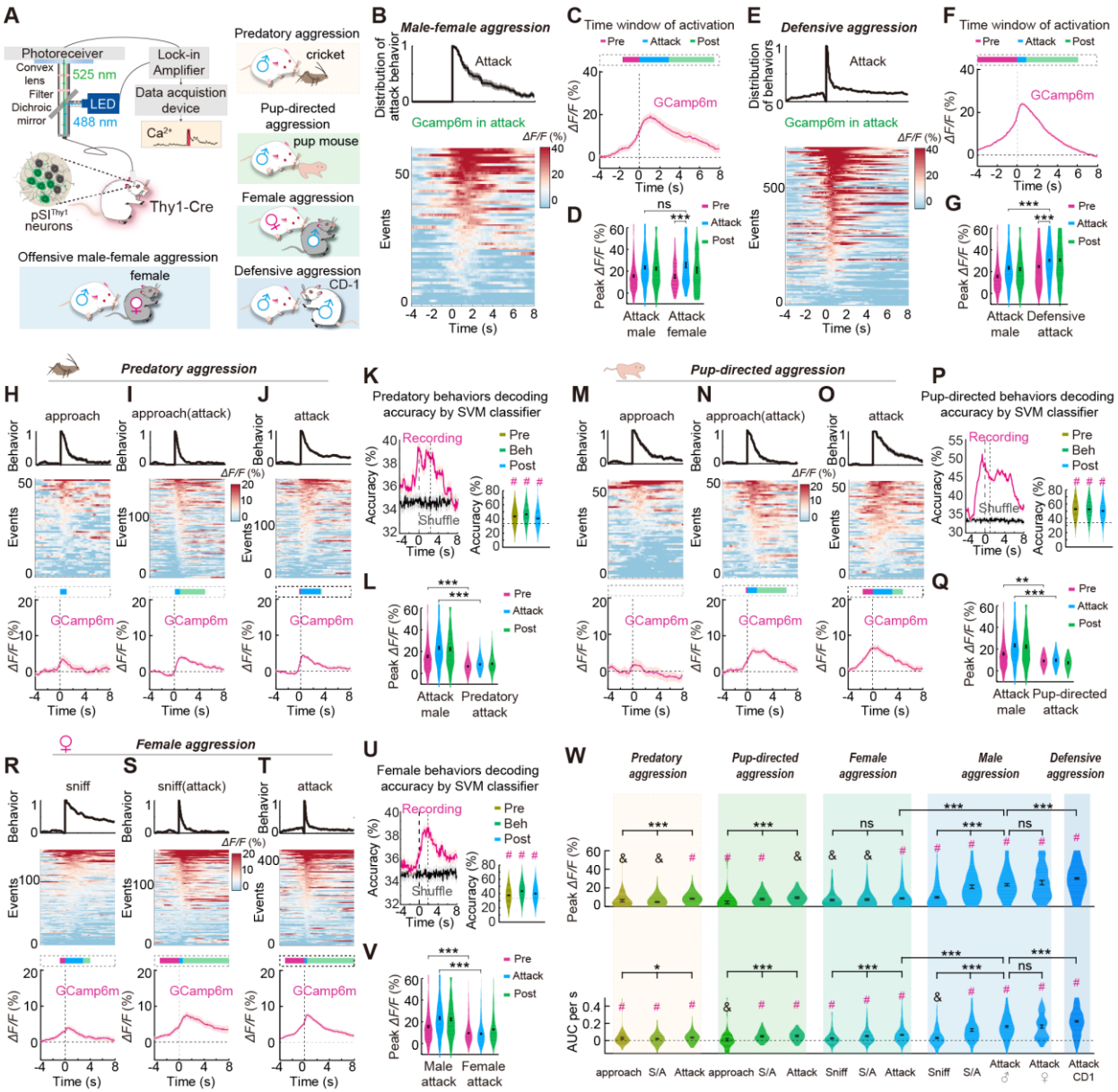
A
Photoreceiver
Convex lens
525 nm
Filter
Dichroic mirror
LED
488 nm
Lock-in Amplifier
Data acquistion device
Ca2+
pSI Thy1 neurons
Thy1-Cre
Offensive male-female aggression
female
Predatory aggression
cricket
Pup-directed aggression
pup mouse
Female aggression
Defensive aggression
CD-1
B
Male-female aggression
Distribution of attack behavior
Attack
Gcamp6m in attack
Events
Time (s)
C
Time window of activation
Pre
Attack
Post
GCamp6m
ΔF/F (%)
Time (s)
D
Peak ΔF/F (%)
ns
***
Attack male
Attack female
E
Defensive aggression
Distribution of behaviors
Attack
Gcamp6m in attack
F
Time window of activation
G
Attack male
Defensive attack
Predatory aggression
H approach
I approach(attack)
J attack
Behavior
Events
GCamp6m
K
Predatory behaviors decoding accuracy by SVM classifier
Recording
Shuffle
Accuracy (%)
L
Attack male
Predatory attack
Pup-directed aggression
M approach
N approach(attack)
O attack
P
Pup-directed behaviors decoding accuracy by SVM classifier
Q
Attack male
Pup-directed attack
Female aggression
R sniff
S sniff(attack)
T attack
U
Female behaviors decoding accuracy by SVM classifier
V
Male attack
Female attack
W
Predatory aggression
Pup-directed aggression
Female aggression
Male aggression
Defensive aggression
Peak ΔF/F (%)
AUC per s
approach
S/A
Attack
Sniff
Attack ♂
Attack ♀
Attack CD1

Figure 5

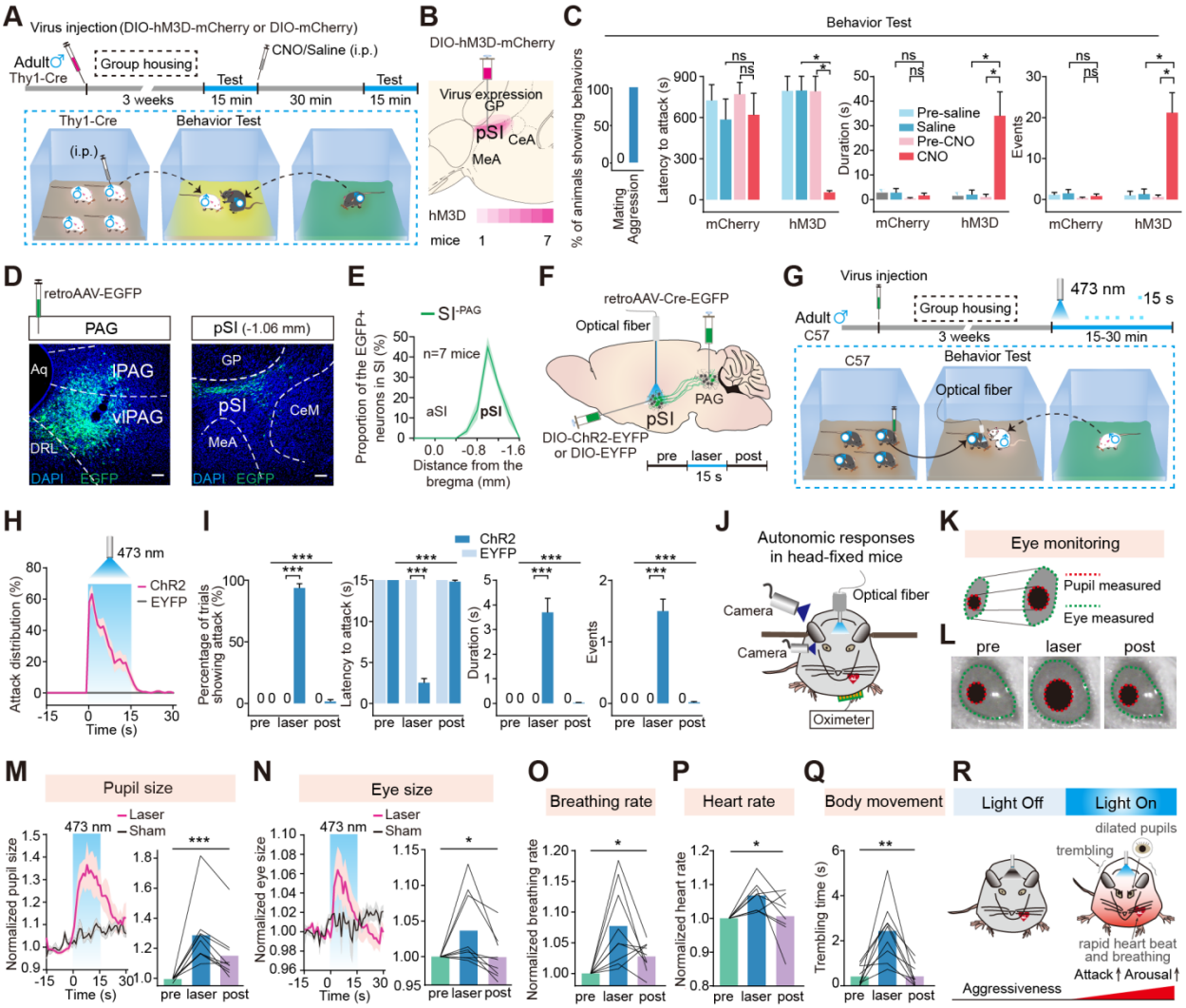
A
Virus injection (DIO-hM3D-mCherry or DIO-mCherry)
Adult♂
Thy1-Cre
Group housing
CNO/Saline (i.p.)
Test
Test
3 weeks
15 min
30 min
15 min
Thy1-Cre
Behavior Test
(i.p.)
B
DIO-hM3D-mCherry
Virus expression
GP
pSI
CeA
MeA
hM3D
mice 1 7
C
Behavior Test
% of animals showing behaviors
Mating
Aggression
Latency to attack (s)
Duration (s)
Events
Pre-saline
Saline
Pre-CNO
CNO
ns
*
mCherry
hM3D
D
retroAAV-EGFP
PAG
pSI (-1.06 mm)
Aq
lPAG
vlPAG
DRL
GP
pSI
CeM
MeA
DAPI EGFP
E
SI-PAG
n=7 mice
aSI
pSI
Proportion of the EGFP+ neurons in SI (%)
Distance from the bregma (mm)
F
retroAAV-Cre-EGFP
Optical fiber
PAG
pSI
DIO-ChR2-EYFP or DIO-EYFP
pre
laser
post
15 s
G
Virus injection
473 nm
15 s
Adult♂
C57
Group housing
3 weeks
15-30 min
C57
Behavior Test
Optical fiber
H
473 nm
ChR2
EYFP
Attack distribution (%)
Time (s)
I
ChR2
EYFP
Percentage of trials showing attack (%)
Latency to attack (s)
Duration (s)
Events
pre laser post
J
Autonomic responses in head-fixed mice
Camera
Camera
Optical fiber
Oximeter
K
Eye monitoring
Pupil measured
Eye measured
L
pre
laser
post
M
Pupil size
473 nm
Laser
Sham
Normalized pupil size
Time (s)
pre laser post
N
Eye size
473 nm
Laser
Sham
Normalized eye size
Time (s)
pre laser post
O
Breathing rate
Normalized breathing rate
pre laser post
P
Heart rate
Normalized heart rate
pre laser post
Q
Body movement
Trembling time (s)
pre laser post
R
Light Off
Light On
dilated pupils
trembling
rapid heart beat and breathing
Attack↑ Arousal↑
Aggressiveness

Figure 6

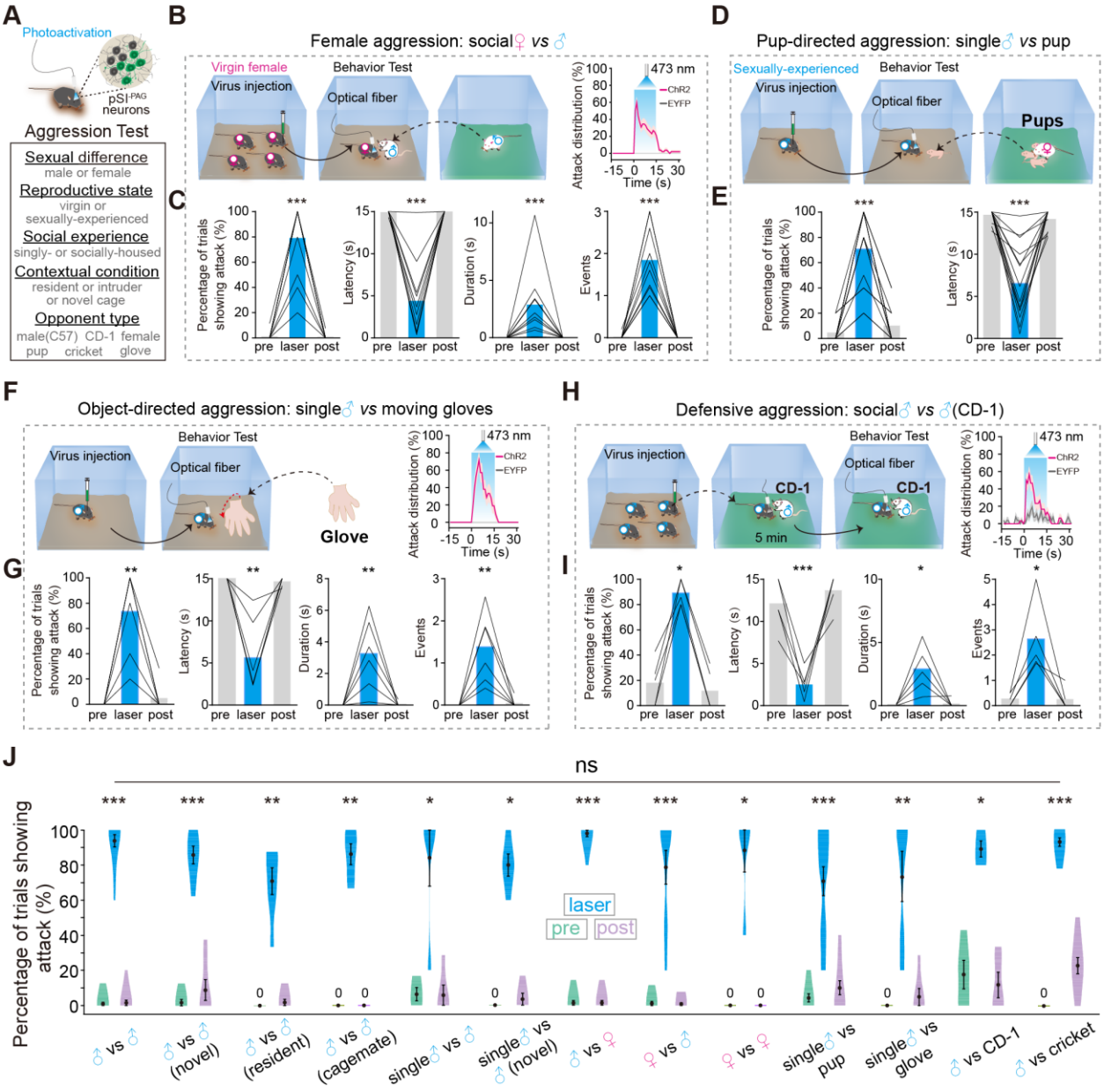
A
Photoactivation
pSI-PAG neurons
Aggression Test
Sexual difference
male or female
Reproductive state
virgin or sexually-experienced
Social experience
singly- or socially-housed
Contextual condition
resident or intruder or novel cage
Opponent type
male(C57) CD-1 female
pup cricket glove
B
Female aggression: social♀ vs ♂
Virgin female
Virus injection
Behavior Test
Optical fiber
473 nm
ChR2
EYFP
Attack distribution (%)
Time (s)
C
Percentage of trials showing attack (%)
Latency (s)
Duration (s)
Events
pre laser post
D
Pup-directed aggression: single♂ vs pup
Sexually-experienced
Virus injection
Behavior Test
Optical fiber
Pups
E
F
Object-directed aggression: single♂ vs moving gloves
Virus injection
Behavior Test
Optical fiber
Glove
G
H
Defensive aggression: social♂ vs ♂(CD-1)
Virus injection
Behavior Test
Optical fiber
CD-1
5 min
I
J
ns
laser
pre
post
Percentage of trials showing attack (%)
♂ vs ♂
♂ vs ♂ (novel)
♂ vs ♂ (resident)
♂ vs ♂ (cagemate)
single♂ vs ♂
single♂ vs ♂ (novel)
♂ vs ♀
♀ vs ♂
♀ vs ♀
single♂ vs pup
single♂ vs glove
♂ vs CD-1
♂ vs cricket

Figure 7

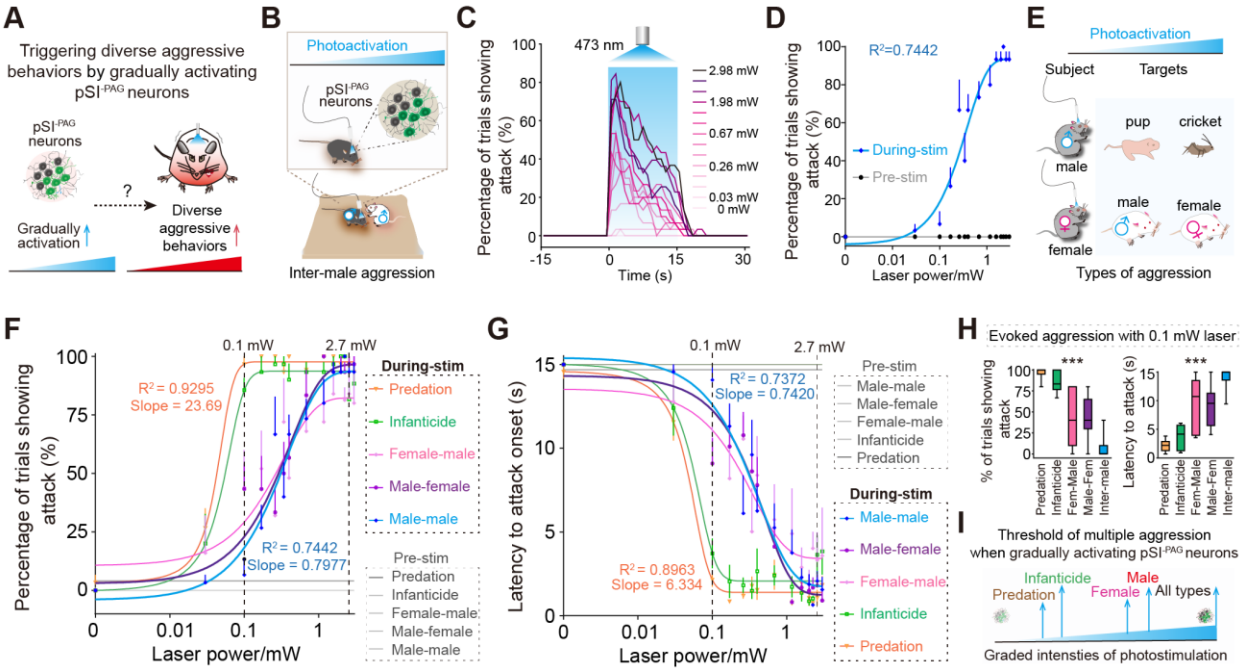
A
Triggering diverse aggressive behaviors by gradually activating pSI-PAG neurons
pSI-PAG neurons
?
Diverse aggressive behaviors
Gradually activation
B
Photoactivation
pSI-PAG neurons
Inter-male aggression
C
473 nm
2.98 mW
1.98 mW
0.67 mW
0.26 mW
0.03 mW
0 mW
Percentage of trials showing attack (%)
Time (s)
D
R²=0.7442
During-stim
Pre-stim
Percentage of trials showing attack (%)
Laser power/mW
E
Photoactivation
Subject
Targets
male
female
pup
cricket
male
female
Types of aggression
F
0.1 mW
2.7 mW
R² = 0.9295
Slope = 23.69
R² = 0.7442
Slope = 0.7977
During-stim
Predation
Infanticide
Female-male
Male-female
Male-male
Pre-stim
Predation
Infanticide
Female-male
Male-female
Male-male
Percentage of trials showing attack (%)
Laser power/mW
G
0.1 mW
2.7 mW
R² = 0.7372
Slope = 0.7420
R² = 0.8963
Slope = 6.334
Pre-stim
Male-male
Male-female
Female-male
Infanticide
Predation
During-stim
Male-male
Male-female
Female-male
Infanticide
Predation
Latency to attack onset (s)
Laser power/mW
H
Evoked aggression with 0.1 mW laser
***
***
% of trials showing attack
Latency to attack (s)
Predation
Infanticide
Fem-Male
Male-Fem
Inter-male
I
Threshold of multiple aggression when gradually activating pSI-PAG neurons
Infanticide
Predation
Male
Female
All types
Graded intensities of photostimulation

Figure 8

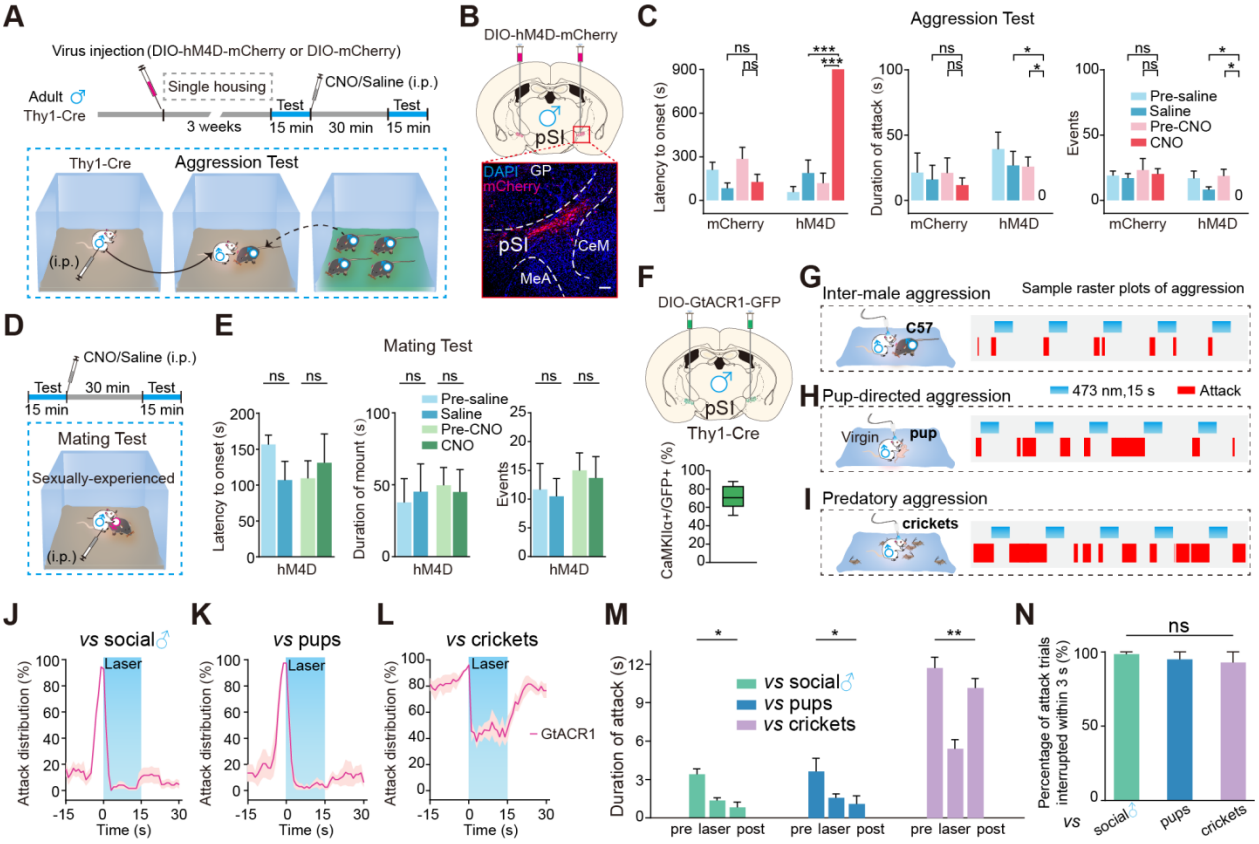
A
Virus injection (DIO-hM4D-mCherry or DIO-mCherry)
Single housing
CNO/Saline (i.p.)
Adult ♂
Thy1-Cre
3 weeks
Test
15 min
30 min
15 min
Thy1-Cre
Aggression Test
(i.p.)
B
DIO-hM4D-mCherry
pSI
DAPI GP
mCherry
pSI
CeM
MeA
C
Aggression Test
Latency to onset (s)
Duration of attack (s)
Events
Pre-saline
Saline
Pre-CNO
CNO
mCherry
hM4D
D
CNO/Saline (i.p.)
Test
30 min
Test
15 min
15 min
Mating Test
Sexually-experienced
(i.p.)
E
Mating Test
Latency to onset (s)
Duration of mount (s)
Events
Pre-saline
Saline
Pre-CNO
CNO
hM4D
F
DIO-GtACR1-GFP
pSI
Thy1-Cre
CaMKIIα+/GFP+ (%)
G
Inter-male aggression
Sample raster plots of aggression
C57
H
Pup-directed aggression
473 nm,15 s
Attack
Virgin
pup
I
Predatory aggression
crickets
J
vs social♂
Laser
Attack distribution (%)
Time (s)
K
vs pups
Laser
L
vs crickets
Laser
GtACR1
M
Duration of attack (s)
vs social♂
vs pups
vs crickets
pre laser post
N
Percentage of attack trials interrupted within 3 s (%)
vs social♂
pups
crickets

Figures S1-S8

Figure S1

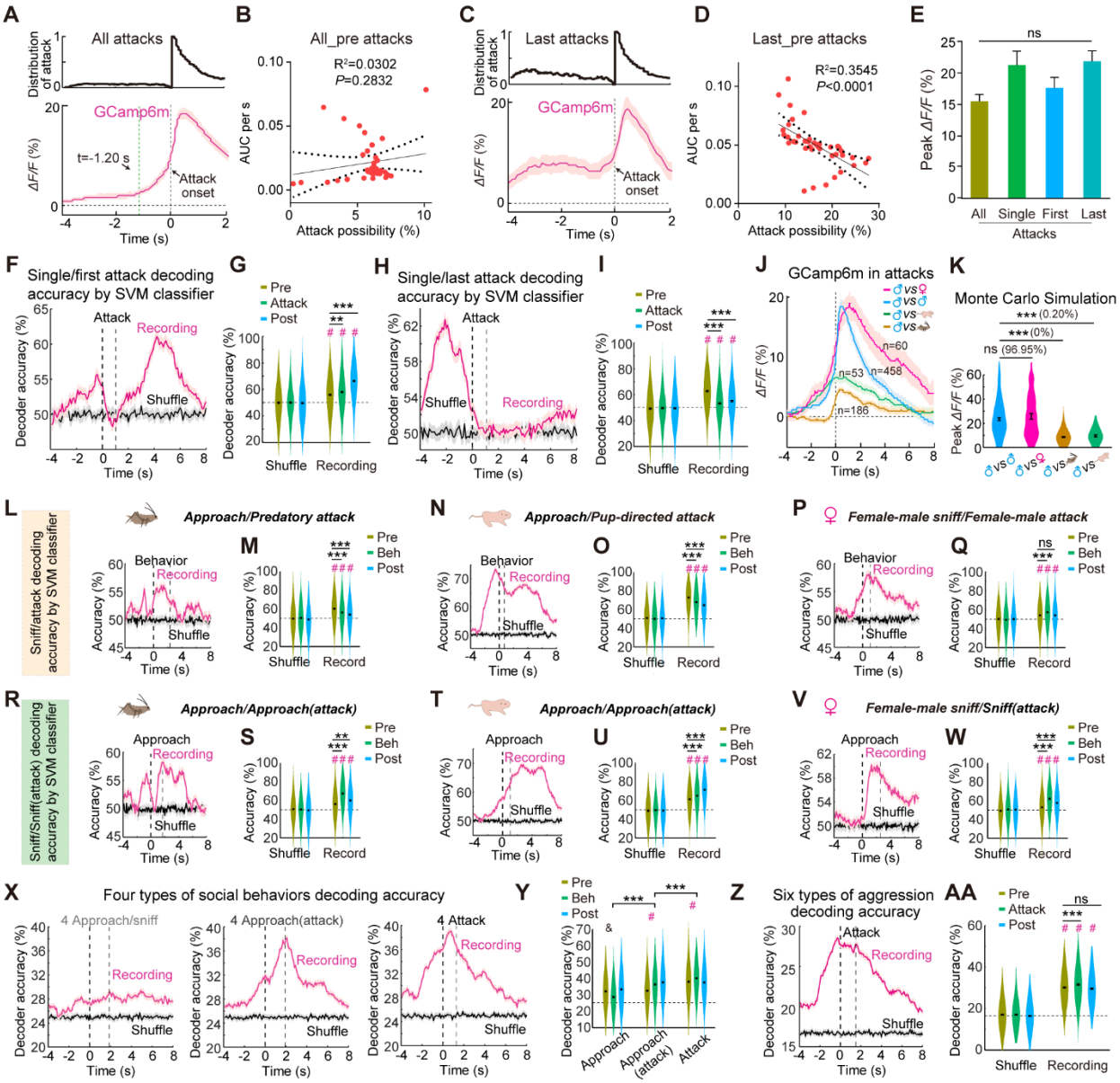

Figure S2

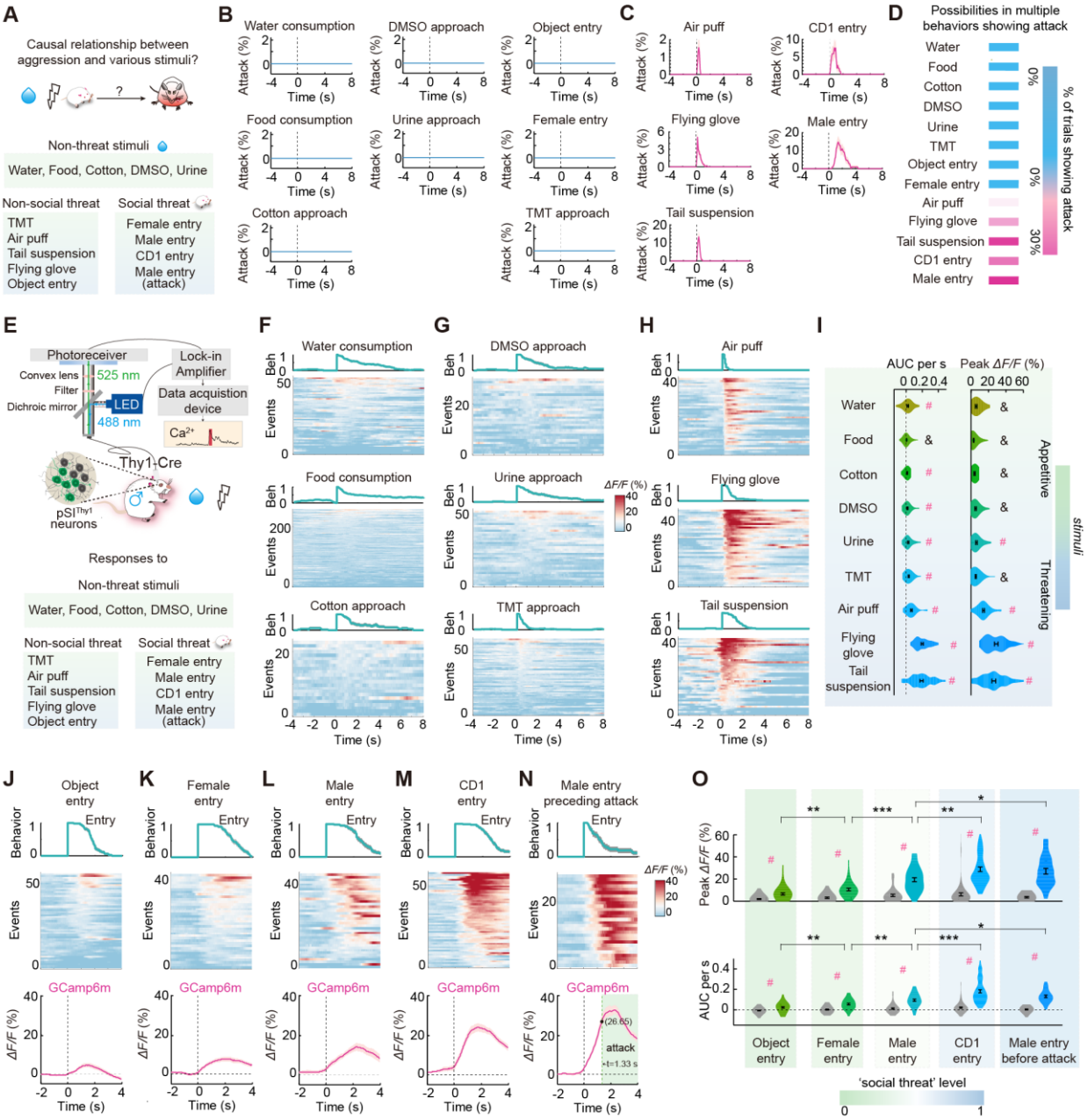
A
Causal relationship between aggression and various stimuli?
Non-threat stimuli
Water, Food, Cotton, DMSO, Urine
Non-social threat
TMT
Air puff
Tail suspension
Flying glove
Object entry
Social threat
Female entry
Male entry
CD1 entry
Male entry (attack)
B
Water consumption
DMSO approach
Object entry
Food consumption
Urine approach
Female entry
Cotton approach
TMT approach
C
Air puff
CD1 entry
Flying glove
Male entry
Tail suspension
Attack (%)
Time (s)
D
Possibilities in multiple behaviors showing attack
% of trials showing attack
E
Photoreceiver
Convex lens
Filter
Dichroic mirror
525 nm
LED
488 nm
Lock-in Amplifier
Data acquistion device
Ca2+
Thy1-Cre
pSI Thy1 neurons
Responses to
Non-threat stimuli
Water, Food, Cotton, DMSO, Urine
Non-social threat
TMT
Air puff
Tail suspension
Flying glove
Object entry
Social threat
Female entry
Male entry
CD1 entry
Male entry (attack)
F
Water consumption
Food consumption
Cotton approach
G
DMSO approach
Urine approach
TMT approach
H
Air puff
Flying glove
Tail suspension
Beh
Events
ΔF/F (%)
Time (s)
I
AUC per s
Peak ΔF/F (%)
Water
Food
Cotton
DMSO
Urine
TMT
Air puff
Flying glove
Tail suspension
Appetitive
Threatening
stimuli
J
Object entry
K
Female entry
L
Male entry
M
CD1 entry
N
Male entry preceding attack
Behavior
Entry
Events
GCamp6m
ΔF/F (%)
Time (s)
(26.65)
attack
t=1.33 s
O
Peak ΔF/F (%)
AUC per s
Object entry
Female entry
Male entry
CD1 entry
Male entry before attack
'social threat' level

Figure S3

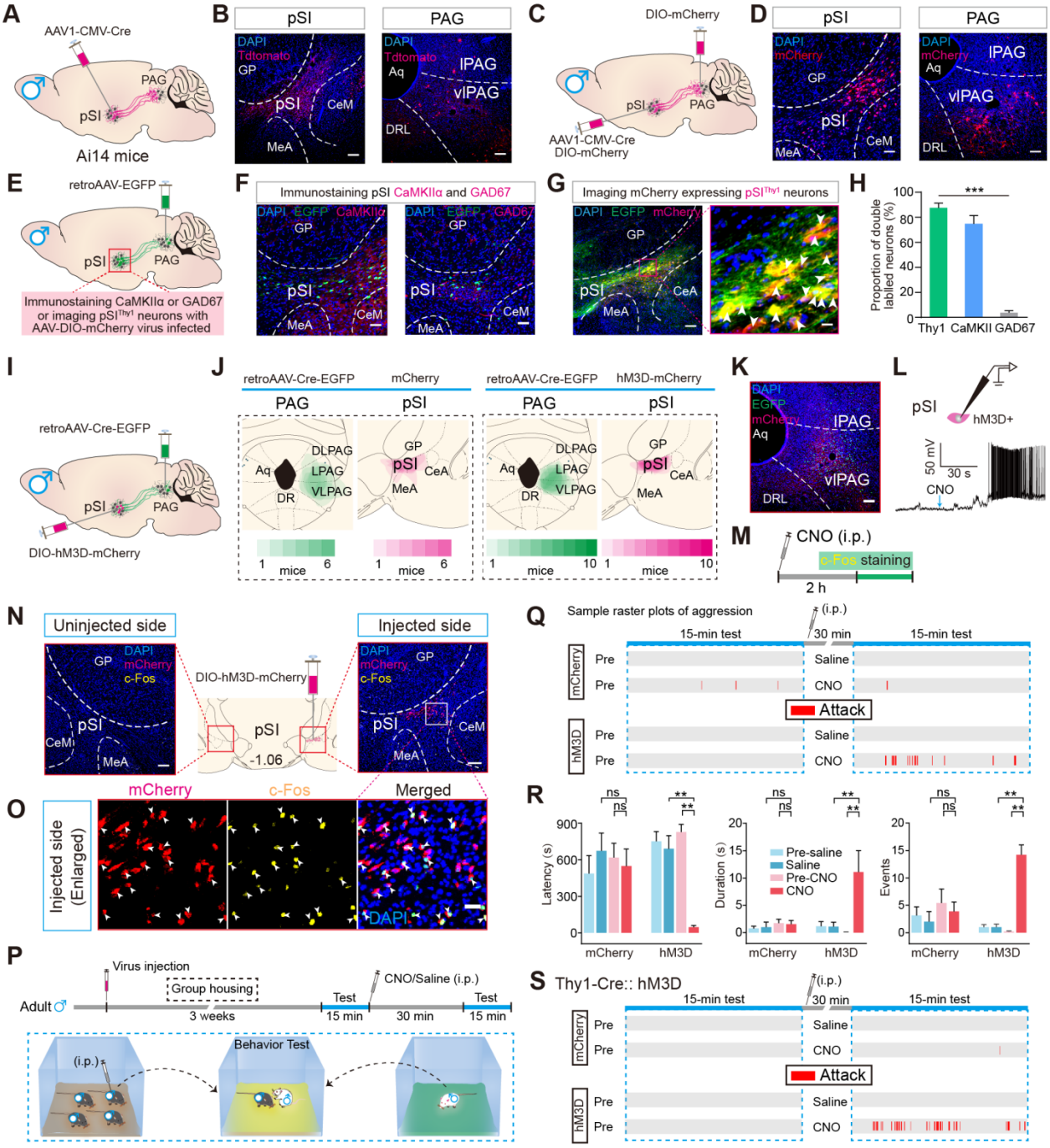
A
AAV1-CMV-Cre
PAG
pSI
Ai14 mice
B
pSI
PAG
DAPI
Tdtomato
GP
CeM
MeA
Aq
lPAG
vlPAG
DRL
C
DIO-mCherry
AAV1-CMV-Cre
DIO-mCherry
D
mCherry
E
retroAAV-EGFP
Immunostaining CaMKIIα or GAD67 or imaging pSI^Thy1 neurons with AAV-DIO-mCherry virus infected
F
Immunostaining pSI CaMKIIα and GAD67
EGFP
CaMKIIα
GAD67
G
Imaging mCherry expressing pSI^Thy1 neurons
CeA
H
Proportion of double labled neurons (%)
Thy1
CaMKII
GAD67
I
retroAAV-Cre-EGFP
DIO-hM3D-mCherry
J
retroAAV-Cre-EGFP
mCherry
hM3D-mCherry
DLPAG
LPAG
VLPAG
DR
mice
K
L
hM3D+
50 mV
30 s
CNO
M
CNO (i.p.)
c-Fos staining
2 h
N
Uninjected side
Injected side
c-Fos
-1.06
O
Injected side (Enlarged)
mCherry
c-Fos
Merged
P
Virus injection
Group housing
Adult
3 weeks
Test
15 min
CNO/Saline (i.p.)
30 min
Behavior Test
(i.p.)
Q
Sample raster plots of aggression
15-min test
30 min
Pre
Saline
CNO
Attack
R
Latency (s)
Duration (s)
Events
Pre-saline
Pre-CNO
ns
S
Thy1-Cre:: hM3D

Figure S4

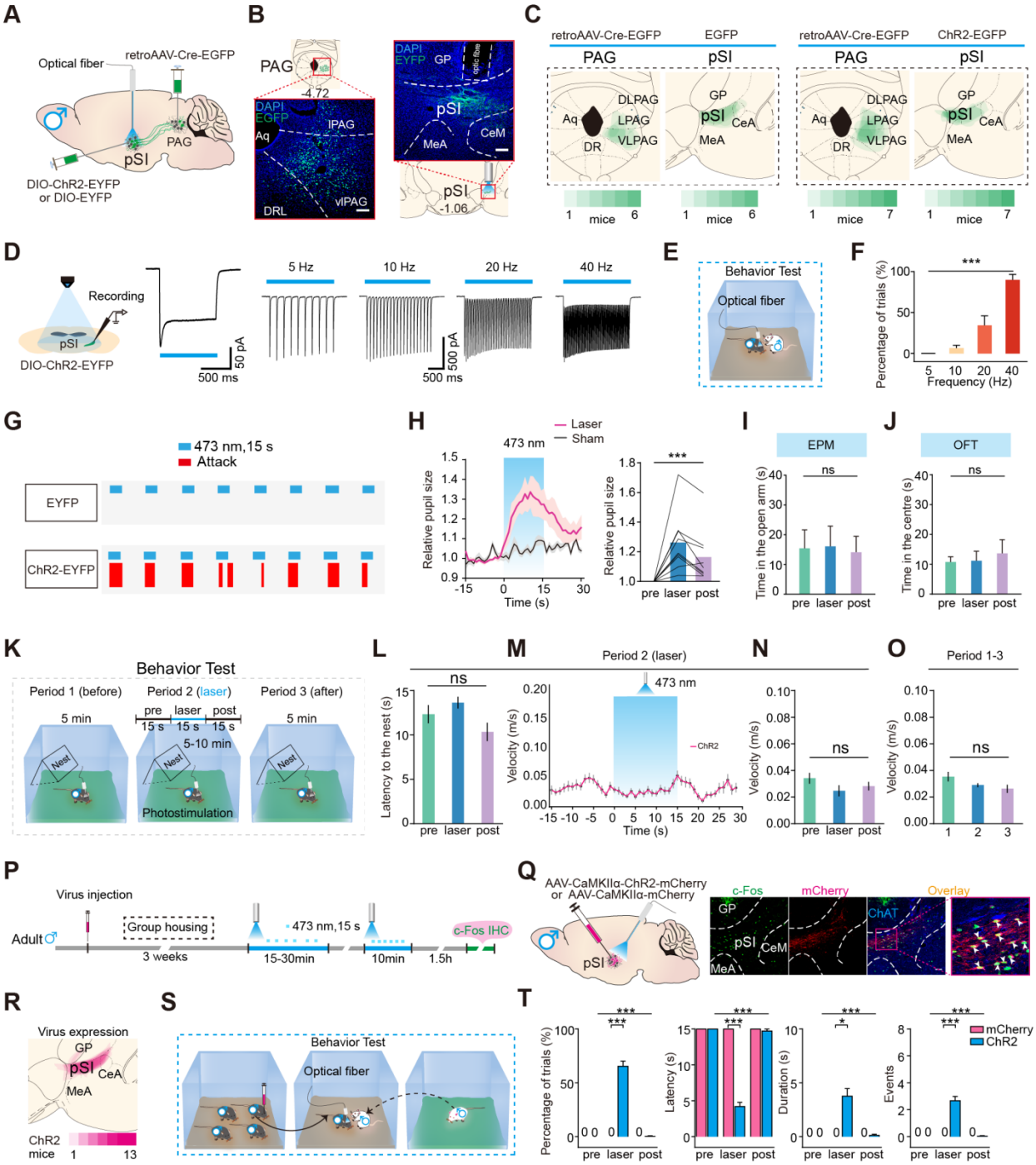
A
Optical fiber
retroAAV-Cre-EGFP
PAG
pSI
DIO-ChR2-EYFP
or DIO-EYFP
B
PAG
-4.72
DAPI
EGFP
IPAG
Aq
DRL
vlPAG
DAPI
EYFP
GP
pSI
MeA
CeM
-1.06
C
retroAAV-Cre-EGFP
EGFP
PAG
pSI
DLPAG
LPAG
VLPAG
Aq
DR
GP
CeA
MeA
mice
ChR2-EGFP
D
Recording
DIO-ChR2-EYFP
50 pA
500 ms
5 Hz
10 Hz
20 Hz
40 Hz
E
Behavior Test
Optical fiber
F
Percentage of trials (%)
Frequency (Hz)
G
473 nm,15 s
Attack
EYFP
ChR2-EYFP
H
Laser
Sham
473 nm
Relative pupil size
Time (s)
pre laser post
I
EPM
Time in the open arm (s)
ns
J
OFT
Time in the centre (s)
K
Behavior Test
Period 1 (before)
Period 2 (laser)
Period 3 (after)
5 min
pre laser post
15 s 15 s 15 s
5-10 min
Nest
Photostimulation
L
Latency to the nest (s)
M
Period 2 (laser)
473 nm
Velocity (m/s)
ChR2
N
O
Period 1-3
P
Virus injection
Adult
Group housing
3 weeks
473 nm,15 s
15-30min
10min
1.5h
c-Fos IHC
Q
AAV-CaMKIIα-ChR2-mCherry
or AAV-CaMKIIα-mCherry
c-Fos
mCherry
Overlay
GP
pSI
CeM
MeA
ChAT
R
Virus expression
GP
pSI
CeA
MeA
ChR2
mice 1 13
S
Behavior Test
Optical fiber
T
Percentage of trials (%)
Latency (s)
Duration (s)
Events
mCherry
ChR2
pre laser post

Figure S5

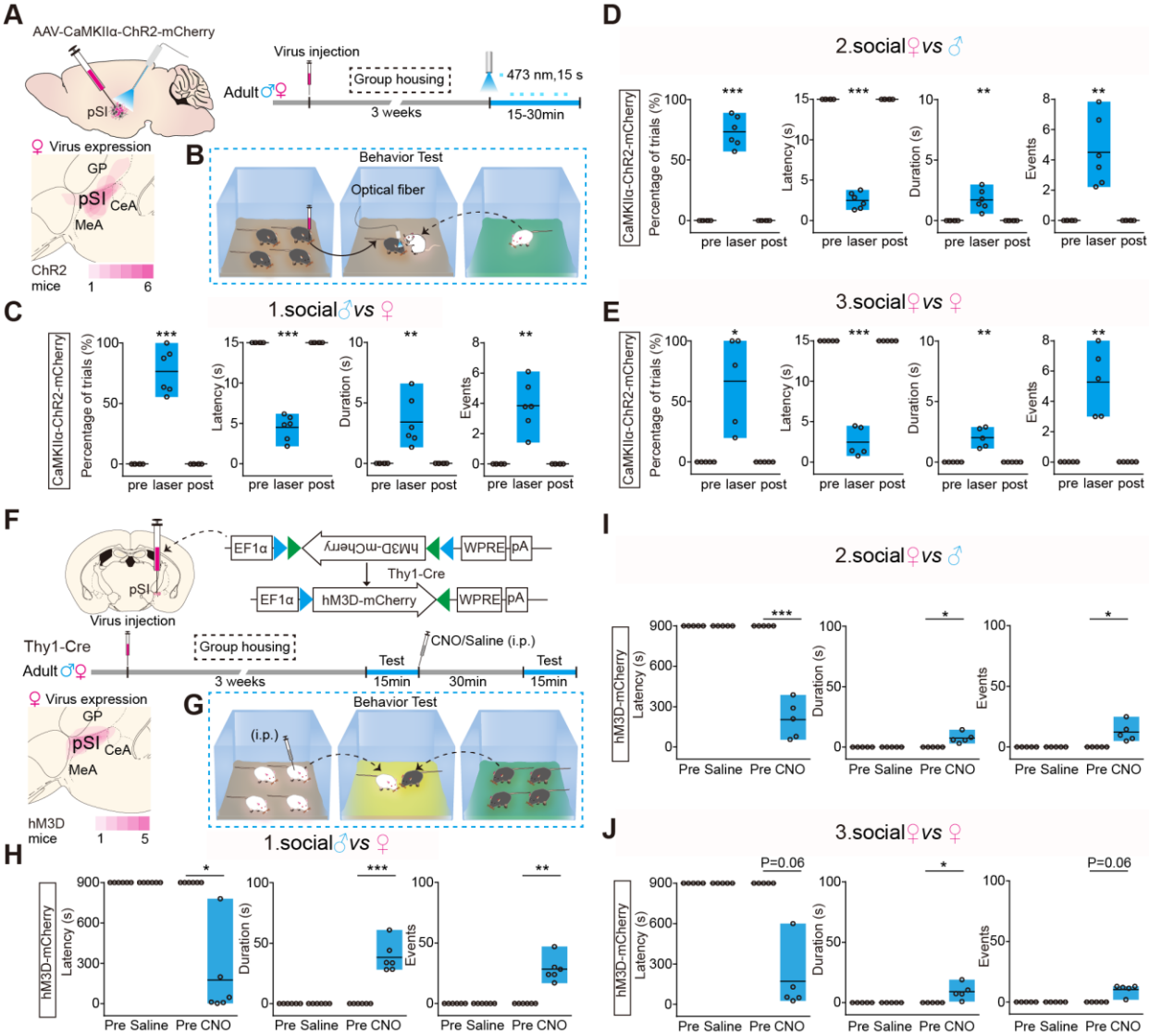
A
AAV-CaMKIIα-ChR2-mCherry
pSI
Virus injection
Adult ♂♀
Group housing
473 nm,15 s
3 weeks
15-30min
♀ Virus expression
GP
pSI
CeA
MeA
ChR2 mice
1
6
B
Behavior Test
Optical fiber
C
1.social♂vs♀
CaMKIIα-ChR2-mCherry
Percentage of trials (%)
Latency (s)
Duration (s)
Events
pre laser post
D
2.social♀vs♂
E
3.social♀vs♀
F
EF1α
hM3D-mCherry
WPRE
pA
Thy1-Cre
pSI
Virus injection
Thy1-Cre
Adult ♂♀
Group housing
CNO/Saline (i.p.)
Test
3 weeks
15min
30min
15min
♀ Virus expression
GP
pSI
CeA
MeA
hM3D mice
1
5
G
Behavior Test
(i.p.)
H
1.social♂vs♀
hM3D-mCherry
Latency (s)
Duration (s)
Events
Pre Saline
Pre CNO
I
2.social♀vs♂
J
3.social♀vs♀
P=0.06

Figure S6

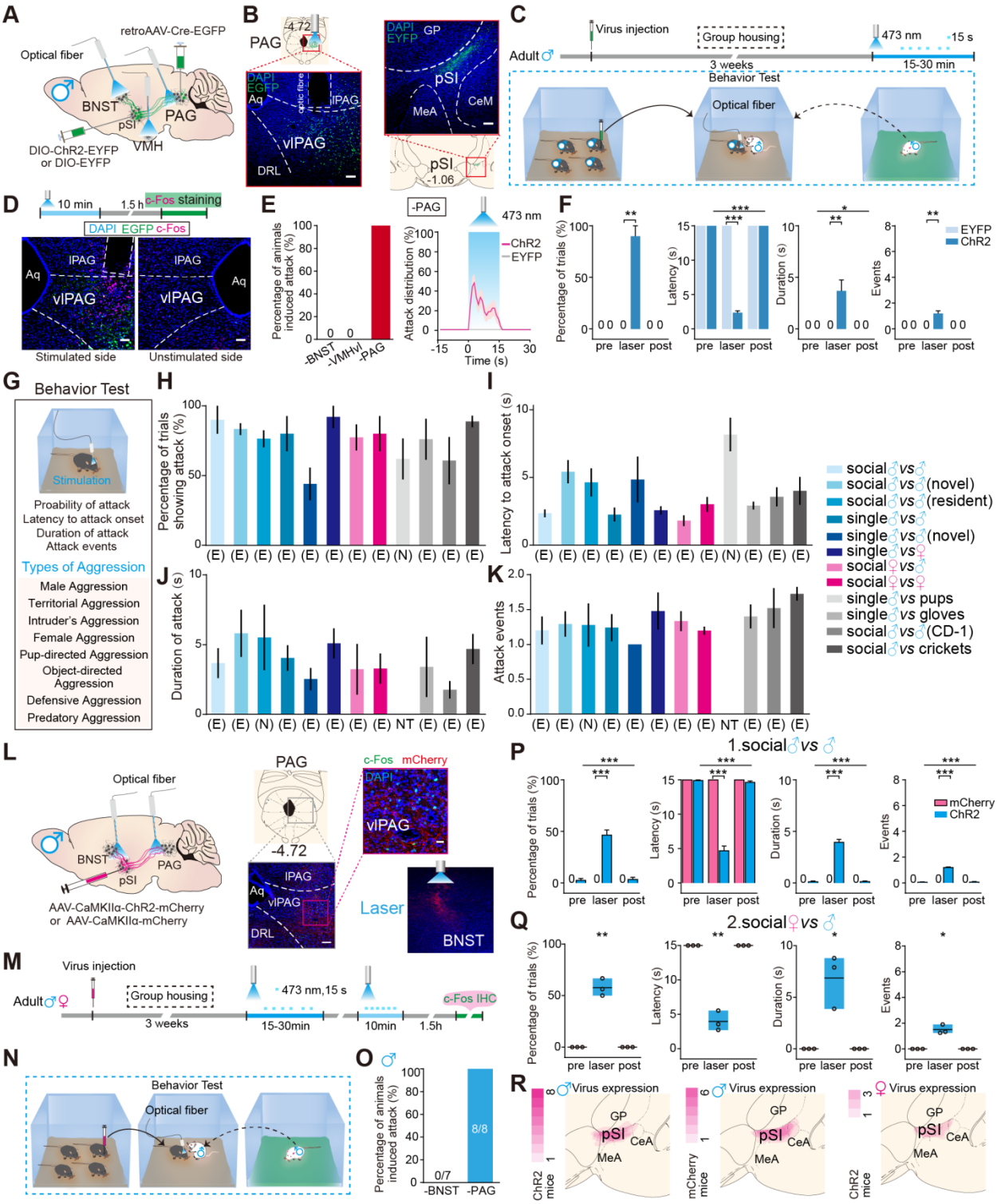
A
retroAAV-Cre-EGFP
Optical fiber
BNST
pSI
PAG
VMH
DIO-ChR2-EYFP
or DIO-EYFP
B
PAG
-4.72
DAPI EGFP
Aq
optic fibre
lPAG
vlPAG
DRL
DAPI EYFP GP
pSI
CeM
MeA
pSI
-1.06
C
Virus injection
Group housing
473 nm
15 s
Adult
3 weeks
15-30 min
Behavior Test
Optical fiber
D
10 min
1.5 h
c-Fos staining
DAPI EGFP c-Fos
lPAG
vlPAG
Aq
Stimulated side
Unstimulated side
E
Percentage of animals induced attack (%)
-BNST
-VMHvl
-PAG
-PAG
473 nm
Attack distribution (%)
ChR2
EYFP
Time (s)
F
Percentage of trials (%)
Latency (s)
Duration (s)
Events
pre laser post
EYFP
ChR2
G
Behavior Test
Stimulation
Proability of attack
Latency to attack onset
Duration of attack
Attack events
Types of Aggression
Male Aggression
Territorial Aggression
Intruder's Aggression
Female Aggression
Pup-directed Aggression
Object-directed Aggression
Defensive Aggression
Predatory Aggression
H
Percentage of trials showing attack (%)
I
Latency to attack onset (s)
J
Duration of attack (s)
K
Attack events
social♂vs♂
social♂vs♂(novel)
social♂vs♂(resident)
single♂vs♂
single♂vs♂(novel)
single♂vs♀
social♀vs♂
social♀vs♀
single♂vs pups
single♂vs gloves
social♂vs♂(CD-1)
social♂vs crickets
L
Optical fiber
BNST
pSI
PAG
AAV-CaMKIIα-ChR2-mCherry
or AAV-CaMKIIα-mCherry
PAG
-4.72
c-Fos mCherry
DAPI
vlPAG
lPAG
Aq
vlPAG
DRL
Laser
BNST
M
Virus injection
Adult
Group housing
473 nm,15 s
c-Fos IHC
3 weeks
15-30min
10min
1.5h
N
Behavior Test
Optical fiber
O
Percentage of animals induced attack (%)
0/7
8/8
-BNST
-PAG
P
1.social♂vs♂
Percentage of trials (%)
Latency (s)
Duration (s)
Events
mCherry
ChR2
Q
2.social♀vs♂
R
Virus expression
GP
pSI
CeA
MeA
ChR2 mice
mCherry mice
ChR2 mice

Figure S7

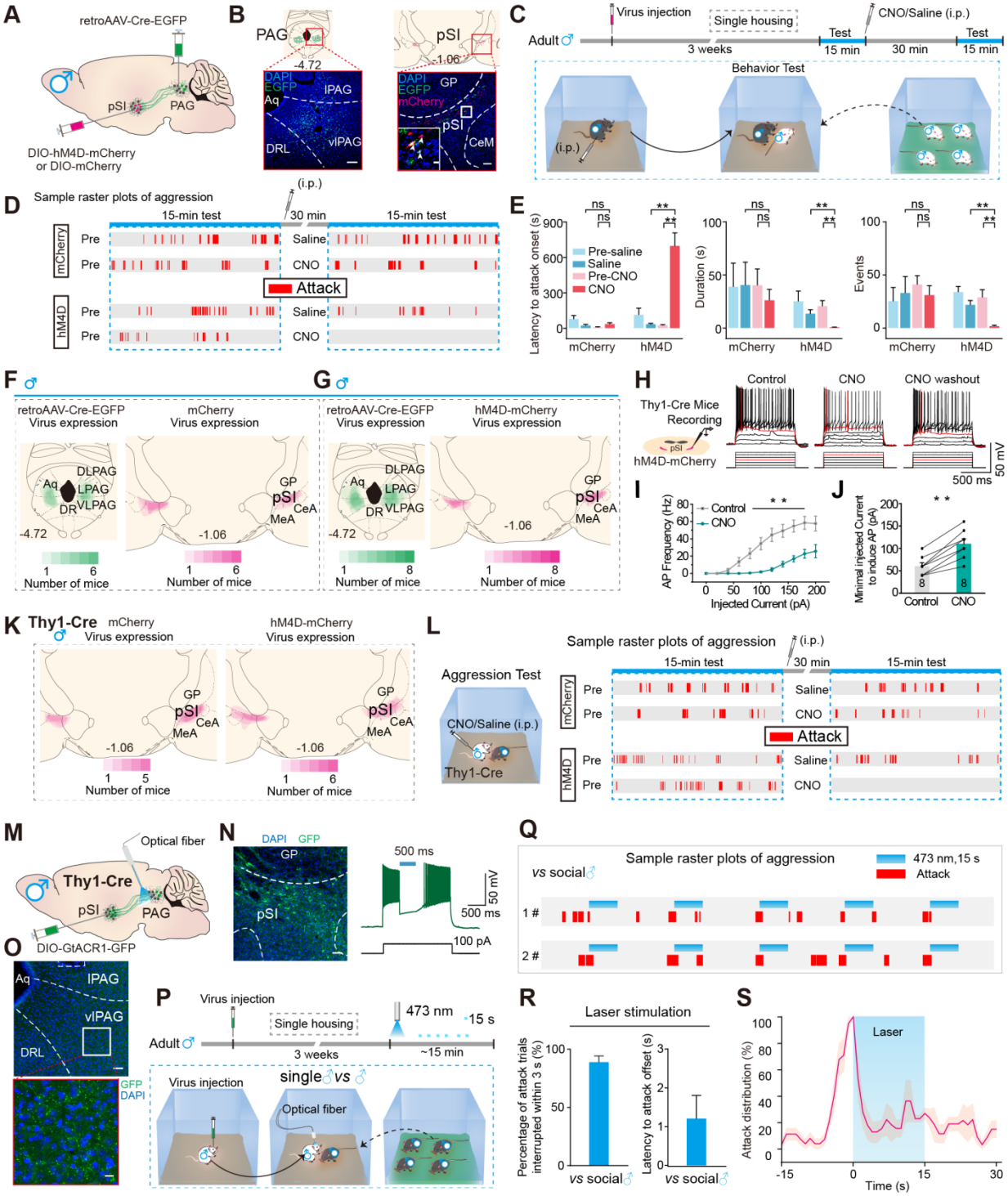
A
retroAAV-Cre-EGFP
pSI
PAG
DIO-hM4D-mCherry
or DIO-mCherry
B
PAG
-4.72
DAPI
EGFP
Aq
IPAG
DRL
vlPAG
pSI
-1.06
GP
mCherry
CeM
C
Virus injection
Single housing
CNO/Saline (i.p.)
Adult
3 weeks
Test
15 min
30 min
Behavior Test
(i.p.)
D
Sample raster plots of aggression
(i.p.)
15-min test
30 min
15-min test
mCherry
hM4D
Pre
Saline
CNO
Attack
E
Latency to attack onset (s)
Pre-saline
Saline
Pre-CNO
CNO
Duration (s)
Events
ns
**
mCherry
hM4D
F
retroAAV-Cre-EGFP
Virus expression
mCherry
Virus expression
DLPAG
LPAG
VLPAG
DR
Aq
GP
pSI
CeA
MeA
-4.72
-1.06
Number of mice
G
retroAAV-Cre-EGFP
Virus expression
hM4D-mCherry
Virus expression
H
Thy1-Cre Mice
Recording
hM4D-mCherry
Control
CNO
CNO washout
500 ms
50 mV
I
AP Frequency (Hz)
Control
CNO
Injected Current (pA)
J
Minimal injected Current to induce AP (pA)
Control
CNO
K
Thy1-Cre
mCherry
Virus expression
hM4D-mCherry
Virus expression
L
Aggression Test
CNO/Saline (i.p.)
Thy1-Cre
Sample raster plots of aggression
(i.p.)
15-min test
30 min
15-min test
M
Optical fiber
Thy1-Cre
pSI
PAG
DIO-GtACR1-GFP
N
DAPI
GFP
GP
pSI
500 ms
50 mV
100 pA
O
Aq
IPAG
vlPAG
DRL
GFP
DAPI
P
Virus injection
Single housing
473 nm
15 s
Adult
3 weeks
~15 min
Virus injection
single♂ vs ♂
Optical fiber
Q
Sample raster plots of aggression
vs social♂
473 nm,15 s
Attack
1 #
2 #
R
Laser stimulation
Percentage of attack trials interrupted within 3 s (%)
Latency to attack offset (s)
vs social♂
S
Laser
Attack distribution (%)
Time (s)

Figure S8

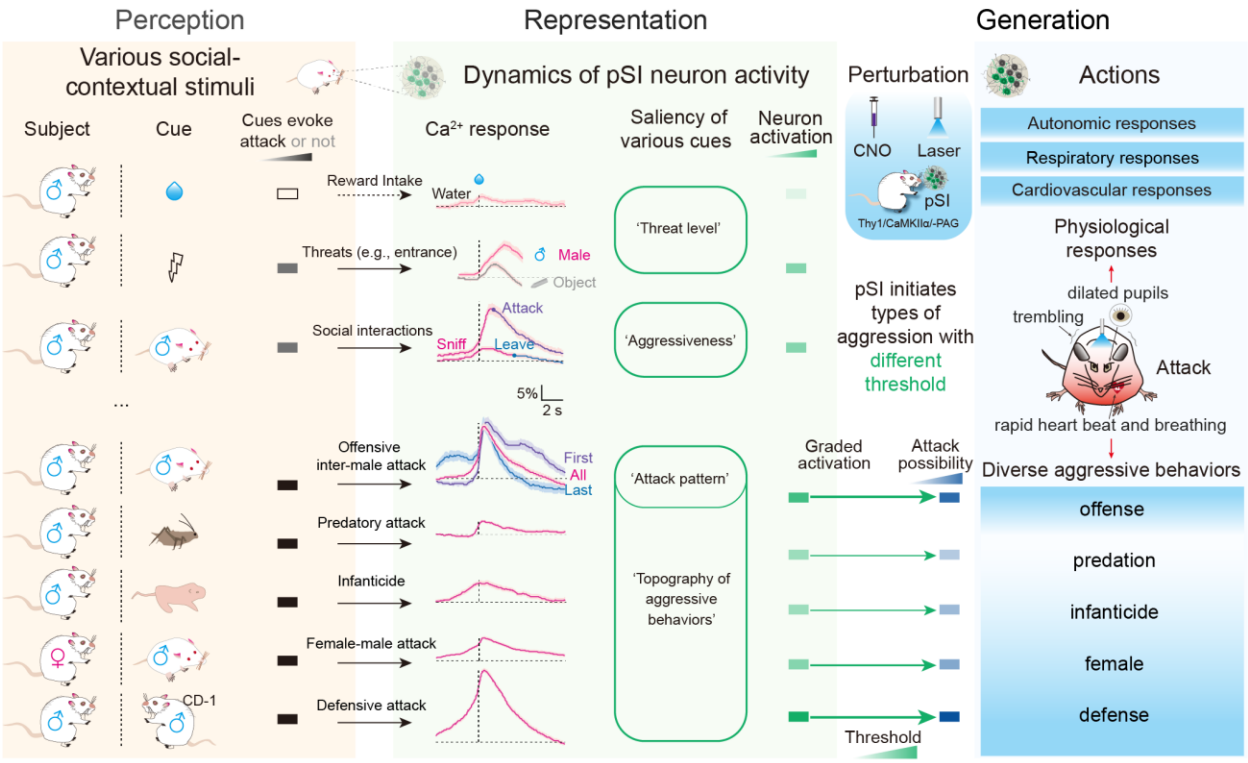
Perception
Representation
Generation
Various social-contextual stimuli
Dynamics of pSI neuron activity
Perturbation
Actions
Subject
Cue
Cues evoke attack or not
Ca2+ response
Saliency of various cues
Neuron activation
CNO
Laser
pSI
Thy1/CaMKIIα/-PAG
Autonomic responses
Respiratory responses
Cardiovascular responses
Reward Intake
Water
'Threat level'
Threats (e.g., entrance)
Male
Object
Physiological responses
dilated pupils
trembling
Attack
rapid heart beat and breathing
Social interactions
Attack
Sniff
Leave
'Aggressiveness'
pSI initiates types of aggression with different threshold
5%
2 s
Offensive inter-male attack
First
All
Last
'Attack pattern'
Graded activation
Attack possibility
Diverse aggressive behaviors
Predatory attack
offense
Infanticide
predation
infanticide
Female-male attack
female
CD-1
Defensive attack
defense
'Topography of aggressive behaviors'
Threshold